Validation of non-equilibrium kinetics in CO 2 –N 2 plasmas

C Fromentin, T Silva, T Dias, E Baratte, O Guaitella, V Guerra

Validation of non-equilibrium kinetics in CO_2-N_2 plasmas

C. Fromentin[1], T. Silva[1], T. C. Dias[1], E. Baratte[2], O. Guaitella[2] and V. Guerra[1]

[1] Instituto de Plasmas e Fusão Nuclear, Instituto Superior Técnico, Universidade de Lisboa, Portugal

[2] Laboratoire de Physique des Plasmas (UMR 7648), CNRS, Univ. Paris Saclay, Sorbonne Université, École Polytechnique, France

Abstract

This work explores the effect of N_2 addition on CO_2 dissociation and on the vibrational kinetics of CO_2 and CO under various non-equilibrium plasma conditions. A self-consistent kinetic model, previously validated for pure CO_2 and CO_2-O_2 discharges, is further extended by adding the kinetics of N_2. The vibrational kinetics considered include levels up to v = 10 for CO, v = 59 for N_2 and up to v_1 = 2 and v_2 = v_3 = 5, respectively for the symmetric stretch, bending and asymmetric stretch modes of CO_2, and account for electron-impact excitation and de-excitation (e-V), vibration-to-translation (V-T) and vibration-to-vibration energy exchange (V-V) processes. The kinetic scheme is validated by comparing the model predictions with recent experimental data measured in a DC glow discharge operating in pure CO_2 and in CO_2-N_2 mixtures, at pressures in the range 0.6 - 4 Torr (80.00 – 533.33 Pa) and a current of 50 mA. The experimental results show a higher vibrational temperature of the different modes of CO_2 and CO and an increased dissociation fraction of CO_2, that can reach values as high as 70 %, when N_2 is added to the plasma. On the one hand, the simulations suggest that the former effect is the result of the CO_2-N_2 and CO-N_2 V-V transfers and the reduction of quenching due to the decrease of atomic oxygen concentration; on the other hand, the dilution of CO_2 and dissociation products, CO and O_2, reduces the importance of back reactions and contributes to the higher CO_2 dissociation fraction with increased N_2 content in the mixture, while the $N_2(B^3\Pi_g)$ electronically excited state further enhances the CO_2 dissociation.

I. Introduction

To reach climate neutrality (balance between greenhouse gas emission sources and sinks [1]) and limit the irreversibility, severity and likelihood of climate hazards and their widespread impacts on human and natural ecosystems [2,3], by holding the temperature increase below 2°C in line with the Paris Agreement [4], breakthrough innovations are required. Some existing and under-development technologies for CO_2 valorisation in the world are briefly reviewed in [5]. The conversion of CO_2 into value-added chemicals and liquid fuels, via the CO_2 Capture and Utilization (CCU) approach is a potential way to not only decrease the CO_2 emissions, but also generate more economic value, reduce the dependence of fossil fuels and create the possibility to recycle CO_2 and close the carbon cycle [6]. The dissociation of CO_2 into CO is the critical step of any CCU process. Indeed, CO_2 is, thermodynamically, a very stable molecule so there are large energy barriers to overcome for its conversion. A very promising approach to achieve efficient dissociation of CO_2 is the use of non-thermal plasmas (NTPs) [7–18] benefiting from non-equilibrium conditions where high energy electrons coexist with cold ions and neutrals. The kinetics of nonequilibrium processes can be stimulated by vibrational excitation of molecules in the plasma [19]. Depending mainly on the electron temperature [20], NTPs can selectively transfer energy from the electrons (gaining energy from the electric fied) to the heavy particles in the plasma to initiate certain chemical processes like the dissociation of CO_2 with lower energy compared to conventional methods [21]. CO_2 dissociation has been the focus of many studies, exploring electron-impact [22–24], vibrationally driven [19,24–27] and thermal [28–30] dissociation routes.

In the last few years, a combination of computational simulations and experimental campaigns have contributed to a better understanding of CO_2-containing discharges [31–38] and to the development of the corresponding “reaction mechanisms”, i.e., a set of reactions and rate coefficients validated

against benchmark experiments. In particular, our modelling results were validated step-by-step against experimental data obtained using direct current (DC) glow discharges (plasmas sustained by high voltages inside a pair of electrodes) and advanced plasma diagnostics, namely Fourier Transform Infrared (FTIR) absorption spectroscopy [36] and optical emission spectroscopy (OES) [39]. By selecting specific working conditions in low-pressure glow discharges, the accuracy of the Electron Energy Distribution Function (EEDF) calculations, electron-impact vibrational excitation and de-excitation (e-V), vibration-to-vibration (V-V) and vibration-to-translation (V-T) energy transfer processes coefficients, and the rate coefficients of the main plasma processes could be tested in low CO_2 excitation regime. Our previous modelling research works were focused on:

(i) The electron-neutral scattering cross sections for CO_2 [40] and CO [41],
(ii) The validation of the electron-impact dissociation cross sections of CO_2 [22],
(iii) The study of the time-resolved evolution of the lower vibrationally excited CO_2 levels during the afterglow of CO_2 discharges, validating a set of V-V and V-T processes involving the lower ~ 70 states and the corresponding rate coefficients [32],
(iv) The extension of the model by including the e-V processes and studying the effect of electrons on the distribution of vibrationally excited CO_2 levels in pulsed and continuous glow discharges [33] to understand the transfer of electron energy toward CO_2 vibrations,
(v) The study of the dynamics of gas heating in the afterglow of pulsed CO_2 and CO_2–N_2 glow discharges, further validating the V-V and V-T mechanisms and rate coefficients [35],
(vi) The preliminary study of the N_2 influence on CO_2 the vibrational distribution functions in pulsed glow discharges using a simplified kinetic scheme [34],
(vii) The development of a reaction mechanism for 'vibrationally cold CO_2 plasmas' taking into account the CO_2 dissociation products in CO_2 discharges in conditions where the vibrational kinetics can modify the EEDF but has no direct influence on chemical reactions [42],
(viii) The elucidation of the role of the electronically excited metastable state $CO(a^3\Pi_r)$ in CO_2 dissociation and CO recombination [36,38,42,43],
(ix) The study of the CO_2 dissociation under Martian environment for oxygen production [31,44],
(x) The inclusion of a self-consistent description of the CO_2 and CO vibrational kinetics involving the dissociation products, namely CO, O_2, O validated in CO_2 and CO_2-O_2 discharges [38].

Herein we extend the study of the coupled electron, vibrational and chemical kinetics developed in [31–34,38,42], already tested and validated in CO_2-containing discharges and afterglows and for various operating conditions, with the addition and validation of the N_2 electron, vibration and chemical kinetics. For this purpose we include 59 vibrational levels of N_2, as was initiated in [31,34]. The V-T and V-V processes for these levels with CO_2 and N_2 molecules and the dissociation products are included, as well as the heavy-particle reactions involving nitrogen species. The model predictions are compared with measurements in DC discharges ignited in different CO_2–N_2 mixtures.

Several reasons motivate the study of CO_2-N_2 low temperature plasmas. N_2 represents a large fraction in most industrial flue gas [45] along with other impurities like oxygen and water, so the influence it may have on the kinetics and chemistry of the plasma must be investigated, as done previously for O_2 [38] and H_2O [46,47]. Moreover, the combined presence of nitrogen and oxygen species is bound to lead to the formation of N_xO_y by-products which are dangerous compounds [48] but could also be an intermediary for nitrogen fixation [49,50]. Furthermore, by varying the N_2 content in CO_2-N_2 mixtures we enlarge the parameter space and can have a thorough validation of the model and gain a deeper understanding of the kinetics of CO_2 plasmas. In the context of in situ resource utilization (ISRU) on Mars, studying the effect of N_2 on CO_2 dissociation is relevant given the presence of N_2 in the Martian atmosphere (96 % CO_2 – 2 % Ar – 2 % N_2). Decomposition of CO_2 under Martin environment would

promote the local production of breathable O_2, fertilizers and transportation fuel on Mars [31,44,51–54], where the conditions are optimal for CO_2 dissociation by plasmas [31]. Moreover, once oxygen has been made available, extracted from CO_2 thanks to membranes for instance [52], N_2 from the Martian atmosphere can be used for the local production of N_xO_y essential for the synthesis of fertilizers on site [54]. Finally, our model for the simulation of CO_2-N_2 DC discharges is a first step towards the simulation of $CO_2/N_2/H_2O$ mixtures as investigated in [55–57] where the chemistry induced by atmospheric pressure DC discharges above a water surface is studied. Since this mixture represents a model of prebiotic atmosphere of the Earth, it is interesting for the study of amino acids formation and for the verification of the theory of the origins of life. Some recent works have studied CO_2–N_2 mixtures, with a focus on the entry problems [58–62], the characterisation of electrical discharges in $CO_2/Ar/N_2$ mixtures [31,63–65] and the CO_2 conversion [63,66–71].

Current research on plasma-based CO_2 conversion in presence of N_2 is done mainly with dielectric barrier discharges (DBD) [67,69,72,73], microwave plasmas (MW) [68,74], ns pulse discharges [75–77] and DC glow discharges [34,66,78,79] where CO_2 dissociation pathways and energy efficiency are analysed. It has been shown that the admixture of N_2 has a beneficial impact on the CO_2 decomposition by plasmas [34,70]. Several reasons can be assigned to this effect: the enhancement of the reduced electric field, the effect of electronically and vibrationally excited states on CO_2 dissociation directly [66,80] or via changes of the EEDF [24,26,31,42], and the dilution with N_2 limiting the influence of back reaction mechanisms producing CO_2 from CO [34]. Favouring the excitation of the asymmetric vibrational mode of CO_2 by adding N_2 is well known in the context of CO_2–N_2 maser/laser systems extensively studied in the 60s [81–84]. The selective excitation of the asymmetric mode of CO_2 by nearly resonant vibrational energy transfers from N_2 was reported to enhance lasing power. Indeed, the first excited level of N_2 has an energy very close to the first asymmetric level of CO_2 ($\Delta E = 18\ cm^{-1} = 2.23 \cdot 10^{-3} eV$), which is smaller than the typical average kinetic energy kT [85], allowing nitrogen to easily exchange vibration quanta with the asymmetric mode of CO_2. This near-resonant transfer can be beneficial for vibrational dissociation of CO_2 as vibrationally excited CO_2 can undergo molecular dissociation through the so-called ladder climbing mechanism or by electron-impact stepwise processes. The anharmonicity of the molecule creates a preferential excitation of molecules in higher vibrational levels compared to those in lower levels, in V-V collisions, which leads to an overpopulating of the higher vibrational levels [86,87] and possible dissociation of highly vibrating CO_2 molecules without a significant amount of kinetic energy required. This purely vibrational mechanism requires $\sim$ 5.5 eV and the products are obtained in the ground state, whereas the CO_2 dissociation by direct electron-impact excitation requires more than 7 eV and leads to the formation of an O atom in an electronically excited state [21]. The asymmetric mode v_3 is of major interest here to reach an efficient dissociation by molecular collisions. While in principle any highly excited mode can lead to dissociation, the excited vibrational levels corresponding to the asymmetric stretch has a relatively long lifetime and its relaxation is thus much slower than that of the symmetric stretch and bending modes [84].

To establish a reaction mechanism for vibrationally excited CO_2-N_2 plasmas a DC glow discharge is used here as it generates a stable (axially) homogeneous plasma (in the positive column) and is accessible to different diagnostics [21]. Despite its evident limitations, namely, fairly low energy efficiency and CO_2 dissociation fractions, these plasma sources are optimal for validation of volume averaged 0D self-consistent kinetic models with detailed and complex kinetics and therefore for the fundamental study of CO_2-containing plasmas. The CO_2, CO and NO densities and the vibrational kinetics are diagnosed by FTIR absoprtion spectroscopy, and actinometry is used to determine the O atom density and loss frequency.

The paper is structured as follows. After the introduction, Section 2 briefly gives information on the experimental set-up and the diagnostics used. This is followed in Section 3 by a description of the model and the kinetic scheme used to study the CO_2-N_2 discharge. Moreover, in this section we report rate coefficients for electron-impact reactions and vibration-translation and vibration-vibration exchanges involving CO_2, N_2 and the dissociation products. The comparison between the experiments

and the simulations is presented and discussed in section 4 to gain further insight into the underlying kinetics. Finally, perspectives and conclusions are reported in section 5.

II. Experiments

Experiments are performed in non-thermal plasmas sustained by a continuous DC glow discharge, operating at pressures in the range P = 0.6 - 4 Torr and discharge current I = 50 mA, in a cylindrical Pyrex tube of radius R = 1 cm. Two tube lengths are used throughout this study, 23 cm for the Fourier transform infrared (FTIR) measurements and 67 cm for the actinometry and reduced field measurements. The experimental setup and diagnostics used are very similar to those described in [36,88,89]. In this section we provide a less detailed but essential description of the experiments.

For all measurements, the pressure, flow and current are imposed. The experiments are conducted both in pure CO_2 and in a CO_2-N_2 mixture (Air Liquide Alphagaz 1 standard for both CO_2 and N_2). The gas flows are controlled using mass flow controllers (Bronkhorst F-210CV) and a total gas flow of 7.4 sccm has been used in the present experiments as done previously in [31,34,36,38,88,89]. The electric field in the positive column of the discharge is estimated by measuring the voltage drop between two tungsten pins placed 20 cm apart and pointing radially inside the reactor. Since the positive column can be considered homogeneous, the electric field measurement is representative of the average field in the plasma bulk. The error on the reduced electric field, E/N, was calculated taking into account the uncertainty on the T_{rot} (see below) used for the calculation of the plasma density N.

In situ FTIR absorption spectroscopy was used to determine the different vibrationally excited states densities of CO_2 and CO from which are deduced the characteristic vibrational temperatures of CO and of the different modes of CO_2, namely, bending, symmetric stretching and asymmetric stretching modes, corresponding to T_1, T_2 and T_3 respectively [20]. The detected IR spectra contain several lines of CO and CO_2 vibrational transitions which are fitted using a MATLAB® algorithm, according to the procedure described in [36,88]. The measurements further give information on the rotational temperature of both CO_2 and CO which is assumed to be representative of the gas temperature [89]. By default, the fit assumes a Treanor vibrational distribution for the three vibrational modes of CO_2 [36,88,90] and bending and symmetric modes are assumed to be in equilibrium i.e. $T_1 = T_2 = T_{1,2}$ and this assumption was confirmed in [33,37,89]. During the experiments, an FTIR resolution of 0.2 cm^{-1} is used and the error on the different temperatures was estimated to be 30 K and 27 K for T_{rot} and $T_{1,2}$ respectively, 67 K for T_3 and 357 K for T_{CO} at 5 Torr, 50 mA and in pure CO_2 [36]. As an outcome of the fitting procedure, the dissociation fraction

$$\alpha = \frac{[CO]}{[CO] + [CO_2]}, \quad (1)$$

where [CO] and [CO_2] represent the gas phase concentrations of CO and CO_2 molecules, respectively, is also obtained. Due to the small dimensions of the sample chamber of the FTIR spectrometer (Bruker V70??), these measurements are done in the 23 cm long reactor. The temperatures for the same pressure and current are assumed to be the same in both reactors due to the fast timescales of temperature evolution in comparison with the residence times in our experimental conditions [89]. Finally, note that the measured vibrational temperatures are only representative of the populations of the lower vibrational levels and do not bring any information regarding the populations of the higher ones, which may deviate from equilibrium Boltzmann and/or Treanor distributions and are modified by the presence of N_2.

Downstream measurements, in which the same plasma reactor is placed upstream a measurement cell installed in the FTIR sample compartment, were also performed, similarly to what has been done by Morillo-Candas *et al.* [91]. Indeed, due to the small fraction of N_xO_y species in the discharge, we had to use a multipass cell placed after the plasma reactor, to increase the optical path to 5 m. Thanks to this configuration, we could reach sufficient sensitivity to observe NO and nitrogen dioxide (NO_2) absorption lines and capturing a wavenumber range of 950–3350 cm^{-1} ensured the simultaneous

measurement of NO, NO_2 as well as CO_2 and CO absorption bands. The NO_2 signal was at the noise level, so that the uncertainty obtained on the NO_2 density was so large that the data obtained are not reliable and therefore not provided here.

O atom densities and wall loss frequencies are measured in pure CO_2 by actinometry in a 67 cm length tube [89]. The absolute O atom densities obtained rely on several parameters for which large discrepancies exist in the literature which leads to an error estimation for this specie density above 30% [89,91]. The loss probability of O atoms at the wall, γ_O, is given in [89] as a function of pressure, for a current of 50 mA, and is deduced from the experimental determination of O atom loss frequencies, in pure CO_2, and was extrapolated at lower pressure. The values are summarized in Table 1.

*Table 1: O loss probabilities from [89] obtained experimentally, in pure CO_2, for a discharge current of 50 mA and used in our calculations. *Extrapolated value.*

Pressure (Torr)	O loss probability γ_O
0.6	$8.87 \cdot 10^{-4}$*
0.8	$6.50 \cdot 10^{-4}$
1	$5.33 \cdot 10^{-4}$
2	$4.50 \cdot 10^{-4}$
3	$4.91 \cdot 10^{-4}$
4	$5.33 \cdot 10^{-4}$

Overall, the set of measurements provides the gas temperature, vibrational temperatures of CO and the various modes of CO_2, the reduced field E/N, the fraction of atomic oxygen, [O]/N, and the densities of $O(^3P)$, $CO(X^1\Sigma^+)$, $CO_2(X^1\Sigma^+_g)$ and $NO(X^2\Pi_r)$ which are compared with the simulation results for the validation of the model described in section IV. The density of the gas, N, is calculated from the ideal gas law with the pressure and gas temperature obtained with the FTIR measurements.

III. Model

The development and validation of self-consistent models constitute a powerful tool to access quantities that are not available experimentally, to obtain insight into the processes occurring in the plasma, to interpret the experimental results and to predict the behaviour of important physical and chemical quantities in different plasma systems. In particular, 0D kinetic models can describe a detailed plasma chemistry with a significant number of processes included and therefore can provide very useful information on the main source and loss mechanisms of the species of interest like CO and NO. However, the reliability of these models depends strongly on the accuracy of the cross sections and/or rate coefficients used to describe the energy transfers, electron-impact mechanisms and heavy-particle chemical reactions.

The calculations are done with the LisbOn KInetics (LoKI) simulation tool developed in-house under MATLAB® and solving a Boltzmann-chemistry global model [92,93]. Since electrons play an important role in low-temperature plasmas, an accurate description of the electron energy distribution function (EEDF) and macroscopic electron parameters, including rate coefficients of electron-impact processes, is required. This is achieved here using the open-source Boltzmann solver LoKI-B, which numerically solves a space-independent form of the two-term electron Boltzmann equation (EBE) for non-magnetised non-equilibrium low-temperature plasmas, excited by DC or HF electric fields [92] or time-dependent (non-oscillatory) electric fields [94], in different gases or gas mixtures. Moreover, to get a self-consistent description of both electron and heavy species, the homogeneous EBE is coupled with the Chemical solver LoKI-C corresponding to a system of zero-dimensional state-to-state rate-balance equations describing the creation and loss of the most important neutral and charged heavy-particles. The relevant information regarding the model is summarized in this section and a figure of the workflow can be found in [42].

The electron, chemical and vibrational kinetics are coupled into a self-consistent scheme for which the reduced electric field, E/N, corresponds to steady-state conditions where the total rate of production of electrons in ionization events compensates exactly their total loss rate due to ambipolar diffusion to the wall and electron-ion recombination or, in other words, when the densities of negative and positive charges are the same, satisfying the quasi-neutrality condition. Moreover, it is guaranteed, thanks to the coupling between LoKI-B and LoKI-C, that the EEDF and electron parameters are obtained taking into account the self-consistently calculated concentrations of the parent gas and for a value of reduced electric field also self-consistently obtained. Vice-versa, all the rate coefficients of the electron-impact reactions depend on this self-consistent EEDF.

The electron density, n_e, is such that the current (I) given as input calculated with:

$$I = \pi R^2 |q_e| n_e v_e, \quad (2)$$

must give the experimental current intensity of 50 mA; where q_e is the elementary charge of electrons and v_e is the electron drift velocity obtained from the EBE solution. The diffusion of neutral species, including the vibrationally excited species, is taken as in [34,95], and is based on the formula of Chantry [96] to obtain the loss rate of species interacting with the wall due to the combined effect of transport (due to diffusion) and reaction at the wall (with a certain wall recombination/deactivation probability γ). The diffusion of charged-particles is described by classical ambipolar diffusion [95] and the effect of the negative ions on the electron density radial profiles is taken into account [97,98]. The gas flow is used as input parameter to the model, where we assume a simple mechanism of renewal of gas: new CO_2/N_2 particles enter the reactor while the species produced in the plasma exit at the outlet assuming conservation of atoms in the plasma mixture [42].

Together with the discharge current (I) given in (2), the input parameters of the model are the gas pressure (P), the flow, the initial gas mixture and reactor dimensions (tube length and radius). The loss probability of O atoms at the wall, γ_O, is also an input parameter and is deduced from the experimental determination of O atom loss frequencies (cf. Table 1). Additionally, in the present simulations the gas temperature obtained experimentally is also used as input parameter. The self-consistent calculation of T_g is possible, using a thermal balance equation [35,95,99] but the study of heat transfer mechanisms is not the focus of this work.

III.1 Chemistry

Most of the required electron scattering cross-section data can be found at the open-access website LXCat [100,101]. For this work, we use the IST-Lisbon database [100] including complete sets of electron scattering cross sections (CS) with neutral species in the ground-state (GS) based on [95,102,103] for N_2, [104] for N, [38,40] for CO_2, [41] for CO, and [105,106] for O_2 and O. They are defined as sets of cross sections giving a good description of the main electron energy and momentum losses, yielding electron swarm parameters in agreement with available measured data, when used in a two-term Boltzmann solver [100]. In CO_2-N_2 plasmas, CO, O_2 and O may be present with significant concentrations, therefore, besides CO_2 and N_2, cross sections for electron impact on these three plasma species are of importance. The CS describe the elastic momentum-transfer due to electron collision with the GS, the excitation of electronic and vibrational states from GS and ionisation. The sets of electron scattering cross sections from ground-states CO_2, N_2, CO and O_2 are complemented by additional collisional data, essentially for collisions from their vibrationally excited states, as well as from some of their electronically excited states. They can be found in the IST-Lisbon database [100] but are not part of the complete sets. The list of all the e-V processes and corresponding cross sections for CO_2 are reported in the Supplementary Information of [38]. Notice that the superelastic processes are considered and the corresponding cross sections are deduced from the direct processes using the Klein-Rosseland relation [107]. Due to the lack of data, the dissociation cross sections via electron impact from vibrationally excited states are considered with a threshold shift, while keeping

the same amplitude as for dissociation from the ground-state [31]. The same procedure is used for ionization from vibrationally excited CO and CO_2 molecules as well as attachment for CO_2.

The vibrational excitation of oxygen is included in the calculation of the EEDF, assuming a Boltzmann distribution at T_g for vibrational levels up to 4, but not in the Chemistry module as a strong depopulation of the Vibrational Distribution Function (VDF) in the first vibrational levels was observed experimentally [108] and in the calculations of [109,110]. Vibrationally excited O_2 molecules do not seem to have a direct influence neither in the EEDF nor in the chemistry [111] but may have a relevant contribution to gas heating, due to V–T deactivation by atomic oxygen, affecting indirectly the discharge [98].

For the description of the rotational excitation and deexcitation of the ground-state N_2 and O_2 by electron impact, we adopt the continuous (CAR) approach, using the GCAR rotational operator [95,112], whereas a discrete approach that considers a set of cross sections for rotational transitions involving the states CO ($X^1\Sigma^+$,v = 0, J = 0-17) published also in the IST-Lisbon database is used for CO.

The species considered in the plasma chemistry of the model include: ground-state, vibrationally and/or electronically excited CO, CO_2, O_2, N_2, NO, NO_2 and CN molecules CO($X^1\Sigma^+$,v=0:10), CO($a^3\Pi_r$), CO_2($X^1\Sigma^+_g$,v_1^{max}=2;v_2^{max}=v_3^{max}=5), O_2($X^3\Sigma_g^-$), O_2($a^1\Delta_g$), O_2($b^1\Sigma_g^+$), O_2(A'$^3\Delta_u$, $A^3\Sigma_u^+$, $c^1\Sigma_u^-$), N_2($X\ ^1\Sigma_g^+$,v=0:59), N_2($A\ ^3\Sigma_u^+$), N_2($B^3\Pi_g$), N_2($C\ ^3\Pi_u$), N_2($w\ ^1\Delta_u$), N_2($a\ ^1\Pi_g$), N_2($a'\ ^1\Sigma_u^-$), NO($X\ ^2\Pi_r$), NO($A\ ^2\Sigma^+$), NO($B^2\Pi_r$), NO_2(X^2A_1), NO_2(a^4A_2), CN($X^2\Sigma^+$) and CN($B^2\Sigma^+$); ground-state and electronically excited oxygen and nitrogen atoms, O(^{3}P), O(^{1}D), N(^{4}S), N(^{2}D), N(^{2}P), ground-state carbon C(^{3}P), ground-state ozone and vibrationally excited ozone, O_3, O_3*; and positive and negative ions, O^+, O_2^+, O^-, CO_2^+, CO^+, N_2^+, N_2^+($B\ ^2\Sigma_u^+$), N^+, N_4^+, N_3^+ and NO^+. For O_3* we consider a single effective vibrationally excited state [113]. O_2(A'$^3\Delta_u$, $A^3\Sigma_u^+$, $c^1\Sigma_u^-$) is an effective sum of the Herzberg states. Our model does not take into account directly the kinetics of $N_2(W^3\Delta_u)$. However, it is considered indirectly in the kinetics of the $N_2(B^3\Pi_g)$ state since the collisional data measured in flow systems actually provide the relaxation coefficients for the coupled states as a whole [114]. Besides, the $N_2(B^3\Pi_g)$ state is populated by the radiative cascade $N_2(B'\ ^3\Sigma_u^-) \rightarrow N_2(B^3\Pi_g)$, on the assumption that the $N_2(B'\ ^3\Sigma_u^-)$ is only populated by electron impact and radiatively depopulated (i.e., the populating rate of the $N_2(B^3\Pi_g)$ state due to this mechanism is that for creating the $N_2(B'\ ^3\Sigma_u^-)$ by electron impact) [114,115]. The rate coefficients of heavy-particle reactions are adopted from literature and based on the kinetic schemes of O_2 [98] based on [111,116,117], CO_2 [42], N_2 [114], N_xO_y [95] and CN [118] while the rate coefficients of the electron impact reactions are calculated from the energy-dependent cross sections, in combination with the EEDF. For the kinetics of oxygen, the set proposed in [98] is adopted without modifications except for the exclusion of vibrational states in the heavy-species chemistry. We also added the three-body reaction:

$$NO + O + CO_2 \rightarrow NO_2 + CO_2, \quad (3)$$

with the rate coefficients taken from [68].

III.1.1 Quenching of $N_2(A)$ and $N_2(B)$

Reactions involving $N_2(A\ ^3\Sigma_u^+)$, referred to as $N_2(A)$, and the triplet levels $N_2(B'\ ^3\Sigma_u^-)$, $N_2(B^3\ \Pi_g)$, and $N_2(W\ ^3\Delta_u)$, considered here as a single effective state $N_2(B)$ [119], are relevant for the study of active nitrogen, shock waves and flames [120,121]. Several authors claim that the presence of these species improves the CO_2 dissociation [66–68,71,121] and therefore these studies regained interest more recently for the study of N_2-containing CO_2 discharges. According to [66,121], the most important electronically excited nitrogen state for CO_2 conversion is $N_2(B)$ with the rate coefficients being roughly gas kinetic [122] for $N_2(B)$ quenched by CO_2 and CO, as can be seen in Table 2, where a brief survey of reported rate coefficients for reactions involving $N_2(B)$ and CO_2 or CO is given.

The rate coefficient for CO_2 dissociation due to quenching with $N_2(A)$ is much smaller than with $N_2(B)$ and is two orders lower than those by products of CO_2 dissociation like CO [123]. Indeed, CO is a more efficient acceptor of the electronic energy from $N_2(A)$ [124–127]. Several rate coefficients found in the literature for the quenching of $N_2(A)$ with CO and CO_2 are compiled in Table 3.

The relative importance of $N_2(A)$ and $N_2(B)$ metastable states for CO_2 dissociation seem to depend on the operating conditions. For discharges with high electron energy like DBD $N_2(A)$ was claimed to be important [67,71] for CO_2 dissociation while for a microwave discharge, with lower electron average energy, it was shown that $N_2(A)$ was of minor importance [68]. However, the study done in the DBD [67] used a value for the rate coefficient for the $N_2(A)$ quenching by CO_2 taken from [71], which is two orders of magnitude higher than what is commonly found in literature (see Table 3).

It is worth noting that in the collisional quenching of electronically excited N_2 molecules the branching ratio of the quenching products remains uncertain and can affect the modeling predictions in the most significant way [80]. Finally, it is necessary to note that an important feature of many reaction involving $N_2(A,B)$ is a dependence of the rate coefficients and products ratios on the vibrational levels [120,122,123,128] and that the actual measurements of rate coefficients can be a mix of vibrational levels [123].

process	[120,129]	[71,121,129]	[66,122]	[71]	[120]
$N_2(B) + CO_2 \rightarrow N_2+CO+O$	$1.5\cdot10^{-10}$ (a)	$8.5\cdot10^{-11}$ (b)			
$N_2(B) + CO_2 \rightarrow$ products			**$2\cdot10^{-10}$** (a)		
$N_2(B) + CO_2 \rightarrow N_2+CO_2$				$1\cdot10^{-11}$	
$N_2(B) + CO_2 \rightarrow N_2+CO_2$				$1.9\cdot10^{-10}$	
$N_2(B)+CO \rightarrow$ products			**$2\cdot10^{-10}$** (a)		$8.5\cdot10^{-11}$

Table 2: Rate coefficients in cm^3s^{-1} for processes involving the quenching of $N_2(B)$, measured at (a) 300 K and (b) 196 K. In bold, values used in the model for section IV.2.

process	[71]	[123]	[126]	[120]
$N_2(A) + CO_2 \rightarrow N_2+CO+O$	$1.54\cdot10^{-12}$			
$N_2(A) + CO_2 \rightarrow$ products		**$1.98\cdot10^{-14}$** (c)		
$N_2(A) + CO_2 \rightarrow N_2+CO_2$	$9.9\cdot10^{-15}$			
$N_2(A) + CO \rightarrow$ products		**$1.7\cdot10^{-12}$** (c)	$2.5\cdot10^{-11}$	$2.5\cdot10^{-12}$

Table 3: Rate coefficients in cm^3s^{-1} for processes involving the quenching of $N_2(A)$, (c) measured at 298 K. In bold, values used in the model for section IV.2.

The quenching processes of $N_2(A)$ and $N_2(B)$ are investigated in section IV.2. The values of the rate coefficients used for this study corresponding to the quenching of $N_2(A)$ with CO_2 and CO are, respectively, $1.98\cdot10^{-14}$ cm^3s^{-1} and $1.7\cdot10^{-12}$ cm^3s^{-1} [123] and are assumed to occur via the following processes:

$$N_2(A) + CO2 \rightarrow N_2 + CO + O, \quad (20)$$

$$N_2(A) + CO \rightarrow N_2 + CO, \quad (21)$$

For the quenching of $N_2(B)$ with CO_2 and CO, considered as follows:

$$N_2(B) + CO_2 \rightarrow N_2 + CO + O, \quad (22)$$

$$N_2(B) + CO \rightarrow N_2(A) + CO, \quad (23)$$

we use the values reported in Piper [122] and used as well in Naidis & Babaeva [66], namely $2\cdot10^{-10}$ cm^3s^{-1} for both processes.

III.2 Vibrational kinetics

The vibrational kinetics include excitation/de-excitation mechanisms due to electron-impact collisions (e-V), energy transfer via vibrational–translational (V-T), vibrational–vibrational (V-V) interactions and wall loss of vibrational quanta (W). The VDFs of CO_2, N_2 and CO are obtained from the solution of the rate-balance equations describing the creation and loss of each individual vibrational level,

accounting for these e-V, V-V, V-T, W processes, as well as chemical reactions like electron-impact dissociation from vibrationally-excited molecules and dissociation in pure vibrational mechanisms. The pure CO_2 subsystem was recently addressed in [38], where expressions for the V-T and V-V involving CO_2, CO, O_2 and O, rate coefficients are suggested. The vibrational energy transfers in the nitrogen system have been extensively studied in the past, due to the key role of vibrations in nitrogen plasmas [95,97,109,110,114,115,130]. The rate coefficients used for the pure N_2 subsystem are given in [34,95] and the calculation of the V-T and V-V rate coefficients were benchmarked from the calculations of Billing *et al.* [131,132]. The reader is referred to these papers for further details and figures representing these rate coefficients. The rate coefficients were scaled using either the Schwartz, Slawsky, and Herzfeld (SSH) theory [133] (SSH) or the theory from Sharma and Brau (SB) [134,135] (SB), which are summarized in [32] for the case of CO_2. A comprehensive description of the SSH scaling law can be found in [16]. In regards of rate coefficients used for inverse reactions, we have used the principle of detailed balance [136] for the various V-T and V-V transitions. We only consider dissociation by electron impact from vibrationally excited CO_2 molecules as the higher levels are not significantly populated in our conditions. In other words, we do not consider dissociation through the pure vibrational path ($CO_2(v^*) + CO_2 \rightarrow CO + O + CO_2$), but only stepwise dissociation by electron impact on vibrationally excited CO_2. The validity of this assumption is shown and discussed in [38,42].

In the following subsections, we start by discussing the description of the vibrational levels considered and the e-V processes. We then review our current choice of rate coefficients for the relevant mechanisms in CO_2-N_2 plasmas, namely CO_2-N_2, CO_2-CO and N_2-CO V-V exchanges and different V-T processes. Finally, we report the probabilities of deactivation of vibrationally excited species and atomic oxygen recombination at the walls.

III.2.1 Energy levels and e-V processes

The model considers 59 vibrational levels of N_2, up to the energy of ~10 eV. They are included in the model following the formula given in [137]:

$$\frac{E_{N_2}}{hc} = \sum_{i=1}^{5} a_i \left(v + \frac{1}{2}\right)^i, \tag{4}$$

with the coefficients a_i in cm^{-1} equal to 2378.1, -18.516, 0.26662, $-6.2127 \cdot 10^{-3}$and $3.4215 \cdot 10^{-5}$, respectively, for i=1-5. The energies of the individual CO_2 vibrational levels are calculated according to the anharmonic oscillator approximation [138] and more details can be found in [38]. The CO vibrational energy levels are calculated by the formula of the anharmonic Morse oscillator [114] as done in [38]. By convention, the ground-state energy is set to 0 eV for CO_2, CO and N_2.

As carefully described in [33,40] and briefly reviewed in [38,99], the cross sections for electron-impact excitation (e-V) of CO_2 vibrations are obtained from a direct deconvolution of the available lumped cross sections, according to the statistical weights of the various levels, and the missing cross sections are generated following the approach from [38], based on a modified form of the semi-empirical Fridman's approximation [21]. For the electron-impact excitation of the CO vibrations, we have adopted the cross sections from [139] for the vibrational excitation and de-excitation which are largely based on resonant excitation data from Laporta and co-workers [140], and where contributions from non-resonant collisions for the transition e + CO(v=0) ↔ e + CO(v=1), taken from [141], are also included. Finally, the e–V mechanisms for N_2 are described as follows: (i) in the electron kinetics calculations, e.g. when solving the electron Boltzmann equation, by adopting electron-scattering cross sections for the reactions e + N_2(X,v) → e + N_2(X,v′) ($1 \leq v \leq v' \leq 10$), obtained by applying a threshold shift to the excitation cross sections for the corresponding vibrational transitions from the ground-state N_2(X,v = 0); (ii) in the chemistry model calculations, by using electron rate coefficients satisfying the scaling law:

$$k_{v,v+v'} = \frac{k_{0,v'}}{1 + 0.15v}, \quad (5)$$

For $1 \leq v' \leq 10, 1 \leq v \leq 59$ and where $k_{0,v'}$ are the rate coefficients for vibrational transition from N_2 in the ground state to the first 10 vibrational states. This scaling law given by Colonna in [142] was validated in [103] and used in [34,95,143].

III.2.2 CO_2-N_2 and CO_2-CO V-V exchanges

The transfer between vibrationally excited nitrogen and the asymmetric stretching mode of CO_2, is very efficient and may potentially have a positive effect on CO_2 dissociation via the ladder climbing mechanism [21]. CO_2 is known to couple very strongly to N_2 via

$$N_2(0) + CO_2(00^0 11) \leftrightarrow N_2(1) + CO_2(00^0 01), \quad (6)$$

since the energy difference between the first vibrationally excited levels is only 18 cm^{-1} [135]. For details on the notation used for the CO_2 vibrations, the reader is referred to [32,37,38]. The hypothesis regarding the selective excitation of the upper laser level of CO_2 lasers by resonant transfer of vibrational energy from N_2 molecules, necessary to obtain the population inversion in the CO_2-N_2 laser system, is widely accepted by the scientific community [82,83,85]. Moreover, even though the equivalent reaction between CO_2 and CO is not as close to energy resonance as for N_2, CO molecules can transfer a considerable amount of energy to the v_3 vibration via (7) because the difference between the energies of the vibrational level of CO and the $(00^0 11)$ level of CO_2 is 170 cm^{-1} which is typically smaller than the average kinetic energy kT [81],

$$CO(0) + CO_2(00^0 11) \leftrightarrow CO(1) + CO_2(00^0 01). \quad (7)$$

The importance of these two processes comes from the large populations of vibrationally excited CO and N_2 molecules present in the discharge, most likely due to direct electronic excitation, followed by the transfer of energy to the vibrational levels of CO_2. This is supported by experimental data on the cross sections of collisions between electrons and heavy species (CO and N_2), reported in [144]. Indeed, according to Schulz, the electron-impact excitation cross sections of the vibrational levels of CO and N_2 are unusually large because of the resonance effect of the short-lived negative CO^- and N_2^- ions [145]. The excitation cross section of the first levels of CO and N_2 ($\sim 5 \cdot 10^{-16} cm^{-2}$) is one order of magnitude higher compared to the excitation of CO_2 in the first asymmetric stretch mode level by electron impact [33,40], for electrons of 2 eV energy, typical of our discharge.

Since the energy defect is about 10 times larger for CO than for N_2 it might be anticipated that CO is not as effective as N_2 in exciting the vibration of CO_2. Furthermore since the CO molecule has a dipole moment, it has also a spontaneous decay whereas N_2 can only decay via collisions with the wall or with other molecules [85]. It appears, however, that the additional dipole-dipole attractive forces between CO_2 and CO more than compensate for this disparity, as the CO_2-CO transfer can even be more efficient than the CO_2-N_2 transfer. This could come from the observation that near resonant V-V transfer processes are more likely to occur when the vibrational modes involved are infrared active [146].

The CO_2-CO V-V rate coefficient comes from our previous work [38] and is based on [147], while the rate coefficient for CO_2-N_2 V-V used in the present work is taken from [148]. We compare in Figure 1 the rate coefficients used in this work for the processes (6) and (7) with experimental data available in literature obtained with laser-excited vibrational fluorescence and shock tube techniques by Taylor *et al.* [149], Rosser *et al.* [150], Taylor & Bitterman [151], Stephenson *et al.* [146], Moore *et al.* [152], Starr & Hancock [153], Rosser *et al.* [154], Blauer and Nickelson [148]. Although there are considerable data for CO_2-N_2, a large scatter can be observed. Above 1000 K there are similarities between the CO_2-CO and CO_2-N_2 V-V rate coefficients as might be expected based on the similarities between N_2 and CO molecules. At lower temperatures, however, the situation may seem puzzling.

The positive temperature dependence for the CO_2-CO V-V rate coefficient is the reverse of that found for CO_2-N_2. It is clear that the Schwartz, Slawsky, and Herzfeld (SSH) theory [133] cannot explain the low-temperature behaviour for CO_2-N_2, as this theory predicts an increase of the reaction rates with temperature. Sharma and Brau (SB) [134,135] have explained the negative temperature dependence of the CO_2-N_2 V-V energy exchange, at low temperatures, on the basis of the long range force between the dipole moment of CO_2 and the quadrupole moment of N_2, being more important than the short range repulsive forces normally used in vibrational relaxation theories. Such an interaction is more important at low temperatures and for processes of near energy resonance.

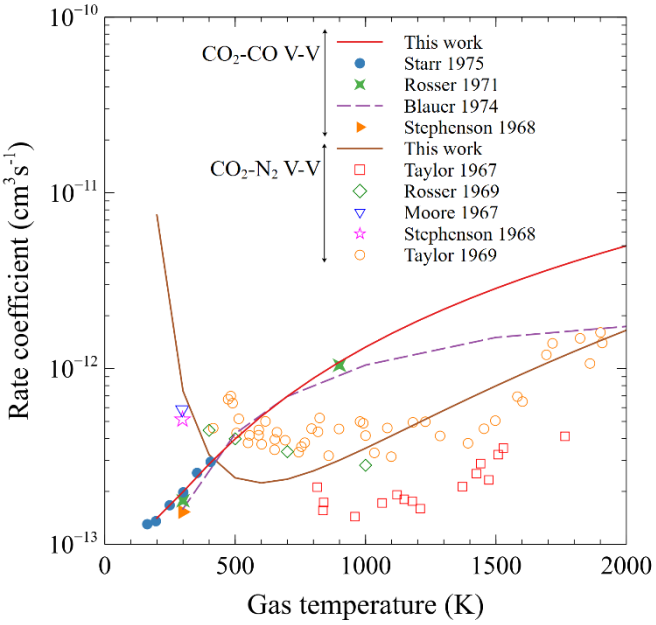

Figure 1: Comparison of the rate coefficients used in this work with experimental data for the near-resonant V-V exchange between the mode v_3 of CO_2 and N_2 and CO, $CO_2(00^01) + N_2/CO(v=0) \rightarrow CO_2(00^01) + N_2/CO(v=1)$.

Only a few vibrational levels of the CO_2 asymmetric stretching mode are considered in the present model ($v_3 \leq 5$) and for simplicity the rate coefficients for the process

$$N_2(w_i) + CO_2(00^0v_i1) \rightarrow N_2(w_f = w_i + 1) + CO_2(00^0(v_f = v_i - 1)1), \quad (8)$$

can be considered with the same value as for the low lying levels ($i.e. w_i = 0, v_i = 1$) as done in [34]. However, in this work, we scale the rate coefficients for the upper levels since they have a noticeable influence on the results, especially the vibrational temperatures, as verified in section IV (cf. Fig. 12). The rate coefficient for the process (6) with $w_i = 0, v_i = 1$, is described by:

$$k(cm^3s^{-1}) = 1{,}66 \cdot 10^{-24} \cdot \exp(a + b \cdot T^{-1/3} + c \cdot T^{-2/3}), \quad (9)$$

where a = 43.8, b = −306 and c = 1288 [148] and is represented in Figure 1. The rate coefficient of the reverse process is calculated from the principle of the detailed balance [136], by multiplying the coefficients of the direct process with the Boltzmann factor, $\exp\left(\frac{-\Delta E}{T_g}\right)$, where T_g is the gas temperature and ΔE the energy difference in K.

To be able to use the SB and SSH theories separately for the scaling of the rate coefficient from [148] (plotted in Fig. 1), we separate it into two parts, one for the long range corresponding to the 'SB part', L_{SB}, and one for the short range corresponding to the 'SSH part', S_{SSH}. To facilitate the scaling of rate coefficients at low and high temperatures with both theories, the function shown in (9) is then split into SSH and SB parts. The sum of these contributions (L_{SB}+S_{SSH}) for the mechanism $N_2(0) + CO_2(00^01) \rightarrow N_2(1) + CO_2(00^001)$ is given in figure 2 to show that we can recover the original

rate coefficient for the process (6) after the fitting procedure. Note that in this case we have a_{SB} = -6.28496, b_{SB} = 379.838, c_{SB} = -1059.2, for L_{SB}, and a_{SSH} = 27.221, b_{SSH} = 10.8178, c_{SSH} = -224.158 for S_{SSH}. We then scale separately the rate coefficients with SB and SSH and add the two contributions to recover the characteristic 'U shaped' curve. All the rate coefficients are given in the Supplementary Information and a comprehensive description of the SSH scaling law can be found in [16].

According to the SB theory and retaining only the terms involving the vibrational levels of CO_2 and N_2 (and not the rotational distributions) for the only non-vanishing contribution, namely the interaction of the N_2 quadrupole moment, Q, with the CO_2 dipole moment, μ, an analytical expression for the probability of the transition (8) is [155]:

$$\frac{k_{v_i,w_i}^{v_f,w_f}}{k_{1,0}^{0,1}} = \frac{\left|< w_f|Q|w_i >\right|^2 * \left|< v_f|\mu|v_i >\right|^2 * I\left(z(\Delta E)\right)}{|< 1|Q|0 >|^2 * |< 0|\mu|1 >|^2 * I\left(z(\Delta E_{10})\right)}, \quad (10)$$

with $k_{1,0}^{0,1}$ the rate coefficient for the forward direction of the transition (1) and $\left|< w_f|\mu/Q|w_i >\right|^2$ the matrix elements of the dipole moment of CO_2 (μ) and quadrupole moments of N_2 (Q). They can be approximated by the harmonic oscillator relation [155]:

$$\left|< w_f = n|\mu/Q\ |w_i = n-1 >\right|^2_{CO_2/N_2} = n * \left|< w_f = 1|\mu/Q\ |w_i = 0 >\right|^2_{CO_2/N_2}, \quad (11)$$

$I(z)$ is the resonance function defined as follows [155]:

$$I(z) = \exp(-z)\,(0.1339 + 01223z + 0.1477z^2 - 0.0283z^3 + 0.0078z^4 - 0.0007z^5), \quad (12)$$

with $z = \Delta E d \left(\frac{M}{2k_B T_g}\right)^{1/2}$ and $\Delta E = \left|E_f - E_i\right|/\hbar$ is the energy mismatch, d is the average of the hard sphere diameters of the two molecules, E_i and E_f the total energies of the initial states and final states, respectively, of CO_2 and N_2, M the reduced mass of the collision pair and ΔE_{10} is the energy mismatch in process (6). By substitution of (11) into (12), we obtain:

$$\frac{k_{v_i,w_i}^{v_f,w_f}}{k_{1,0}^{0,1}} = \frac{w_f * |< 1|Q|0 >|^2 * v_i * |< 0|\mu|1 >|^2 * I\left(w(\Delta E)\right)}{|< 1|Q|0 >|^2 * |< 0|\mu|1 >|^2 * I\left(w(\Delta E_{10})\right)} = k_{1,0}^{0,1} * \frac{w_f * v_i * I\left(w(\Delta E)\right)}{I\left(w(\Delta E_{10})\right)}. \quad (13)$$

The SB theory is only used for near resonant processes as the resonance function, I(w), has a fast decay with increasing ΔE. Considering that the resonance function for values above 50 cm^{-1} provides ~$8 \cdot 10^{-3}$, which leads to rate coefficients below $6 \cdot 10^{-14}$$cm^3s^{-1}$, we used the SB theory only for the processes which fulfil $\Delta E < 50\ cm^{-1}$. A few rate coefficients are given in Figure 3. When $\Delta E > 50\ cm^{-1}$ we only consider the S_{SSH} contribution to the rate coefficient and we scale using the harmonic oscillator.

Our scaling approach is only valid for 300 < T_g < 1000 K as the fitting of L_{SB} and S_{SSH} with expression (9) fails outside of this range. Besides, the V-V transfer involving vibrationally excited N_2 molecules and the bending and symmetric modes of CO_2 is not included in the model as the corresponding rate coefficients are three orders of magnitude lower than the transfer with the asymmetric stretching mode in the gas temperature range of interest [300 K; 1000 K] [156,157].

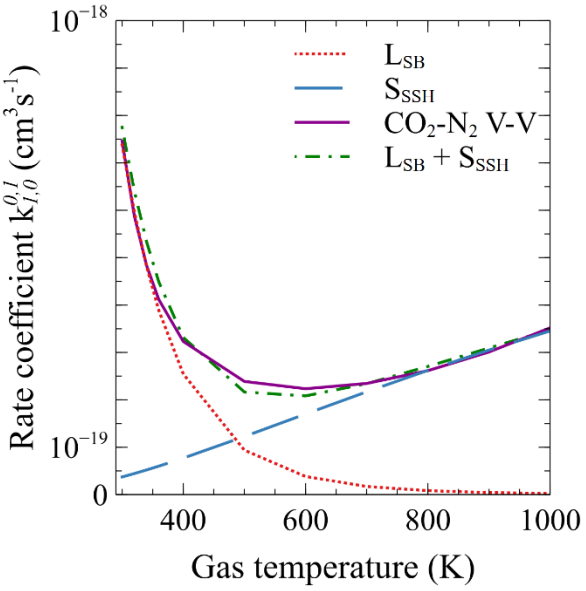

Figure 2: Fitting of the low temperature (⋯) and high temperature ranges (--) of the rate coefficient corresponding to the CO_2-N_2 V-V transfer, $N_2(0) + CO_2(00^01) \rightarrow N_2(1) + CO_2(00^00)$ (—) from [148] and the sum of these two contributions (L_{SB}+S_{SSH}) (-·-).

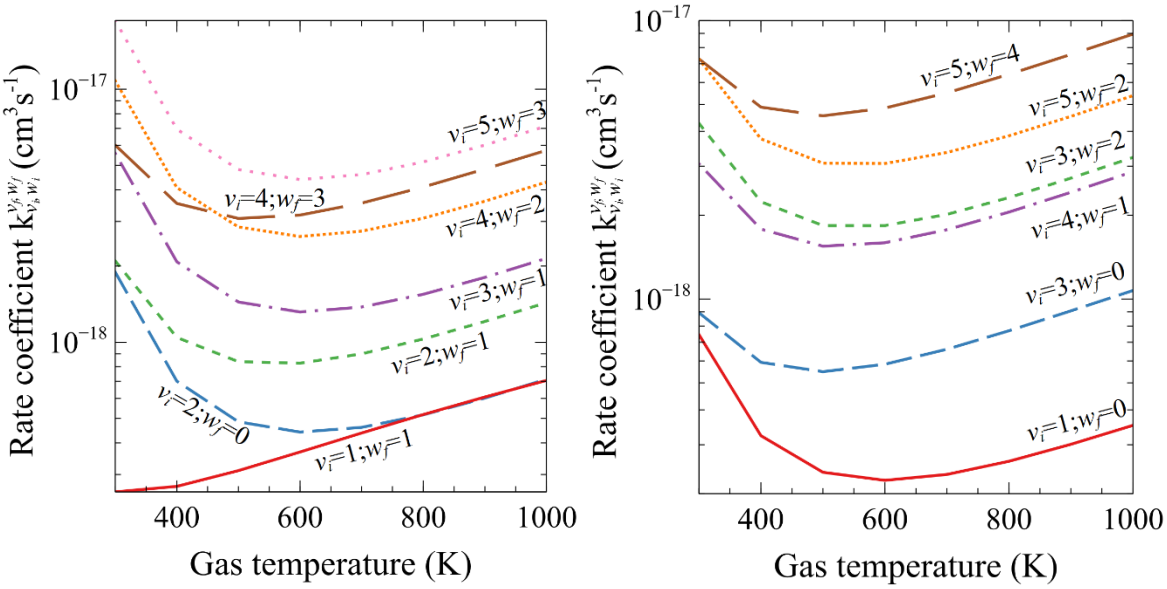

Figure 3: Rate coefficients ($k_{v_i,w_i}^{v_f,w_f}$) of the process $N_2(w_i) + CO_2(00^0v_i1) \rightarrow N_2(w_f = w_i + 1) + CO_2(00^0(v_f = v_i - 1)1)$ scaled with the procedure described in this section as a function of T_g.

III.2.3 N_2-CO V-V exchanges

The V–V exchange $N_2(1)$ + CO(0) → $N_2(0)$ + CO(1) has an equivalent importance to the V–V exchange $N_2(1)$ + $CO_2(00^01)$ → $N_2(0)$ + $CO_2(00^011)$ due to the high density of vibrationally excited CO and N_2 molecules in the plasma, despite a lower rate coefficient. To obtain accurate rate coefficients we use the analytical expression from Kurnosov *et al.* [158] which seems to be a good approximation to experimental and semiclassical rate coefficients for a large range of near resonant vibrational transitions in the N_2–CO system. This expression takes into account short range repulsive and van der Waals forces (first term) as well as quadrupole-quadrupole interaction (second term):

$$k\left(v,u\middle|v-1,u+1;T_g\right)=a\cdot Z\cdot T_g\cdot z(v)\cdot z(u+1)\cdot\exp\left(\frac{\Delta E}{2T_g}\right)\cdot F(y)\cdot F_S+$$

$$\frac{b}{T_g}\cdot Z\cdot z(v)\cdot|\langle u+1|q|u\rangle|^2\cdot\exp\left(\frac{\Delta E}{2T_g}\right)\cdot\exp\left(-\frac{\Delta E^2}{CT_g}\right), \quad (20)$$

with $Z=(\pi\sigma^2)V_M$ the gas kinetic collision rate coefficient, with V_M the average relative translational velocity, $\pi\sigma^2$ the gas kinetic collision cross section. ΔE is defined as $[E_{CO}(u+1)+E_{N_2}(v-1)]-[E_{CO}(u)+E_{N_2}(v)]$ and should be in Kelvin. $z(v)=\frac{v}{1-v\cdot\chi_e}$, with the anharmonicity factor $\chi_{e_{CO}}=0.00612$ and $\chi_{e_{N_2}}=0.00607$ and *F(y)* and the argument of the adiabatic function *y* are defined as (18) and (19). F_S is Shin's factor

$$F_S=\exp\left[\frac{4}{\pi\cdot\sqrt{T^*}}\cdot y^{\frac{1}{3}}+\frac{16}{3\cdot\pi^2\cdot T^*}\right], \quad (21)$$

with $T^*=\frac{T}{\varepsilon_{ST}}$, $|\langle u+1|q|u\rangle|^2$ is the matrix element of the quadrupole moment of N_2 and ε_{ST} is the well depth taken to be equal to the Lennard-Jones potential well depth. The semi-empirical parameters in equation (20) were obtained by fitting the rate coefficients from [159,160] in the temperature range 80 K < T_g < 700 K and assuming that $|\langle u+1|q|u\rangle|^2\approx(u+1)$, $a=6.6\times10^{-8}\,K^{-1}, b=0.04\,K, C=145\,K$. According to [158], the best-fitted interaction length L used in *y* is equal to 0.185 Å. With this value, equation (20) adequately reproduces all the semiclassical data for resonant and non-resonant transitions [158].

The various coefficients are fitted through the exponential expression (9) and the fitting parameters can be found in the Supplementary Information. In Figure 4, we represent the rate coefficients obtained in this work following the procedure from Kurnosov *et al.* [158] for the process $N_2(1)$ + CO(0) → $N_2(0)$ + CO(1) as a function of the gas temperature. Figure 4 shows as well the rate coefficients calculated using a mixed quantum-classical method by Hong *et al.* [161], a fitting of experimental data from Sato *et al.* [162] found in a survey of vibrational relaxation rate coefficients from Blauer & Nickerson [148], calculated by Shin [163] and other rate coefficients determined experimentally by Zittel & Moore [164], Stephenson & Mosburg [165], Starr *et al.* [166], Allen & Simpson [159] Green & Hancock [167] and Mastrocinque *et al.* [160] and found a good agreement with the experiments. Our rate coefficients are valid for T_g < 1000 K. For higher gas temperatures the Quantum-classical rate coefficients calculated by Hong *et al.* [161] should be used instead, as they are in good agreement with the experimental data from Sato *et al.* [162] (not shown here) measured for T_g > 1600 K.

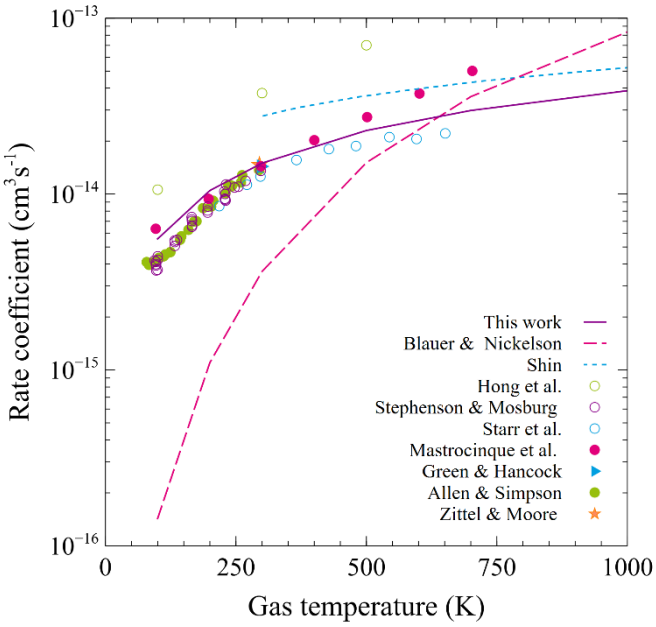

Figure 4: Comparison of the rate coefficients used in this work (—) with experimental data (symbols), fitting at high T_g (— —) and calculation (--) for the near resonant VV exchange between N_2 and CO, $N_2(1) + CO(0) \rightarrow N_2(0) + CO(1)$.

III.2.4 M(*v*)-M' V-T

The rate coefficients for the V-T relaxation from level *v* to *v*-1 of N_2 by collision with CO are obtained following the work of Plonjes *et al.* [168]. For the $N_2(v)$-N_2 V-T, the expressions recommended in [95,115,130] were favoured in the present paper as they lead to rate coefficients in a good agreement with the semiclassical calculations from [131,132] in the range 300 K < T_g < 1000 K. Vibrational dissociation by V-T processes is included as a transition from the last bound vibrational level of N_2 (v = 59 here) to a pseudo-level in the continuum as done in [95,102,130] for N_2 and originally for H_2 in [169]. Note that, Terraz *et al.* [34] extended the applicability to temperatures in the range [200 K; 300 K] compared with the rate coefficients previously used in [95,115,130]. To do so the results from the semi-classical model of [131,132] available only for a few temperatures in the range [200 K ; 8000 K] were fitted as a function of the gas temperature and over two different temperature regimes, according to the exponential form (9). All the details for the determination of the $N_2(v)$-N_2/CO_2 rate coefficients using this procedure can be found in [34] as well as all the necessary coefficients to calculate the rate coefficients until v = 20 for N_2 (supplementary appendix).

For the other M(*v*)-M' V-T rate coefficients we scale them according to the theoretical dependences from the SSH theory on the vibrational levels and gas temperature, as done in [95] for $N_2(v)$-O_2 and in [34] for $N_2(v)$-CO_2 energy transfers, calculated from the V-T $N_2(v)$-N_2. To illustrate this method, the rate coefficient $k_{v,v-1}$ (N_2) for deactivation of a vibrational level of CO by N_2, corresponding to the process CO(v) + N_2 → CO(v-1) + N_2, is estimated from the rate coefficient for the relaxation of CO due to CO(v)-CO collisions, $k_{v,v-1}$ (CO) [38,170].

$$k_{v,v-1}(N_2)(T_g) = C_{radius} \times C_{mass} \times k_{v,v-1}(CO)(T_g) \times \frac{F\left(Y_{v,v-1}^{CO-N_2}\right)}{F\left(Y_{v,v-1}^{CO-CO}\right)}, \quad (14)$$

$$C_{radius} = \left(\frac{r_{CO-N_2}}{r_{CO-CO}}\right)^2 \; where \; r_{i-j} = \frac{1}{2}(r_i + r_j), \quad (15)$$

with r_i the diameter of the molecule i in the hard sphere collision model

$$C_{mass} = \left(\frac{\mu_{CO-N_2}}{\mu_{CO-CO}}\right)^{\frac{1}{2}}, \quad (16)$$

where $\mu_{i-j} = \frac{m_i \times m_j}{m_i + m_j}$ is the reduced mass of the collision and m_i the mass of molecule i.

F(y) is the adiabacity function given by

$$F(y)\begin{cases} \frac{1}{2}\left[3 - e^{\frac{2y}{3}}\right] e^{-\frac{2y}{3}}, y < 21.622 \\ 8\left(\frac{\pi}{3}\right)^{\frac{1}{2}} y^{\frac{7}{3}} e^{-\frac{2y}{3}}, y \geq 21.622 \end{cases}, \quad (17)$$

with *y* the adiabacity factor

$$y_{v,v-1} = \Delta E_{v,v-1} \times \left(\frac{\pi L}{\hbar}\right) \times \sqrt{\frac{\mu}{2k_B T_g}}, \quad (18)$$

with $\Delta E_{v,v-1}$ the energy difference between the vibrational levels *v* and *v*-1 of N_2, k_B the Boltzmann constant, T_g the gas temperature and L is the 'interaction length' calculated from the expression [16]:

$$L = \frac{1}{\frac{17.5}{r_0}}, \quad (19)$$

with r_0 the Lennard Jones potential distance from [171]. The same approach was adopted in our previous work [38] for CO(*v*)-M (M=CO_2, O_2) using the rate coefficient from CO(v)-CO V-T and CO_2(*v*)-M' (M'=CO, O_2) using the rate coefficient from CO_2(v)-CO_2 V-T.

III.3 Surfaces processes

An important process in the vibrational kinetics, in our experimental conditions, is the deactivation of vibrationally excited CO_2, CO and N_2 molecules through collisions at the reactor wall. This deactivation of vibrationally excited states is shown to have a significant influence on the vibrational characteristic temperatures, especially for pressures below 1 Torr [38,172]. Due to the lack of experimental values, we set the same value of deactivation probability, γ_v, for any mode of CO_2 i.e. $\gamma_v(CO_2(v>0)) = 0.2$ for a Pyrex surface (average value from Table 1 of [173]) where the CO_2 molecule is assumed to deactivate to the vibrational ground state. We use a constant value of $4 \cdot 10^{-2}$ for the deactivation probability for all levels of CO and $4.9 \cdot 10^{-4}$ for the deactivation probability for all levels of N_2 both taken from [173]. As opposed to CO_2, we consider single-quantum transitions for CO and N_2 as done for N_2 and O_2 in [95], where only one vibrational quantum is lost upon collision with the wall. We also investigate the impact of changing the deactivation probability for the bending, symmetric stretch and mixed modes of CO_2, from 0.2 to 0.05, on the vibrational temperatures (cf. Section (IV.1, Fig. 9 and 10). Note that the gas mixture might influence the wall de-excitation probability of vibrationally excited molecules. For instance, a linear enhancement of the $N_2(v)$ wall deactivation probability from $1.3 \cdot 10^{-3}$ to $2.6 \cdot 10^{-3}$ with an increase in the admixture of CO_2 (from 0.066 % to 0.5 %) in a low-pressure N_2 plasma was observed for a Pyrex surface [174].

The importance of the CO_2-O V-T exchanges calls for a verification of the accuracy of the calculation of the atomic oxygen concentration. In turn, the loss of O atoms is mainly controlled by recombination at the walls to form O_2 molecules characterized by the wall O loss/recombination probability, γ_O. In this study, γ_O is assumed to remain constant for the different mixture compositions, equal to the probability measured in pure CO_2 [89] as a function of pressure and at 50 mA (cf. Table 1). Changes in γ_O are not expected to significantly modify the CO_2 dissociation fraction, as shown in

[38,175], but could lead to an increase/decrease in O atom fractions affecting the vibrational temperatures because of the strong CO_2-O V-T deactivation. It is known that the recombination probability depends on the nature of the gas ignited in the reactor [89,176]. In CO_2-N_2 plasmas, CO molecules, C and N atoms or even CO_2 molecules are likely to be chemisorbed or physisorbed on the reactor walls, changing the surface configuration and competing for the adsorption sites with O atoms limiting the recombination into O_2. The possibility of CO adsorbed at the walls was already suggested by Cenian *et al.* [177] where the rate for the O recombination at the wall is assumed to depend on the CO concentration in the gas phase (see reaction 11 in Table 3.1 of [177]). We thus expect γ_O to be lower for a CO_2-N_2 plasma than for a pure O_2 plasma. However, at present it is difficult to draw any conclusions on the values of γ_O in CO_2-N_2 with regards to the pure CO_2 case.

IV. Results

IV.1 Model validation

In this section, the results of our model are compared with experimental data measured in a CO_2-N_2 DC discharge for pressures between 0.6 and 4 Torr and a current of 50 mA. The calculated reduced electric field, vibrational temperatures, atomic oxygen and NO fractions and CO_2 dissociation fraction are compared with the ones obtained experimentally. For completeness, tables with the calculated concentrations of all the species considered in the model are given in the Supplementary Information for a few selected conditions.

The model shows a satisfactory quantitative agreement and reproduces very well the dependencies of the measured quantities for different pressures and initial CO_2 fractions in the different CO_2-N_2 mixtures. Once validated against the benchmark experiments, the model is used for the interpretation of the measured quantities and the identification of the main processes ruling the discharge.

In Figures 5 and 6 we represent E/N and [O]/N, respectively, as a function of pressure for a pure CO_2 plasma and for a CO_2-N_2 plasma with a ratio of 1:1. A decrease of E/N with increasing pressure can be observed in experiments and simulations for pure CO_2 and for the mixture. There is, in general, a quite good agreement between the model predictions and the experimental values, although the absolute value of E/N is somewhat overestimated in the calculations at the low pressures, especially for the pure CO_2 discharge. A maximum of [O]/N around 1 Torr can be observed in experiments and simulations for pure CO_2 which is mostly due to the O loss frequency showing a minimum at 1 Torr [89]. However, the maximum of experimental [O]/N seems to be shifted for CO_2-N_2 which is not reproduced in the simulations. Since the simulations consider the same recombination probability for atomic oxygen at the wall via $O + wall \xrightarrow{\gamma_O} O_2$, γ_O, for pure CO_2 and for the CO_2-N_2 mixture (cf. section III.2.5), the results suggest that the dependence on pressure of γ_O might be different in the CO_2-N_2 mixtures than in pure CO_2. To investigate the importance of this quantity on the [O]/N simulation results, we multiply by two the γ_O and the resulting [O]/N are given in Figures 6 and 7.

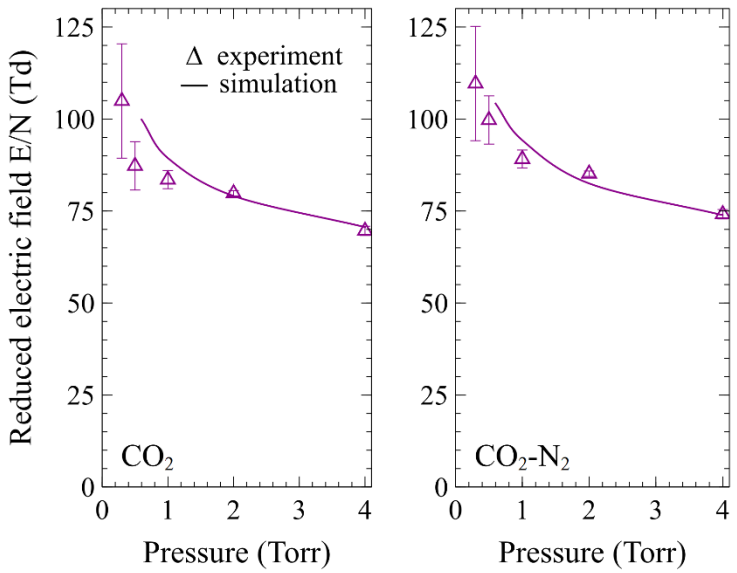

Figure 5: Reduced electric field E/N as a function of pressure for pure CO_2 (left) and a 50/50 CO_2-N_2 mixture, at a current of 50 mA: experiment (Δ) and model calculations (—).

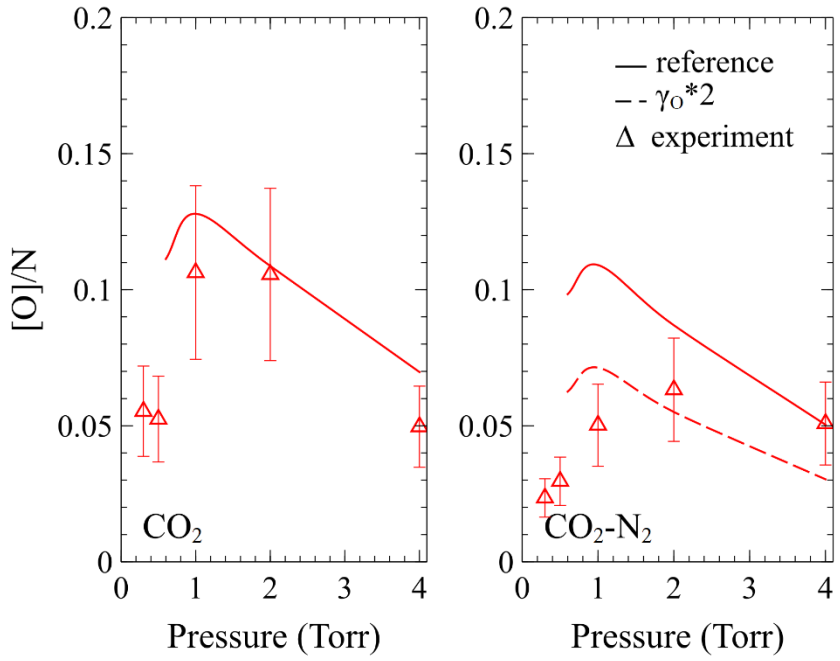

Figure 6: Atomic oxygen fraction, [O]/N, as a function of pressure for pure CO_2 (left) and a 50/50 CO_2-N_2 mixture, at a current of 50 mA: experiment (Δ), model calculations with the default γ_O values from [89] (—) and γ_O values multiplied by two (– –).

Figure 7 shows the measured and calculated values of the reduced electric field, E/N, and the atomic oxygen fraction, [O]/N, as a function of the CO_2 initial fraction for a discharge current of 50 mA, at 2 Torr. Overall, the self-consistently calculated reduced electric field variation with the CO_2 initial fraction agrees well with the experimentally measured E/N. These results prove that the ionization rates and ion chemistry (transport and charge exchange) are well characterized and that the model can be used as a predictive tool when no experimental data for E/N are available. The atomic oxygen fraction, [O]/N, also shows a proper trend with the CO_2 fraction but remains too high for all conditions except for the pure CO_2 case. One possibility to justify this discrepancy would be a too strong O_2 dissociation by electron impact associated with Phelps cross section, as suggested by

several authors [178,179] and further discussed in [38,111]. The agreement could be improved by using Polak's cross section for O_2 dissociation by electron impact [180] as discussed in [38] in the context of CO_2-O_2 plasmas. Another possibility would be a larger recombination probability at the wall for the different mixtures in comparison to the pure CO_2 case. A dependence of γ_O on the CO_2 fraction in the different CO_2-N_2 mixtures seems plausible, as discussed in section III.2.5. Upon multiplying γ_O by two, we can observe that [O]/N decreases by 24 % and 38 % for CO_2 initial fractions of 0.1 and 0.9 respectively, leading to a [O]/N too low for CO_2 fractions higher than 0.25 and too high for CO_2 fractions below. From this analysis it can be inferred that [O]/N is very sensitive to the recombination probability of atomic oxygen γ_O at the wall and that to obtain a good agreement between the simulations and experiment the γ_O should increase with the N_2 fraction.

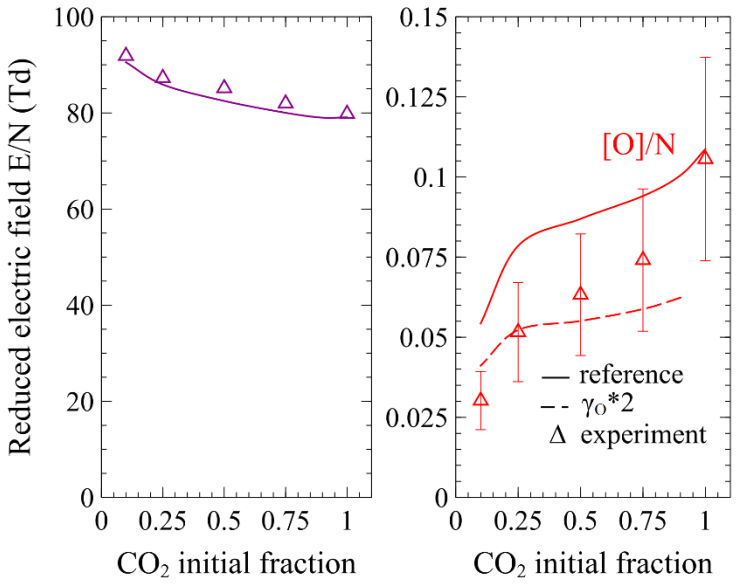

Figure 7: Measured and calculated reduced electric field, E/N, and atomic oxygen fraction, [O]/N, of a CO_2-N_2 discharge as a function of the CO_2 fraction in the initial mixture, at 2 Torr and 50 mA: from experiment (Δ) and model calculations with the default γ_O values from [89] (—) and γ_O values multiplied by two (– –).

Our state-to-state model also provides the populations of each individual vibrational levels of the different modes of CO_2 and of CO and N_2. The vibrational temperature is then calculated assuming a Treanor distribution [90], as:

$$T_{v,ij} = \left(\frac{E_1}{\ln(p_i/p_j) - \frac{E_j - E_i - E_1}{k_B T_g}} \right) / k_B, \qquad (24)$$

where E_1 is the energy of the first level, p_i and p_j and E_i and E_j are the population and energy of levels i and j, respectively, T_g is the gas temperature and k_B the Boltzmann constant. We use an average of the temperatures calculated using the first three vibrational levels. Note that for the specific case of the CO_2 bending mode corresponding to v_2, we assume a Boltzmann distribution to obtain the vibrational temperature T_2 (see equation 5 in [99]). Moreover, for simplicity in the presentation of the results, we define a common temperature of the bending and symmetric stretching modes denoted $T_{1,2}$ [33,89] which is enough for a simple description of the vibrational kinetics even though this is not imposed in the model [38].

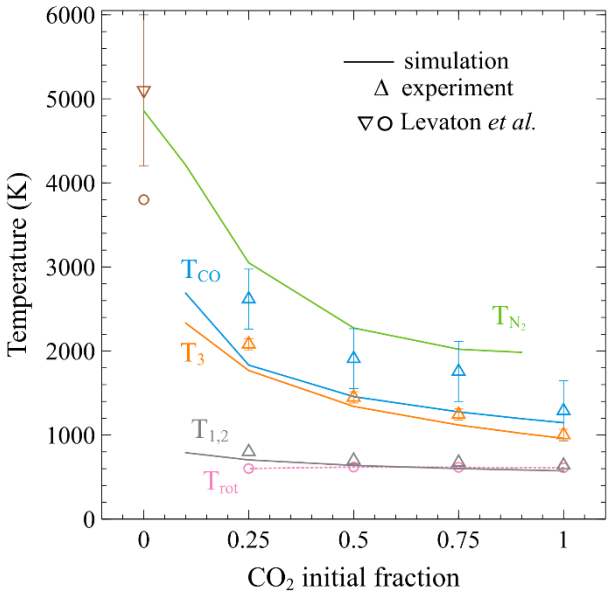

Figure 8: Experimental values (Δ) and calculated values (line) of the common vibrational temperature of the CO_2 bending and symmetric modes $T_{1,2}$, the vibrational temperature of the asymmetric stretching mode T_3, the CO and N_2 vibrational temperatures T_{CO} and T_{N2} and the rotational temperature T_{rot} (o) (used as input parameter for the model) when a discharge is ignited in different mixtures of CO_2-N_2, at 50mA, and a pressure of 2 Torr.

Figure 8 shows the vibrational temperatures of CO and of the different modes of CO_2 obtained from the model and experiment as well as the experimental rotational temperature T_{rot} used as input parameter for the model and the calculated vibrational temperature of N_2 as a function of the CO_2 initial fraction. Note that the vibrational temperatures are calculated with expression (24) using the very first points (v=0, 1 and 2) of the vibrational distributions (see Fig. 11). All the vibrational temperatures increase with the N_2 content. This trend can be partly explained by the reduced quenching of vibrations of CO_2/CO/N_2 by O atoms as [O]/N decreases with decreasing the CO_2 initial fraction (cf. Fig. 7). Indeed, O atoms are very efficient quenchers of the CO_2 vibrations as already discussed in section III.2.5. Besides, the vibrational deactivation of N_2 also takes place essentially by V-T deactivation with O atoms and to a lesser extent through the Zel'dovich reaction forming NO, as also shown in [95]. Note that, the CO_2-N_2 V-V and CO-N_2 V-V transfers play a major role to explain the trends observed and this is discussed in more details at the end of the section (Fig. 12). The rotational temperature T_{rot} remains almost constant with N_2 addition as already observed in [70]. The temperature $T_{1,2}$ is very close to T_{rot}, as expected from the small energy difference between levels of symmetric and bending modes that favours the V-T deexcitation. The V–V up pumping and CO_2-N_2 V-V mechanism produce important concentrations of vibrationally excited states of CO_2 in the asymmetric stretch mode. The large energy difference between the asymmetric stretch mode levels of CO_2 and the anharmonic V-V up pumping and CO_2-N_2 V-V transfers are beneficial to reach high concentration of vibrationally excited CO_2. However, part of the energy stored in ν_3 is lost through the intermode V-V transfer ($CO_2(\nu_3)+CO_2(\nu_{1,2}) \rightarrow CO_2(\nu_3-1)+CO_2(\nu_{1,2}+1)$), and through quenching by O atoms. T_{CO} systematically showing larger values than T_3 for all the conditions reported can be explained by different rate coefficients for V-T relaxation, the lack of inter-mode V-V relaxation processes for CO, and more efficient vibrational excitation through electron-to-vibrational energy transfers for CO [38,89]. Finally, T_{N2} is higher than T_{CO} and two main reasons can be evoked. First, the quenching of vibrationally excited molecules by O atoms is more efficient for CO than N_2. Indeed, the rate coefficient included in this work for the N_2-O V-T, as described in [22, 53], is at least 10 times lower than for CO [38,136] in the temperature range [300 K;1000 K]. Second, the deactivation of vibrationally excited states at the wall is more important in the case of CO than N_2 as the deactivation probability is two orders of magnitude lower for N_2 (cf. section III.2.5).

The calculated and measured vibrational temperatures of N_2 obtained for a flowing DC glow discharge in pure N_2 by Levaton *et al.* [181] are given on Fig. 8 as an indicator since we do not have

access to experimental values for T_{N2} with FTIR spectrometry. The experimental conditions are very similar to the ones used in the present work in terms of current, radius of the glass tube, pressure, and type of discharge. The main difference comes from the flow with a rate around 10 times higher in [181]. Since the T_{rot} obtained by FTIR does not change for the different mixtures studied in this work (cf. Fig. 10), we use the same for the pure N_2 simulation. The T_{N2} calculated with our model is in very good agreement with the data point obtained in [181] by Optical Emission Spectroscopy, but higher than the value calculated using the state-to-state kinetic model from the same author [181]. To further validate the vibrational kinetics in CO_2-N_2 plasmas, future measurements (similar to what was done in [75]) require the detection of the vibrational temperature of N_2.

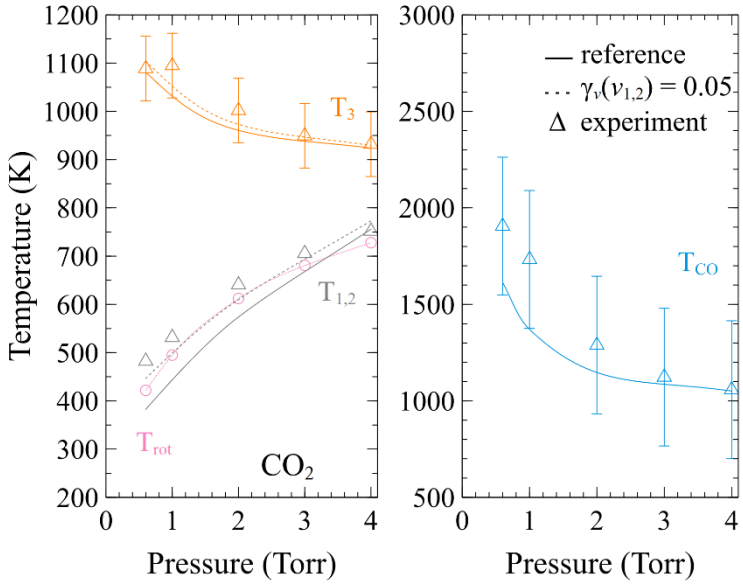

Figure 9: Experimental values (Δ) and calculated values (line) of the common vibrational temperature of the CO_2 bending and symmetric modes $T_{1,2}$, the vibrational temperature of the asymmetric stretching mode T_3, the CO and N_2 vibrational temperatures T_{CO} and T_{N2} and the rotational temperature T_{rot} (o) (used as input parameter for the model) when a discharge is ignited in pure CO_2, at 50mA, as a function of pressure. The model calculations were done including with the default probabilities of deactivation of the vibrationally excited states of CO and N_2 and the different modes of CO_2, at the wall from section IV.6. (—) and $\gamma_v(v_{1,2}) = 0{,}05$ (···)

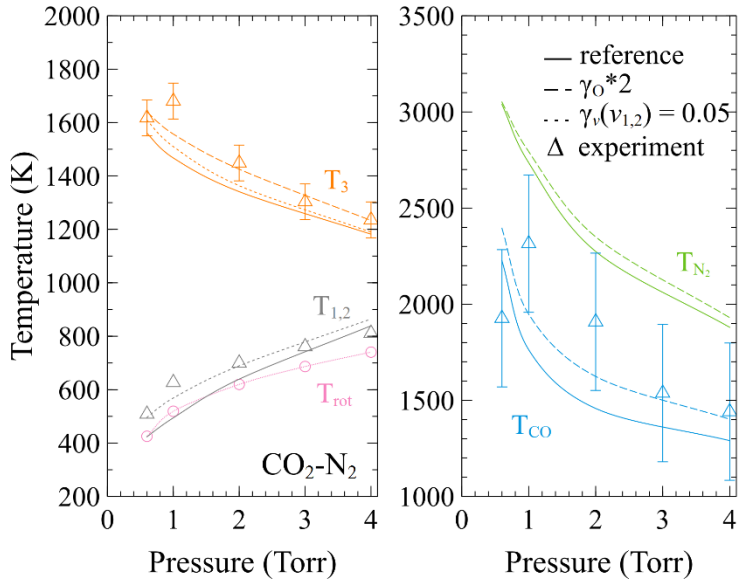

Figure 10: Experimental values (Δ) and calculated values (line) of the common vibrational temperature of the CO_2 bending and symmetric modes $T_{1,2}$, the vibrational temperature of the asymmetric stretching mode T_3, the CO and N_2 vibrational

temperatures T_{CO} and T_{N2} and the rotational temperature T_{rot} (o) (used as input parameter for the model) when a discharge is ignited in CO_2-N_2 (50 % of each) at 50mA, as a function of pressure. The model calculations were done including with the default probabilities of deactivation of the vibrationally excited states of CO and N_2 and the different modes of CO_2, at the wall from section IV.6. (—), $\gamma_v(v_{1,2}) = 0{,}05$ (···) and multiplying the default γ_O values from [89] by two (– –).

Figures 9 and 10 show the vibrational temperatures of CO and of the different modes of CO_2 obtained from the model and experiment as well as the experimental rotational temperature T_{rot} used as input parameter for the model and the calculated vibrational temperature of N_2 as a function of pressure for pure CO_2 and a CO_2-N_2 mixture with 50 % CO_2, respectively. The increase of T_{rot} with the pressure can be explained by the higher power dissipated in the plasma because of the higher voltage (and therefore power) required to maintain the current as the pressure is increased. The exact mechanisms responsible for the conversion of electrical energy into gas heating are complex, but include enhanced V-T transfers at higher pressure and possible exothermic reactions [35,70,99]. The influence of deactivation of vibrationally excited CO_2 and CO at the walls, described in section III.2.5., is illustrated in Figure 9 for the case of pure CO_2 and Figure 10 for the CO_2-N_2 mixture. Including the wall deactivation for vibrationally excited CO_2, CO and N_2 molecules mostly affects the vibrational temperatures of these molecules at lower pressures as observed in [38,172]. The default deactivation probabilities of the different modes of CO_2 are 0.2 (Section III.2.5.) and lead to simulated $T_{1,2}$ values lower than in the experiment. The results labelled $\gamma_v(v_{1,2}) = 0.05$ correspond to simulations with a deactivation probability for the bending, symmetric stretch and mixed modes of CO_2 of 0.05, instead of 0.2, as proposed for pure CO_2 in [38] and lead to a better agreement of the calculated $T_{1,2}$ with experiment. Since no experimental values for the wall deactivation probability (on Pyrex) of the bending mode of CO_2 was reported in the literature to our knowledge, the present results suggest a value for $\gamma_v(v_{1,2})$ smaller than for $\gamma_v(v_3)$. Finally, we observe that T_{CO} and T_3 increase upon multiplying the γ_O by two as a consequence of the reduced deactivation through V-T with O. Note that for readability of the figure we do not represent this case for $T_{1,2}$ as it changes by a maximum of 3 % only.

The vibrational distribution functions (VDFs) of the asymmetric stretch mode of CO_2, and bending mode of CO_2, of N_2 and CO, calculated for a DC glow discharge operating at 2 Torr for different CO_2-N_2 gas mixtures are represented in Figure 11. The simulations evince a remarkable deviation from equilibrium for N_2 and CO, and to a lesser extent for CO_2, emphasizing the importance of detailed state-to-state models to understand the vibrational energy transfers taking place in the system, as already pointed out in [54]. To maintain this non-equilibrium, the gas temperature must be kept low to suppress the quenching of vibrations. Indeed, V-T relaxation poses an inherent loss mechanism of vibrational energy and increases the gas temperature, which in turn enhances the V-T relaxation creating a positive feedback loop between gas heating and quenching [8]. The VDFs for 90 % and 75% of CO_2 are only represented for the asymmetric stretch of CO_2 for readability of the figure as they almost overlap with each other in the other cases.

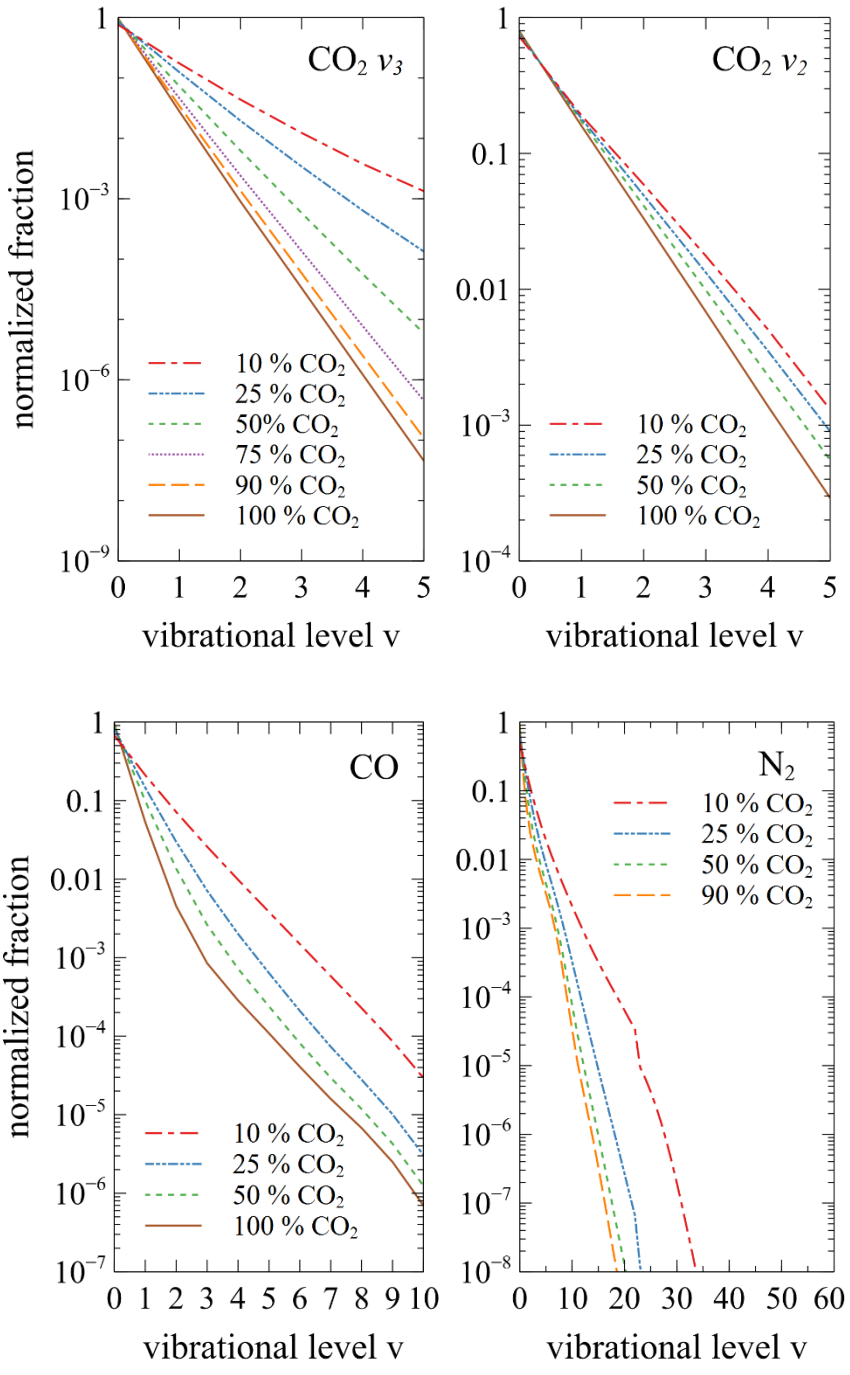

Figure 11: Vibrational distribution functions of the asymmetric stretch mode of CO_2 (v_3), bending mode of CO_2 (v_2), of N_2 and CO, calculated for a DC glow discharge operating at 2 Torr and I = 50 mA for different CO_2-N_2 gas mixtures.

It is well-known that an important part of electron energy is transferred into the vibrational excitation of CO_2, CO and N_2, in the range of E/N between 1 and 100 Td [172,182]. This emphasizes the necessity of having a correct description of the vibrational energy transfers between these species. In particular, it is expected that near resonant CO_2-N_2 and CO-N_2 transfers may have an impact shaping the VDFs. To quantify the importance of these transfers, we removed them from the simulations and checked the changes in the vibrational temperatures. The vibrational temperatures T_3, T_{CO} and T_{N2} are represented as a function of the CO_2 initial fraction in Figure 12. We can notice that without the CO_2-N_2 V-V transfer T_3 is almost constant, and far from experimental values, for all the mixtures considered and the same can be said for T_{CO} and the CO-N_2 V-V transfer. In the case of T_{N2} both transfers are also playing a significant role but the increase of T_{N2} with decreasing the CO_2 initial

fraction also comes from the enhancement of the electron-impact excitation of vibrations of N_2 as the fraction of N_2 increases in the mixture.

The scaling of CO_2-N_2 V-V, according to the Sharma Brau theory, explained in detail in section III.2.2., also influences T_3 and T_{N2}. Therefore, we represent these vibrational temperatures as a function of the CO_2 initial fraction keeping the rate coefficient for the CO_2-N_2 V-V as represented in Figure 1 regardless of the vibrational levels involved (no SB scaling) and scaling this rate coefficient (reference). From this examination it can be concluded that the increase of T_3 with N_2 is mostly due to the CO_2-N_2 V-V and similarly for T_{CO} with CO-N_2 V-V. Both processes (and the SB scaling) significantly improve the agreement between the simulations and experiment for T_3 and T_{CO} further conveying the importance of including these processes in the model.

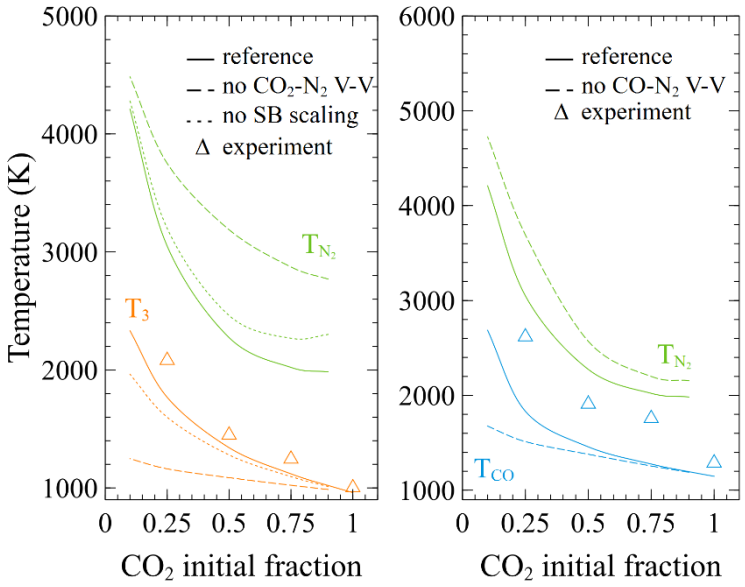

Figure 12: Experimental values (Δ) and calculated values (line) of the common vibrational temperature of the CO_2 of the asymmetric stretching mode T_3, the CO and N_2 vibrational temperatures T_{CO} and T_{N2} as a function of the CO_2 initial fraction, at 50mA. The model calculations were done excluding (– –), including the CO_2-N_2 V-V transfer with (—) and without scaling (···) (left) and including (—) and excluding (– –) the CO-N_2 V-V transfer (right). The error bars are not represented here but are the same as in Fig. 13.

IV.2 Effect of N_2 on CO_2 dissociation

In this section the beneficial effect of admixture of N_2 on the CO_2 dissociation, already observed experimentally and by modeling in [34,68,70,71,183], is investigated. Several reasons can be assigned to this effect. For instance, the enhancement of the reduced electric field, the effect of electronically excited states on the CO_2 dissociation directly or via changes of the EEDF, the vibrational excitation of nitrogen and its transfer to the CO_2 asymmetric stretching mode and the dilution with N_2 limiting the influence of back reaction mechanisms are possibilities often advanced [8,66,172].

Figure 13 shows the absolute (α) and effective (α_{eff}) CO_2 dissociation fraction as a function of the CO_2 initial fraction at 2 Torr. The latter takes into account the initial fraction of CO_2 in the gas mixture (for instance, when only 10 % CO_2 is present in the gas mixture, the absolute conversion needs to be multiplied by a factor 0.1). The increase of the absolute CO_2 dissociation fraction, α, (cf. equation 1) with N_2, both in the experimental data and the calculations, indicates that N_2 has a beneficial effect on CO_2 splitting. Dissociation fractions up to 70 % are observed, a very encouraging result considering that the present setup is designed for fundamental studies only. However, it might be more relevant to use the effective dissociation instead as it takes into account the initial fraction of CO_2 in the gas mixture. The effective CO_2 conversion decreasing linearly when adding N_2 can be explained by the lower CO_2 fraction in the mixture, which compensates the enhancement of the absolute conversion of CO_2 in the presence of N_2. the decrease of α_{eff} was already observed in the simulations of an unpacked

DBD reactor [183] and of a MW discharge [68]. Note that no significant dissociation of N_2 was observed for all the simulations conducted (below 0.05 %).

Overall, a good agreement is obtained between the experimental and calculated trend for the CO_2 dissociation even when reactions (20)-(23) (cf. section III.1.1) are not included in the simulations (reference case).

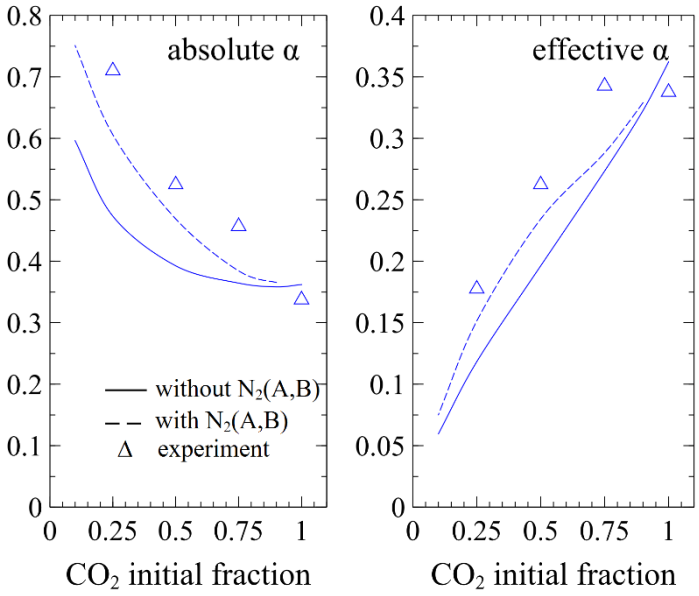

Figure 13: Absolute and effective dissociation fraction for different CO_2/N_2 mixtures for a discharge current of 50 mA and a pressure of 2 Torr. The curve labelled 'with N_2(A,B)' corresponds to the reference case to which we added the processes from Tables 2 and 3.

The agreement is further improved when the dissociative quenching processes with the two metastable states, N_2(A) and N_2(B), are included in the model, as described in section III.1.1. Indeed, these states open a new CO_2 dissociation channel and are claimed to be responsible for the increase of α in the presence of N_2 by several authors [63,66,71,120,121,129,183]. As can be seen in Figure 13, adding these processes noticeably improves the absolute value and trend of the CO_2 dissociation fraction. This shows that the dissociation of CO_2 molecules in collisions with electronically excited states of N_2 gives a substantial contribution to the conversion rate. We have verified that considering the CO_2 dissociation by N_2(A) does not change appreciably the results, which shows that N_2(B) is the main contributor. It is worth pointing out that the dissociation fraction is also increasing when these processes are not accounted for, suggesting that other phenomena are also responsible for the beneficial effect of N_2 on the dissociation of CO_2.

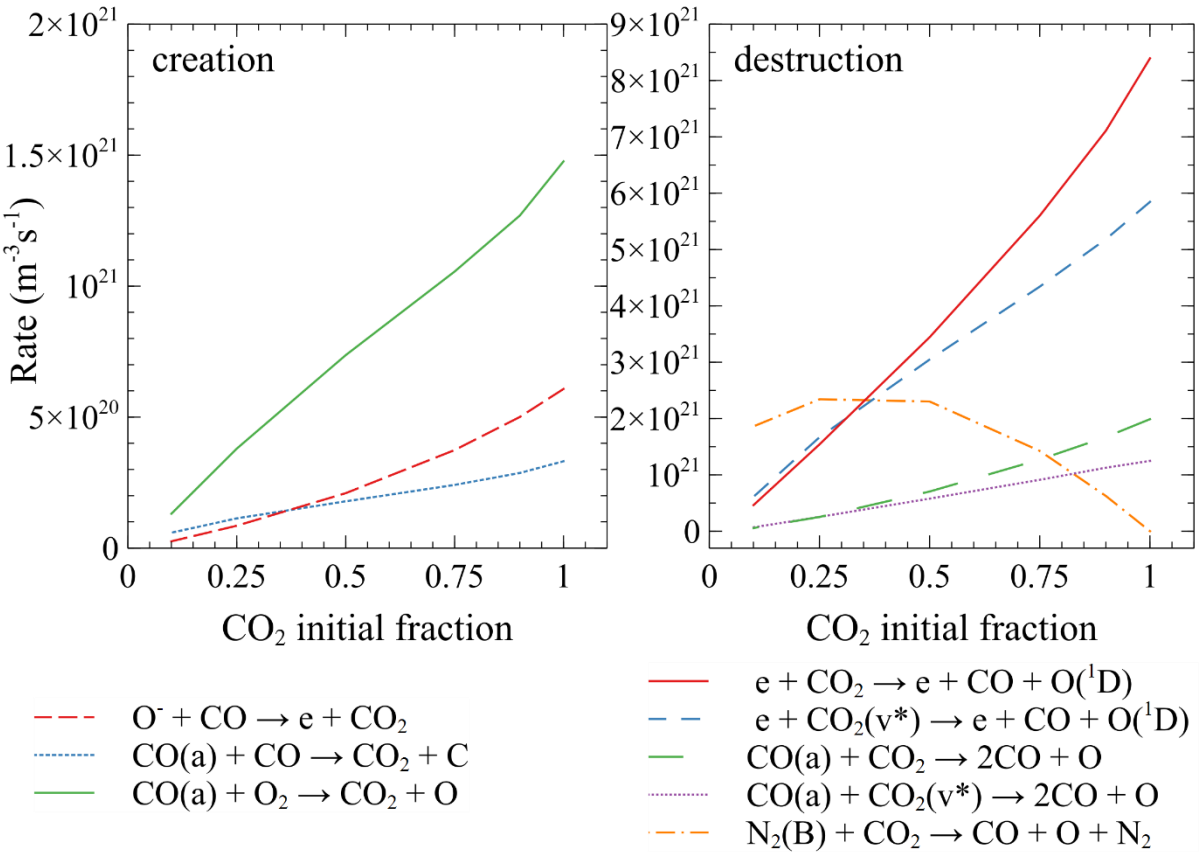

Figure 14: Rate of the most important creation (left) and destruction (right) processes of CO_2, as a function of CO_2 fraction in the CO_2-N_2 gas mixture, at 2 Torr.

To explain the trend of the CO_2 dissociation fraction with the addition of N_2, we plot in Figure 14 the rates of the most important creation and destruction processes of CO_2, as a function of the CO_2 initial fraction for P = 2 Torr and I = 50 mA. In the system under study, CO_2 can be decomposed by direct electron impact, both on molecules in the vibrational ground-state (GS) and in vibrational excited states (VES), noted $CO_2(v^*)$, through $e + CO_2 \rightarrow CO + O(^1D)$. The contribution of the vibrational states comes mainly from the lower-laying levels (01^101), (02^201), (10^002) and (00^011). For high N_2 content, corresponding to a higher vibrational temperature of the asymmetric mode of CO_2 (cf. Fig. 10), the electron-impact dissociation on the VES surpasses the one from the GS. However, this does not have any impact on the CO_2 dissociation fraction because overall the rates of electron impact from GS and VES decrease with the N_2 content due to the decrease of CO_2 density and rate coefficient (cf. discussion of figure 15 concerning the EEDF).

At high N_2 fractions, the contribution of CO_2 dissociation in quenching collisions with $N_2(B)$ via:

$$N_2(B) + CO_2 \rightarrow CO + O + N_2, \quad (25)$$

even exceeds that of dissociation of CO_2 molecules by electron impact. However, this is accompanied by a lower CO_2 content in the mixture, leading to a drop in effective CO_2 conversion (Fig. 13). Above 75% N_2, both the electron-impact dissociation and the dissociation by N_2 metastable molecules rates decrease due to the lower CO_2 concentration, which is not compensated by the higher N_2 concentration (and thus higher dissociation by N_2 metastable molecules). In addition, for small O_2 and CO concentrations, CO_2 dissociation can be stimulated through:

$$CO(a^3\Pi_r) + CO_2 \rightarrow 2\,CO + O. \quad (26)$$

The importance of these two mechanisms shows that despite their low density, electronically excited species can have a large influence on the overall plasma chemistry. The calculated densities of these electronically excited states are given in the Supplementary Information for several conditions. We observe that both the calculated $N_2(A)$ and $N_2(B)$ densities increase with the N_2 content, going from $1.45 \cdot 10^{16}$ m^{-3} and $1.55 \cdot 10^{15}$ m^{-3} at 90 % CO_2 to $1.6 \cdot 10^{18}$ m^{-3} and $6.9 \cdot 10^{16}$ m^{-3} at 10 % CO_2, respectively for $N_2(A)$ and $N_2(B)$ while the CO(a) density remains relatively constant ($3.85 \pm 0.3 \cdot 10^{16}$ m^{-3}) for the different mixtures, at 2 Torr and 50 mA. Even though the density of $N_2(A)$ is always, at least, one order of magnitude higher than $N_2(B)$, the same process as (25) but involving $N_2(A)$ contributes to less than 0.2 % of the CO_2 dissociation for all conditions represented in Fig. 14.

Concerning the creation of CO_2, the electronically excited state $CO(a^3\Pi_r)$, noted CO(a) thereafter, promotes the CO recombination into CO_2 due to bimolecular reactions with O_2 and CO as follows:

$$CO(a) + O_2 \rightarrow CO_2 + O, \quad (27)$$

$$CO(a) + CO \rightarrow CO_2 + C, \quad (28)$$

attesting the complex role that this electronically excited state has on the overall kinetics, as already pointed out in [38,182,184,185]. Finally, another main creation mechanism involving O^- ions is :

$$O^- + CO \rightarrow e + CO_2, \quad (29)$$

playing a significant role for high CO_2 fractions as already mentioned in [38].

As can be observed in Figure 14, the rates of the back reaction processes (27), (28) and (29) forming CO_2 decrease with increasing N_2 content. Indeed, adding N_2 dilutes the dissociation products which limits the back reaction mechanisms and leads to an increase of the CO_2 dissociation fraction. Some studies of CO_2 dissociation by non-thermal plasma have been performed using not only N_2 but also rare gases like Argon or Helium as a diluent [69,74,186–188]. However, investigating how the dilution affects the CO_2 dissociation fraction is not straightforward as adding a diluent changes the plasma electrical properties.

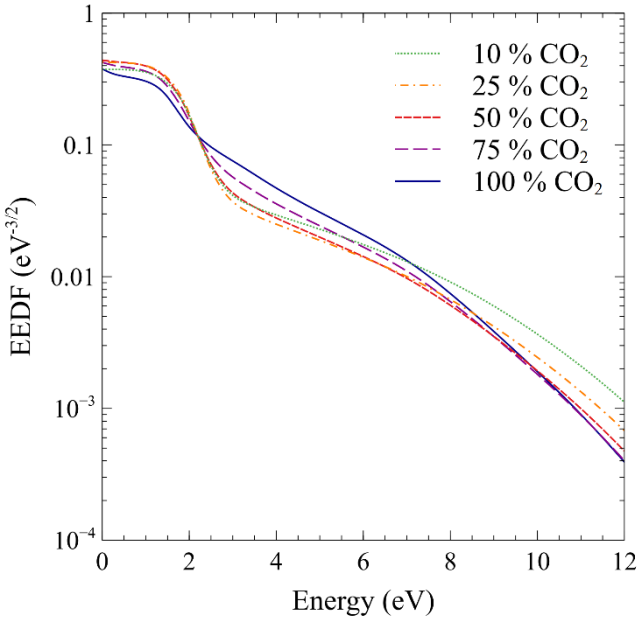

Figure 15: Electron Energy Distribution Function (EEDF) calculated for different CO_2/N_2 mixtures for a discharge current of 50 mA and a pressure of 2 Torr (self-consistent simulations).

Finally, we analyse the changes in the Electron Energy Distribution Function (EEDF) upon addition of N_2. The self-consistently calculated EEDFs for different CO_2/N_2 mixtures for a discharge current of 50 mA and a pressure of 2 Torr are shown in Figure 15. Note that changes in the EEDF are associated

with several factors, including the modifications in E/N, mixture composition (N_2, CO, O_2, O) and/or changes in T_v and superelastic collisions with vibrationally and electronically excited states.

Two main effects explain the shape and dependence (with the N_2 content) of the EEDFs we observe here. On the one hand, the self-consistently calculated reduced electric field increases (from 79 to 90.5 Td) with the nitrogen fraction (cf. Fig. 7) and on the other hand, as the mixture is changing, the effect of N_2 and of the dissociation products, namely CO, O_2 and O is more pronounced in mixtures with higher N_2 content than in pure CO_2. The EEDFs derived for the CO_2-N_2 (above 25% of CO_2) plasmas have a lower population of electrons around the CO_2 dissociation energies (7.5 and 11.9 eV [180]) than in a pure CO_2 plasma, as already observed in [34] for a CO_2-N_2 mixture with 50 % CO_2. Accordingly, the direct electron dissociation rate coefficient for the GS is lower for 50 % CO_2 ($9.4 \cdot 10^{-17}$ m^3s^{-1}) and 75 % CO_2 ($8.9 \cdot 10^{-17}$ m^3s^{-1}), than for pure CO_2 ($9.5 \cdot 10^{-17}$ m^3s^{-1}). Therefore, the enhancement of the reduced electric field is not sufficient to increase the contribution of direct electron-impact dissociation for low N_2 content. We can infer that the increase in the CO_2 dissociation when N_2 is added into the mixture is not due to an enhancement of the direct electron-impact dissociation, but rather to the enhanced contribution of reaction (25) and to the reduction of back reactions as a consequence of dilution with N_2.

IV.3 NO_x formation

Earlier studies in DBD reactors showed that the presence of N_2 during CO_2 splitting, along with the main CO_2 decomposition products (CO and oxygen species), leads to the formation of NO_x compounds, with concentrations in the range of several hundreds of ppm [71,183]. Furthermore, if NO_x compounds are produced, it is important to know whether high enough concentrations might be obtained for two reasons. On the one hand, NO_x can be considered relevant for nitrogen fixation on earth and in the context of ISRU on Mars; on the other hand, these species have a severe negative impact on air quality giving rise to several environmental and health issues [20,21] leading to restriction of their emissions. The mechanisms of NO_x formation in cold plasmas at reduced pressure are relatively well known and have been described in various modeling works [35,191–194].

In this work, downstream measurements were performed to investigate the composition and concentration of the produced NO_x species in the effluent of our CO_2-N_2 DC glow discharge, using FTIR spectroscopy. We could detect NO and nitrogen dioxide (NO_2) but the amount of NO_2 was too low to be quantified.

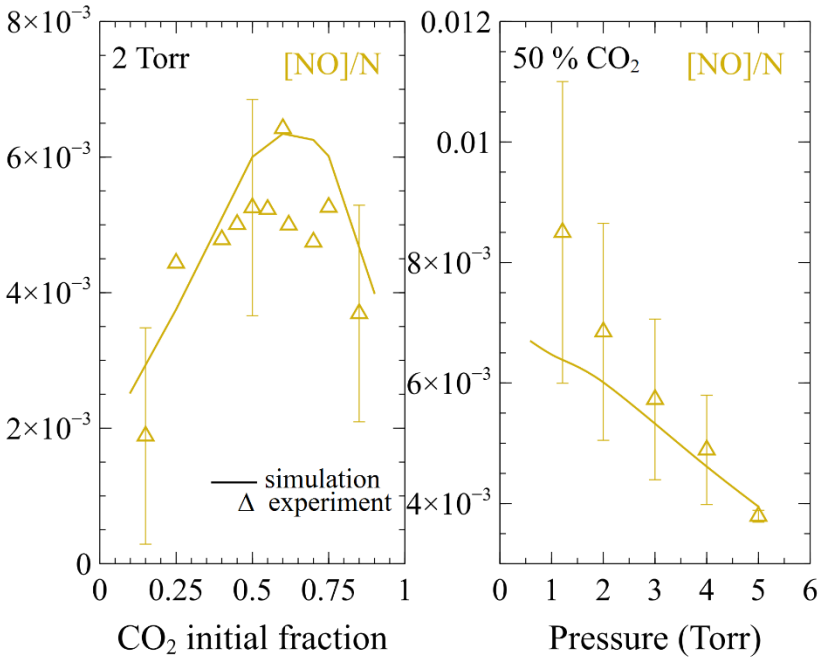

Figure 16: Measured (Δ) and calculated (—) NO fraction, [NO]/N, of a CO_2-N_2 discharge as a function of the CO_2 initial fraction (left) and as a function of pressure for 50% CO_2 (right).

The measured and calculated NO fractions are plotted as a function of the CO_2 initial fraction in the gas mixture and as a function of pressure at a fixed N_2 content of 50% in Figure 16. Experimentally and in the simulations the NO fraction as a function of the CO_2 initial fraction follows a parabolic trend with a maximum around 50% N_2. Concerning the pressure dependence, we can observe that both the measured and calculated [NO]/N decreases with rising pressure. Note that the FTIR measurements were realized in the afterglow while the model results are obtained for the active part of the discharge. However, it was verified that this does not have a significant effect on the NO density measured. Since we find a good agreement between the experiment and simulations (Fig. 16), within the experimental reproducibility error, we believe that our model can be used to explain the observed trends. Therefore, we investigate the contributions of main creation and destruction mechanisms of NO for the different gas mixtures studied at 2 Torr and this is shown in Figure 17. Note that in the simulations the obtained NO fraction is about four orders of magnitude higher than the NO_2 fraction and that the NO density was affected by up to 30% and the maximum was slightly shifted towards 50% when the O recombination probability is multiplied by two in the model (see Section IV.1.).

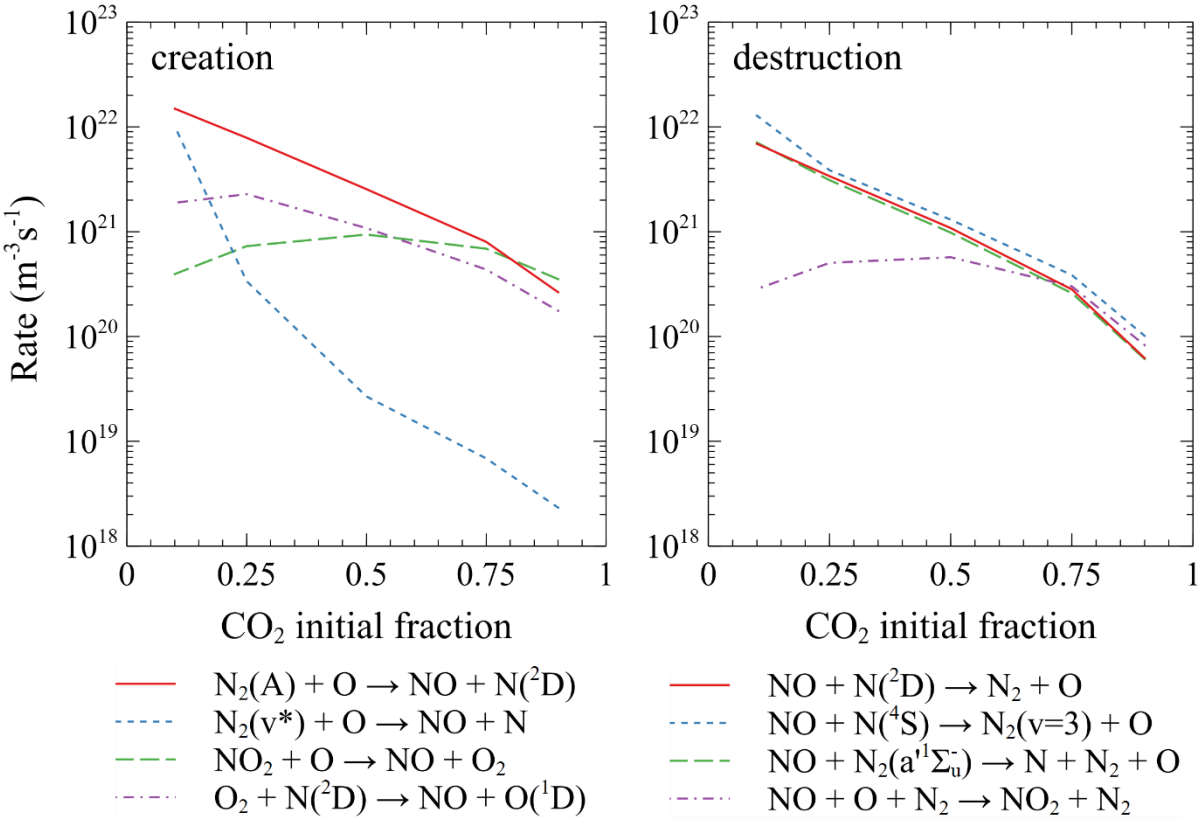

Figure 17: Rate of the most important creation (left) and destruction (right) processes of NO, as a function of CO_2 initial fraction in the CO_2-N_2 gas mixture, at 2 Torr.

In our CO_2-N_2 plasma the NO species are formed out of N reacting with O_2 and $N_2(A^3\Sigma^+_u)$ and $N_2(v\geq13)$ reacting with O atoms, originating from N_2 and CO_2. Thus, it is not unexpected that the maximum of the NO fraction is achieved when both reactants are present in approximately equal concentrations. The dominant formation mechanism of NO at low N_2 content is the reaction between O radicals and NO_2 molecules, forming NO and O_2 molecules. The NO formation via collisions between $N(^2D)$ atoms and O_2 is important even if the density of N atoms is much lower than O (typically, by several orders of magnitude in our conditions). On the other hand, nitrogen atoms also play an important role in the destruction of NO. An important NO loss mechanism is the recombination with O atoms into NO_2 through a three-body reaction (see reaction given in (3)). This third body can be either CO_2 (mainly important above 75 % CO_2), N_2 (especially for N_2 content above 25 %) or O_2. At higher N_2 fractions, the concentrations of N and $N_2(A)$ will rise giving increasing importance to their reactions whilst the amount of atomic and molecular oxygen will decrease. This will encourage the loss of NO through processes involving species coming from N_2. The three-body reaction $NO + O + CO_2 \rightarrow NO_2 + CO_2$ is not represented in Fig. 17 as it only contributes significantly to the NO destruction above 90% of CO_2 (12 % maximum contribution). Regarding charge transfers, it is worth noticing that the process $O_2^+ + NO \rightarrow O_2 + NO^+$ does not constitute a real creation process for NO as more than 99% of NO^+ is transformed back to NO at the wall and is thus not represented in Figure 17.

NO_2 is a significant source of NO production and vice versa. The only important process for NO_2 production is the three-body recombination between NO and O, mostly with N_2 (for CO_2 fraction below 75 %) and with CO_2 and O_2 as a third body. The main destruction mechanism accounting for more than 99% of the NO_2 loss is the reaction of NO_2 with O atoms giving NO and O_2 molecules.

The mechanism of the plasma chemistry of CO_2/N_2 mixtures has been discussed in detail by Snoeckx *et al.* for a DBD reactor [183] and by Heijkers *et al.* for a MW discharge [68]. In both cases the formation of NO was also observed, albeit through a different mechanism. In a microwave plasma, the lower energy of the electrons causes vibrational excitation to become more important than electronic excitation and the vibrationally excited N_2 molecules (with v>13) react with O atoms to form N and NO through the Zel'dovich reaction [95,109], instead of the electronically excited N_2 in the DBD. In our conditions, this mechanism is becoming important only for high N_2 content. In Figure 17 we represent the sum of the rates for all the vibrational states of N_2 above v=13 represented as $N_2(v^*)$.

V. Conclusions

This work reports the validation of a 0D self-consistent kinetic model of CO_2-N_2 plasmas, from the comparison of the model predictions with recent experimental data obtained in a continuous DC glow discharge ignited in different CO_2-N_2 gas mixtures. A good agreement is obtained between the calculated vibrational temperatures of CO_2 and CO, [O]/N, [NO]/N, E/N and dissociation fractions, and the corresponding experimental data measured by in situ FTIR spectroscopy and actinometry. The reaction mechanism (validated set of reactions and corresponding rate coefficients) we propose predicts the quantities mentioned above for pressures between 0.6 and 4 Torr, discharge current of 50 mA and for different compositions ranging from 100 % to only 25 % of CO_2 in a CO_2-N_2 mixture.

Our model includes a self-consistent description of the CO_2, CO and N_2 vibrational kinetics and allows us to evince a remarkable deviation from equilibrium for N_2 and CO vibrational distribution functions, and to a lesser extent for CO_2. This result emphasizes the importance of detailed state-to-state kinetic models and of an understanding of the vibrational energy transfers taking place. In particular, the transfer of vibrational energy from nitrogen to the asymmetric stretching mode of CO_2, described by the CO_2-N_2 V-V transfer in the simulations, greatly influences the vibrational temperature associated to v_3. However, the dissociation fraction does not depend on it and therefore, we can conclude that the degree of vibrational excitation reached remains insufficient for an effective dissociation via the pure vibrational mechanism in our conditions.

The experimental data show an enhanced dissociation of CO_2 when N_2 is added to the plasma. The effect can be attributed to the presence of the metastable $N_2(B^3\Pi_g)$ (creating a new channel for CO_2 dissociation) and to the dilution of dissociation products (limiting the back reactions). The electronically excited state $CO(a^3\Pi_r)$ also influences the plasma chemistry even with the addition of a significant amount of N_2, showing the importance of electronically excited states in the dissociation kinetics. The studies of the self-consistently calculated EEDFs showed that the enhancement of the reduced electric field is not sufficient to increase the contribution of direct electron-impact dissociation for N_2 content below 75 % of the initial mixture. Overall, the admixture of N_2 has a beneficial impact on CO_2 decomposition but it does not compensate for the decrease of the CO_2 initial fraction.

Two main surface processes play a significant role in the plasma kinetics, namely, the recombination of atomic oxygen to form O_2 and the deactivation of the vibrations of CO, N_2 and the different modes of CO_2 at the reactor walls. The O atom densities were shown to strongly depend on the former surface loss process [89]. In turn the vibrational temperatures are greatly affected by the O atoms as they are strong quenchers of vibrations [38,195]. In light of the comparison between the simulations and experimental results in section IV.1., we can infer that the recombination probability of atomic oxygen, γ_O, should increase with the N_2 content. The present results corroborate previous studies that have shown the important role of wall deactivation of vibrationally excited CO_2 and N_2 at pressures around 1 Torr and below, where it changes the vibrational kinetics [34,38] and has a major contribution to gas heating [35]. Similarly, O recombination at the wall and V-T transfers with O atoms greatly contribute to the thermal balance in oxygen discharges [98]. Therefore, an accurate determination of the experimental γ_O and γ_v in realistic gas mixtures, containing CO_2 and N_2 but also

the dissociation products like CO, is therefore needed for further studies of plasmas in CO_2-N_2 mixtures.

It is important to analyse the formation of NO_x compounds in CO_2-N_2 plasmas as NO_x may have a severe negative impact on air quality giving rise to several environmental and health issues, but high enough concentrations can be considered relevant for nitrogen fixation on earth [49,50] and in the context of In Situ Resource and Utilization on Mars [54]. If necessary, one way to prevent the formation of NO_x compounds is to use the separation membrane technology where the oxygen species can be transported away from the reaction mixture and therefore prevent oxygen species to react with N_2. Moreover, an oxygen-permeable membrane placed in the plasma will shift the equilibrium of the CO_2 dissociation reaction towards increased fractions of CO and O [52,196]. However, membranes have only been applied, up to now, to separate O_2 from the gas mixture, and not the O atoms which participate as well in the NO_x production. One solution would be to modify the surface of the plasma reactor to increase the recombination probability of O atoms at the walls as already done in [195] and modeled in [38]. In contrast, to obtain high concentrations of NO_x one solution would be exposing the O_2 coming from the membrane to a N_2 plasma leading to the formation of NO_x, essential for the synthesis of fertilizers and nitrogen fixation [49,50,54].

Overall, the present work adds one more layer to the systematic set-by-step validation strategy of CO_2 non-equilibrium kinetics initiated in [37]. By developing joint experimental, modelling and simulation activities, it has been possible to gather a significant amount of experimental data and simulation results that allow a thorough model validation and can be used to validate or benchmark other models. A similar endeavour is carried out in [98] for pure O_2 plasmas, where the benefits of adopting such paradigm in the development of reaction mechanisms for plasma chemistry is highlighted. Future developments may include a detailed analysis of the surface kinetics, the validation of the kinetics of other species with new measurements performed in the same conditions, such as vibrationally temperatures (or distributions) of N_2 molecules, nitrogen atoms, or molecular nitrogen electronically excited states, or the extension of the domain of validity of the present kinetic scheme to other pressure or excitation conditions.

VI. Acknowledgments

This work was partially supported by the European Union's Horizon 2020 research and innovation programme under grant agreement MSCA ITN 813393, and by Portuguese FCT-Fundação para a Ciência e a Tecnologia, under projects UIDB/50010/2020, UIDP/50010/2020, PTDC/FIS-PLA/1616/2021, EXPL/FIS-PLA/0076/2021 and PD/BD/150414/2019 (PD-F APPLAuSE).

VII. References

[1] J. Rogelj, M. Schaeffer, M. Meinshausen, R. Knutti, J. Alcamo, K. Riahi, W. Hare, Zero emission targets as long-term global goals for climate protection, Environ. Res. Lett. 10 (2015) 105007. https://doi.org/10.1088/1748-9326/10/10/105007.

[2] IPCC, 2022: Summary for Policymakers [H.-O. Pörtner, D.C. Roberts, E.S. Poloczanska, K. Mintenbeck, M. Tignor, A. Alegría, M. Craig, S. Langsdorf, S. Löschke, V. Möller, A. Okem (eds.)]. In: Climate Change 2022: Impacts, Adaptation, and Vulnerability. Contribution of Working Group II to the Sixth Assessment Report of the Intergovernmental Panel on Climate Change [H.-O. Pörtner, D.C. Roberts, M. Tignor, E.S. Poloczanska, K. Mintenbeck, A. Alegría, M. Craig, S. Langsdorf, S. Löschke, V. Möller, A. Okem, B. Rama (eds.)]. Cambridge University Press. In Press., (n.d.).

[3] IPCC, 2014: Climate Change 2014: Synthesis Report. Contribution of Working Groups I, II and III to the Fifth Assessment Report of the Intergovernmental Panel on Climate Change [Core Writing Team, R.K. Pachauri and L.A. Meyer (eds.)]. IPCC, Geneva, Switzerland, 151 pp., (n.d.).

[4] Paris Agreement, Int. Leg. Mater. 55 (2016) 743.
[5] C.-H. Huang, C.-S. Tan, A Review: CO2 Utilization, Aerosol Air Qual. Res. 14 (2014) 480–499. https://doi.org/10.4209/aaqr.2013.10.0326.
[6] G.A. Olah, G.K.S. Prakash, A. Goeppert, Anthropogenic Chemical Carbon Cycle for a Sustainable Future, J. Am. Chem. Soc. 133 (2011) 12881–12898. https://doi.org/10.1021/ja202642y.
[7] B. Ashford, X. Tu, Non-thermal plasma technology for the conversion of CO2, Curr. Opin. Green Sustain. Chem. 3 (2017) 45–49. https://doi.org/10.1016/j.cogsc.2016.12.001.
[8] R. Snoeckx, A. Bogaerts, Plasma technology – a novel solution for CO2 conversion?, Chem. Soc. Rev. 46 (2017) 5805–5863. https://doi.org/10.1039/C6CS00066E.
[9] A.D.N. Kamkeng, M. Wang, J. Hu, W. Du, F. Qian, Transformation technologies for CO2 utilisation: Current status, challenges and future prospects, Chem. Eng. J. 409 (2021) 128138. https://doi.org/10.1016/j.cej.2020.128138.
[10] A. Goede, R. van de Sanden, CO2-Neutral Fuels, Europhys. News. 47 (2016) 22–26. https://doi.org/10.1051/epn/2016304.
[11] A. Bogaerts, G. Centi, Plasma Technology for CO2 Conversion: A Personal Perspective on Prospects and Gaps, Front. Energy Res. 8 (2020). https://www.frontiersin.org/articles/10.3389/fenrg.2020.00111 (accessed October 22, 2022).
[12] L.D. Pietanza, O. Guaitella, V. Aquilanti, I. Armenise, A. Bogaerts, M. Capitelli, G. Colonna, V. Guerra, R. Engeln, E. Kustova, A. Lombardi, F. Palazzetti, T. Silva, Advances in non-equilibrium CO2 plasma kinetics: a theoretical and experimental review, Eur. Phys. J. D. 75 (2021) 237. https://doi.org/10.1140/epjd/s10053-021-00226-0.
[13] A. George, B. Shen, M. Craven, Y. Wang, D. Kang, C. Wu, X. Tu, A Review of Non-Thermal Plasma Technology: A novel solution for CO2 conversion and utilization, Renew. Sustain. Energy Rev. 135 (2021) 109702. https://doi.org/10.1016/j.rser.2020.109702.
[14] A. Berthelot, A. Bogaerts, Modeling of CO2 Splitting in a Microwave Plasma: How to Improve the Conversion and Energy Efficiency, J. Phys. Chem. C. 121 (2017) 8236–8251. https://doi.org/10.1021/acs.jpcc.6b12840.
[15] R. Aerts, W. Somers, A. Bogaerts, Carbon Dioxide Splitting in a Dielectric Barrier Discharge Plasma: A Combined Experimental and Computational Study, ChemSusChem. 8 (2015) 702–716. https://doi.org/10.1002/cssc.201402818.
[16] T. Kozák, A. Bogaerts, Splitting of CO2 by vibrational excitation in non-equilibrium plasmas: a reaction kinetics model, Plasma Sources Sci. Technol. 23 (2014) 045004. https://doi.org/10.1088/0963-0252/23/4/045004.
[17] W. Wang, R. Snoeckx, X. Zhang, M.S. Cha, A. Bogaerts, Modeling Plasma-based CO2 and CH4 Conversion in Mixtures with N2, O2, and H2O: The Bigger Plasma Chemistry Picture, J. Phys. Chem. C. 122 (2018) 8704–8723. https://doi.org/10.1021/acs.jpcc.7b10619.
[18] A. Bogaerts, E.C. Neyts, Plasma Technology: An Emerging Technology for Energy Storage, ACS Energy Lett. 3 (2018) 1013–1027. https://doi.org/10.1021/acsenergylett.8b00184.
[19] V.D. Rusanov, A.A. Fridman, G.V. Sholin, The physics of a chemically active plasma with nonequilibrium vibrational excitation of molecules, Sov. Phys. Uspekhi. 24 (1981) 447–474. https://doi.org/10.1070/PU1981v024n06ABEH004884.
[20] Y. Itikawa, Cross Sections for Electron Collisions With Carbon Dioxide, J. Phys. Chem. Ref. Data. 31 (2002) 749–767. https://doi.org/10.1063/1.1481879.
[21] Fridman A.A., Plasma chemistry., Cambridge University Press, 2012.
[22] A.S. Morillo-Candas, T. Silva, B.L.M. Klarenaar, M. Grofulović, V. Guerra, O. Guaitella, Electron impact dissociation of CO2, Plasma Sources Sci. Technol. 29 (2020) 01LT01. https://doi.org/10.1088/1361-6595/ab6075.
[23] N.Y. Babaeva, G.V. Naidis, On the efficiency of CO2 conversion in corona and dielectric-barrier discharges, Plasma Sources Sci. Technol. 30 (2021) 03LT03. https://doi.org/10.1088/1361-6595/abe6e6.
[24] L.D. Pietanza, G. Colonna, M. Capitelli, Self-consistent electron energy distribution functions, vibrational distributions, electronic excited state kinetics in reacting microwave CO2 plasma: An advanced model, Phys. Plasmas. 27 (2020) 023513. https://doi.org/10.1063/1.5139625.

[25] T. Kozák, A. Bogaerts, Evaluation of the energy efficiency of CO2 conversion in microwave discharges using a reaction kinetics model, Plasma Sources Sci. Technol. 24 (2014) 015024. https://doi.org/10.1088/0963-0252/24/1/015024.
[26] M. Capitelli, G. Colonna, G. D'Ammando, L.D. Pietanza, Self-consistent time dependent vibrational and free electron kinetics for CO2 dissociation and ionization in cold plasmas, Plasma Sources Sci. Technol. 26 (2017) 055009. https://doi.org/10.1088/1361-6595/aa6427.
[27] I. Armenise, E. Kustova, Mechanisms of Coupled Vibrational Relaxation and Dissociation in Carbon Dioxide, J. Phys. Chem. A. 122 (2018) 5107–5120. https://doi.org/10.1021/acs.jpca.8b03266.
[28] F.A. D'Isa, E.A.D. Carbone, A. Hecimovic, U. Fantz, Performance analysis of a 2.45 GHz microwave plasma torch for CO2 decomposition in gas swirl configuration, Plasma Sources Sci. Technol. 29 (2020) 105009. https://doi.org/10.1088/1361-6595/abaa84.
[29] A.J. Wolf, F.J.J. Peeters, P.W.C. Groen, W.A. Bongers, M.C.M. van de Sanden, CO2 Conversion in Nonuniform Discharges: Disentangling Dissociation and Recombination Mechanisms, J. Phys. Chem. C. 124 (2020) 16806–16819. https://doi.org/10.1021/acs.jpcc.0c03637.
[30] A.J. Wolf, T.W.H. Righart, F.J.J. Peeters, W.A. Bongers, M.C.M. van de Sanden, Implications of thermo-chemical instability on the contracted modes in CO2 microwave plasmas, Plasma Sources Sci. Technol. 29 (2020) 025005. https://doi.org/10.1088/1361-6595/ab5eca.
[31] P. Ogloblina, A.S. Morillo-Candas, A.F. Silva, T. Silva, A. Tejero-del-Caz, L.L. Alves, O. Guaitella, V. Guerra, Mars in situ oxygen and propellant production by non-equilibrium plasmas, Plasma Sources Sci. Technol. 30 (2021) 065005. https://doi.org/10.1088/1361-6595/abec28.
[32] T. Silva, M. Grofulović, B.L.M. Klarenaar, A.S. Morillo-Candas, O. Guaitella, R. Engeln, C.D. Pintassilgo, V. Guerra, Kinetic study of low-temperature CO2 plasmas under non-equilibrium conditions. I. Relaxation of vibrational energy, Plasma Sources Sci. Technol. 27 (2018) 015019. https://doi.org/10.1088/1361-6595/aaa56a.
[33] M. Grofulović, T. Silva, B.L.M. Klarenaar, A.S. Morillo-Candas, O. Guaitella, R. Engeln, C.D. Pintassilgo, V. Guerra, Kinetic study of CO2 plasmas under non-equilibrium conditions. II. Input of vibrational energy, Plasma Sources Sci. Technol. 27 (2018) 115009. https://doi.org/10.1088/1361-6595/aadb60.
[34] L. Terraz, T. Silva, A. Morillo-Candas, O. Guaitella, A. Tejero-del-Caz, L.L. Alves, V. Guerra, Influence of N2 on the CO2 vibrational distribution function and dissociation yield in non-equilibrium plasmas, J. Phys. Appl. Phys. 53 (2019) 094002. https://doi.org/10.1088/1361-6463/ab55fb.
[35] T. Silva, M. Grofulović, L. Terraz, C.D. Pintassilgo, V. Guerra, Dynamics of Gas Heating in the Afterglow of Pulsed CO2 and CO2–N2 Glow Discharges at Low Pressure, Plasma Chem. Plasma Process. 40 (2020) 713–725. https://doi.org/10.1007/s11090-020-10061-7.
[36] B.L.M. Klarenaar, R. Engeln, D.C.M. van den Bekerom, M.C.M. van de Sanden, A.S. Morillo-Candas, O. Guaitella, Time evolution of vibrational temperatures in a CO2 glow discharge measured with infrared absorption spectroscopy, Plasma Sources Sci. Technol. 26 (2017) 115008. https://doi.org/10.1088/1361-6595/aa902e.
[37] T. Silva, M. Grofulović, L. Terraz, C.D. Pintassilgo, V. Guerra, Modelling the input and relaxation of vibrational energy in CO2 plasmas, J. Phys. Appl. Phys. 51 (2018) 464001. https://doi.org/10.1088/1361-6463/aadbd7.
[38] C. Fromentin, T. Silva, T.C. Dias, A.S. Morillo-Candas, O. Biondo, O. Guaitella, V. Guerra, Study of vibrational kinetics of CO2 and CO in CO2-O2 plasmas under non-equilibrium conditions, (2022). https://doi.org/10.48550/arXiv.2210.07778.
[39] Tiago DIAS, Atomic oxygen kinetics in CO2 plasmas, INSTITUTO SUPERIOR TÉCNICO, 2019. https://scholar.tecnico.ulisboa.pt/authors/ad9a9348517672649595e209046789e0886527d7d7d96e42ce569f21c5122ad7/records (accessed October 22, 2022).
[40] M. Grofulović, L.L. Alves, V. Guerra, Electron-neutral scattering cross sections for CO2: a complete and consistent set and an assessment of dissociation, J. Phys. Appl. Phys. 49 (2016) 395207. https://doi.org/10.1088/0022-3727/49/39/395207.

[41] P. Ogloblina, A. Tejero-del-Caz, V. Guerra, L.L. Alves, Electron impact cross sections for carbon monoxide and their importance in the electron kinetics of CO2–CO mixtures, Plasma Sources Sci. Technol. 29 (2019) 015002. https://doi.org/10.1088/1361-6595/ab4e72.
[42] A.F. Silva, A.S. Morillo-Candás, A. Tejero-del-Caz, L.L. Alves, O. Guaitella, V. Guerra, A reaction mechanism for vibrationally-cold low-pressure CO2 plasmas, Plasma Sources Sci. Technol. 29 (2020) 125020. https://doi.org/10.1088/1361-6595/abc818.
[43] Time Evolution of the Dissociation Fraction in rf CO2 Plasmas: Impact and Nature of Back-Reaction Mechanisms | The Journal of Physical Chemistry C, (2020). https://pubs.acs.org/doi/abs/10.1021/acs.jpcc.0c03354 (accessed October 29, 2020).
[44] V. Guerra, T. Silva, P. Ogloblina, M. Grofulović, L. Terraz, M.L. da Silva, C.D. Pintassilgo, L.L. Alves, O. Guaitella, The case for in situ resource utilisation for oxygen production on Mars by non-equilibrium plasmas, Plasma Sources Sci. Technol. 26 (2017) 11LT01. https://doi.org/10.1088/1361-6595/aa8dcc.
[45] N. Meunier, S. Laribi, L. Dubois, D. Thomas, G. De Weireld, CO2 Capture in Cement Production and Re-use: First Step for the Optimization of the Overall Process, Energy Procedia. 63 (2014) 6492–6503. https://doi.org/10.1016/j.egypro.2014.11.685.
[46] M. Budde, L.M. Martini, M. Ceppelli, S. Quercetti, R. Engeln, Absolute OH density measurements in a CO2–H2O glow discharge by laser-induced fluorescence spectroscopy, Plasma Sources Sci. Technol. 31 (2022) 055002. https://doi.org/10.1088/1361-6595/ac5ecc.
[47] C. Verheyen, T. Silva, V. Guerra, A. Bogaerts, The effect of H2O on the vibrational populations of CO2 in a CO2/H2O microwave plasma: a kinetic modelling investigation, Plasma Sources Sci. Technol. 29 (2020) 095009. https://doi.org/10.1088/1361-6595/aba1c8.
[48] World Health Organization. Regional Office for Europe, Air quality guidelines: global update 2005: particulate matter, ozone, nitrogen dioxide and sulfur dioxide, World Health Organization. Regional Office for Europe, 2006. https://apps.who.int/iris/handle/10665/107823 (accessed October 28, 2022).
[49] H. Chen, D. Yuan, A. Wu, X. Lin, X. Li, Review of low-temperature plasma nitrogen fixation technology, Waste Dispos. Sustain. Energy. 3 (2021) 201–217. https://doi.org/10.1007/s42768-021-00074-z.
[50] L. Lin, H. Xu, H. Gao, X. Zhu, V. Hessel, Plasma-assisted nitrogen fixation in nanomaterials: fabrication, characterization, and application, J. Phys. Appl. Phys. 53 (2020) 133001. https://doi.org/10.1088/1361-6463/ab5f1f.
[51] M.Y. Ong, S. Nomanbhay, F. Kusumo, P.L. Show, Application of microwave plasma technology to convert carbon dioxide (CO2) into high value products: A review, J. Clean. Prod. 336 (2022) 130447. https://doi.org/10.1016/j.jclepro.2022.130447.
[52] D. Premathilake, R.A. Outlaw, R.A. Quinlan, C.E. Byvik, Oxygen Generation by Carbon Dioxide Glow Discharge and Separation by Permeation Through Ultrathin Silver Membranes, Earth Space Sci. 6 (2019) 557–564. https://doi.org/10.1029/2018EA000521.
[53] V. Guerra, T. Silva, O. Guaitella, Living on mars: how to produce oxygen and fuel to get home, Europhys. News. 49 (2018) 15–18. https://doi.org/10.1051/epn/2018302.
[54] V. Guerra, T. Silva, N. Pinhão, O. Guaitella, C. Guerra-Garcia, F.J.J. Peeters, M.N. Tsampas, M.C.M. van de Sanden, Plasmas for in situ resource utilization on Mars: Fuels, life support, and agriculture, J. Appl. Phys. 132 (2022) 070902. https://doi.org/10.1063/5.0098011.
[55] D. Fitz, H. Reiner, B.M. Rode, Chemical evolution toward the origin of life, Pure Appl. Chem. 79 (2007) 2101–2117. https://doi.org/10.1351/pac200779122101.
[56] M. Janda, V. Martišovitš, M. Morvová, Z. Machala, K. Hensel, Monte Carlo simulations of electron dynamics in N2/CO2 mixtures, Eur. Phys. J. D. 45 (2007) 309–315. https://doi.org/10.1140/epjd/e2007-00254-x.
[57] M. Janda, M. Morvova, Z. Machala, I. Morva, Study of Plasma Induced Chemistry by DC Discharges in CO2/N2/H2O Mixtures Above a Water Surface, Orig. Life Evol. Biospheres. 38 (2008) 23–35. https://doi.org/10.1007/s11084-007-9115-0.
[58] J. Annaloro, A. Bultel, Vibrational and electronic collisional-radiative model in CO2-N2-Ar mixtures for Mars entry problems, Phys. Plasmas. 26 (2019) 103505. https://doi.org/10.1063/1.5114792.

[59] V. Joly, A. Roblin, Vibrational relaxation of CO2 (m, nl, p) in a CO2-N2 mixture. Part 1: Survey of available data, Aerosp. Sci. Technol. 3 (1999) 229–238. https://doi.org/10.1016/S1270-9638(99)80045-5.
[60] V. Joly, C. Marmignon, P. Jacquet, Vibrational relaxation of CO2(m, nl, p) in a CO2 N2 mixture. Part 2: Application to a one-dimensional problem, Aerosp. Sci. Technol. 3 (1999) 313–322. https://doi.org/10.1016/S1270-9638(00)86967-9.
[61] Z. Bouyahiaoui, R. Haoui, A. Zidane, Numerical investigation of a hypersonic flow around a capsule in CO2–N2 environment, Eur. J. Mech. - BFluids. 80 (2020) 146–156. https://doi.org/10.1016/j.euromechflu.2019.12.009.
[62] G.N. Zalogin, P.V. Kozlov, L.A. Kuznetsova, S.A. Losev, V.N. Makarov, Yu.V. Romanenko, S.T. Surzhikov, Radiation excited by shock waves in a CO2-N2-Ar mixture: Experiment and theory, Tech. Phys. 46 (2001) 654–661. https://doi.org/10.1134/1.1379629.
[63] H. Zhang, L. Li, X. Li, W. Wang, J. Yan, X. Tu, Warm plasma activation of CO2 in a rotating gliding arc discharge reactor, J. CO2 Util. 27 (2018) 472–479. https://doi.org/10.1016/j.jcou.2018.08.020.
[64] H.L.K. Manning, I.L. ten Kate, S.J. Battel, P.R. Mahaffy, Electric discharge in the Martian atmosphere, Paschen curves and implications for future missions, Adv. Space Res. 46 (2010) 1334–1340. https://doi.org/10.1016/j.asr.2010.07.006.
[65] G. Garcia-Cosio, H. Martinez, M. Calixto-Rodriguez, A. Gomez, DC discharge experiment in an Ar/N2/CO2 ternary mixture: A laboratory simulation of the Martian ionosphere's plasma environment, J. Quant. Spectrosc. Radiat. Transf. 112 (2011) 2787–2793. https://doi.org/10.1016/j.jqsrt.2011.09.008.
[66] G.V. Naidis, N.Y. Babaeva, Modeling of CO2 conversion in low-pressure glow discharges in CO2-N2 mixtures, J. Phys. Appl. Phys. 55 (2022) 335202. https://doi.org/10.1088/1361-6463/ac7266.
[67] R. Snoeckx, S. Heijkers, K.V. Wesenbeeck, S. Lenaerts, A. Bogaerts, CO2 conversion in a dielectric barrier discharge plasma: N2 in the mix as a helping hand or problematic impurity?, Energy Environ. Sci. 9 (2016) 999–1011. https://doi.org/10.1039/C5EE03304G.
[68] S. Heijkers, R. Snoeckx, T. Kozák, T. Silva, T. Godfroid, N. Britun, R. Snyders, A. Bogaerts, CO2 Conversion in a Microwave Plasma Reactor in the Presence of N2: Elucidating the Role of Vibrational Levels, J. Phys. Chem. C. 119 (2015) 12815–12828. https://doi.org/10.1021/acs.jpcc.5b01466.
[69] M. Schiorlin, R. Klink, R. Brandenburg, Carbon dioxide conversion by means of coplanar dielectric barrier discharges, Eur. Phys. J. Appl. Phys. 75 (2016) 24704. https://doi.org/10.1051/epjap/2016160073.
[70] M. Grofulović, B.L.M. Klarenaar, O. Guaitella, V. Guerra, R. Engeln, A rotational Raman study under non-thermal conditions in pulsed CO2–N2 and CO2–O2 glow discharges, Plasma Sources Sci. Technol. 28 (2019) 045014. https://doi.org/10.1088/1361-6595/ab1240.
[71] W. Wang, R. Snoeckx, X. Zhang, M.S. Cha, A. Bogaerts, Modeling Plasma-based CO_2 and CH_4 Conversion in Mixtures with N_2, O_2, and H_2O: The Bigger Plasma Chemistry Picture, J. Phys. Chem. C. 122 (2018) 8704–8723. https://doi.org/10.1021/acs.jpcc.7b10619.
[72] M.I. Khan, N.U. Rehman, S. Khan, N. Ullah, A. Masood, A. Ullah, Spectroscopic study of CO_2 and CO_2–N_2 mixture plasma using dielectric barrier discharge, AIP Adv. 9 (2019) 085015. https://doi.org/10.1063/1.5096399.
[73] R. Brandenburg, A. Sarani, About the development of single microdischarges in dielectric barrier discharges in CO2 and CO2/N2 gas mixtures: DBD-MDs in CO2 and CO2/N2, Eur. Phys. J. Spec. Top. 226 (2017) 2911–2922. https://doi.org/10.1140/epjst/e2016-60339-8.
[74] S. Mohsenian, D. Nagassou, R. Elahi, P. Yu, M. Nallar, H.-W. Wong, J.P. Trelles, Carbon dioxide conversion by solar-enhanced microwave plasma: Effect of specific power and argon/nitrogen carrier gases, J. CO2 Util. 34 (2019) 725–732. https://doi.org/10.1016/j.jcou.2019.09.002.
[75] C. Richards, E. Jans, D. Mignogna, I.V. Adamovich, Time-resolved CO2, CO, and N2 vibrational population measurements in Ns pulse discharge plasmas, Plasma Sources Sci. Technol. 31 (2022) 094011. https://doi.org/10.1088/1361-6595/ac8f6d.

[76] I. Gulko, E.R. Jans, C. Richards, S. Raskar, X. Yang, D.C.M. van den Bekerom, I.V. Adamovich, Selective generation of excited species in ns pulse/RF hybrid plasmas for plasma chemistry applications, Plasma Sources Sci. Technol. 29 (2020) 104002. https://doi.org/10.1088/1361-6595/abb3a1.
[77] G.V. Pokrovskiy, N.A. Popov, S.M. Starikovskaia, Fast gas heating and kinetics of electronically excited states in a nanosecond capillary discharge in CO_2, Plasma Sources Sci. Technol. 31 (2022) 035010. https://doi.org/10.1088/1361-6595/ac5102.
[78] M. Grofulović, B.L.M. Klarenaar, O. Guaitella, V. Guerra, R. Engeln, A rotational Raman study under non-thermal conditions in pulsed CO2–N2 and CO2–O2 glow discharges, Plasma Sources Sci. Technol. 28 (2019) 045014. https://doi.org/10.1088/1361-6595/ab1240.
[79] M.A. Damen, L.M. Martini, R. Engeln, Temperature evolution in a pulsed CO2–N2 glow discharge measured using quantum cascade laser absorption spectroscopy, Plasma Sources Sci. Technol. 29 (2020) 065016. https://doi.org/10.1088/1361-6595/ab8e50.
[80] D. Mignogna, E.R. Jans, S. Raskar, I.V. Adamovich, Generation and decay of N2(A3Σu +) molecules in reacting CO2 and CH4 plasmas, Plasma Sources Sci. Technol. (2022). https://doi.org/10.1088/1361-6595/ac99fc.
[81] R.L. TAYLOR, S. BITTERMAN, Survey of Vibrational Relaxation Data for Processes Important in the CO2-N2 Laser System, Rev. Mod. Phys. 41 (1969) 26–47. https://doi.org/10.1103/RevModPhys.41.26.
[82] N.N. Sobolev, V.V. Sokovikov, CO2 LASERS, Sov. Phys. Uspekhi. 10 (1967) 153. https://doi.org/10.1070/PU1967v010n02ABEH005861.
[83] C.K.N. Patel, Selective Excitation Through Vibrational Energy Transfer and Optical Maser Action in N2-CO2, Phys. Rev. Lett. 13 (1964) 617–619. https://doi.org/10.1103/PhysRevLett.13.617.
[84] W.J. Witteman, G.V.D. Goot, High-Power Infrared Laser with Adjustable Coupling-Out, J. Appl. Phys. 37 (1966) 2919–2919. https://doi.org/10.1063/1.1782158.
[85] W.J. Witteman, The CO2 Laser, Springer, 2013.
[86] A.W. van de Steeg, T. Butterworth, D.C.M. van den Bekerom, A.F. Silva, M.C.M. van de Sanden, G.J. van Rooij, Plasma activation of N2, CH4 and CO2: an assessment of the vibrational non-equilibrium time window, Plasma Sources Sci. Technol. 29 (2020) 115001. https://doi.org/10.1088/1361-6595/abbae4.
[87] P. Diomede, M.C.M. van de Sanden, S. Longo, Vibrational Kinetics in Plasma as a Functional Problem: A Flux-Matching Approach, J. Phys. Chem. A. 122 (2018) 7918–7923. https://doi.org/10.1021/acs.jpca.8b05623.
[88] B.L.M. Klarenaar, A.S. Morillo-Candas, M. Grofulović, M.C.M. van de Sanden, R. Engeln, O. Guaitella, Excitation and relaxation of the asymmetric stretch mode of CO2 in a pulsed glow discharge, Plasma Sources Sci. Technol. 28 (2019) 035011. https://doi.org/10.1088/1361-6595/aada5e.
[89] A.S. Morillo-Candas, C. Drag, J.-P. Booth, T.C. Dias, V. Guerra, O. Guaitella, Oxygen atom kinetics in CO2 plasmas ignited in a DC glow discharge, Plasma Sources Sci. Technol. 28 (2019) 075010. https://doi.org/10.1088/1361-6595/ab2b84.
[90] C.E. Treanor, J.W. Rich, R.G. Rehm, Vibrational Relaxation of Anharmonic Oscillators with Exchange-Dominated Collisions, J. Chem. Phys. 48 (1968) 1798–1807. https://doi.org/10.1063/1.1668914.
[91] A. Morillo candas, Investigation of fundamental mechanisms of CO2 plasmas, doctoral thesis, Université Paris-Saclay (ComUE), 2019. https://www.theses.fr/2019SACLX091 (accessed October 22, 2022).
[92] A. Tejero-del-Caz, V. Guerra, D. Gonçalves, M.L. da Silva, L. Marques, N. Pinhão, C.D. Pintassilgo, L.L. Alves, The LisbOn KInetics Boltzmann solver, Plasma Sources Sci. Technol. 28 (2019) 043001. https://doi.org/10.1088/1361-6595/ab0537.
[93] LoKI - IPFN, (n.d.). https://nprime.tecnico.ulisboa.pt/loki/ (accessed January 20, 2023).
[94] A. Tejero-del-Caz, V. Guerra, N. Pinhão, C.D. Pintassilgo, L.L. Alves, On the quasi-stationary approach to solve the electron Boltzmann equation in pulsed plasmas, Plasma Sources Sci. Technol. 30 (2021) 065008. https://doi.org/10.1088/1361-6595/abf858.

[95] V. Guerra, A. Tejero-del-Caz, C.D. Pintassilgo, L.L. Alves, Modelling N2–O2 plasmas: volume and surface kinetics, Plasma Sources Sci. Technol. 28 (2019) 073001. https://doi.org/10.1088/1361-6595/ab252c.
[96] P.J. Chantry, A simple formula for diffusion calculations involving wall reflection and low density, J. Appl. Phys. 62 (1987) 1141–1148. https://doi.org/10.1063/1.339662.
[97] V. Guerra, J. Loureiro, Kinetic model of a low-pressure microwave discharge in O2-H2 including the effects of O- ions on the characteristics for plasma maintenance, Plasma Sources Sci. Technol. 8 (1999) 110. https://doi.org/10.1088/0963-0252/8/1/014.
[98] T. C. Dias, C. Fromentin, L. L. Alves, A. T. del Caz, T. Silva, and V. Guerra, Reaction mechanisms for O2 plasmas, In preparation to submit to the Special Issue on Verification, Validation and Benchmarking of Low-temperature Plasma Models of Plasma Sources Sci. Technol. (2022).
[99] O. Biondo, C. Fromentin, T. Silva, V. Guerra, G. van Rooij, A. Bogaerts, Insights into the limitations to vibrational excitation of CO_2: validation of a kinetic model with pulsed glow discharge experiments, Plasma Sources Sci. Technol. 31 (2022) 074003. https://doi.org/10.1088/1361-6595/ac8019.
[100] L.L. Alves, The IST-LISBON database on LXCat, J. Phys. Conf. Ser. 565 (2014) 012007. https://doi.org/10.1088/1742-6596/565/1/012007.
[101] IST-Lisbon database, (n.d.). www.lxcat.net (accessed November 22, 2022).
[102] J. Loureiro, C.M. Ferreira, Coupled electron energy and vibrational distribution functions in stationary N2 discharges, J. Phys. Appl. Phys. 19 (1986) 17. https://doi.org/10.1088/0022-3727/19/1/007.
[103] P. Coche, V. Guerra, L.L. Alves, Microwave air plasmas in capillaries at low pressure I. Self-consistent modeling, J. Phys. Appl. Phys. 49 (2016) 235207. https://doi.org/10.1088/0022-3727/49/23/235207.
[104] Y. Wang, O. Zatsarinny, K. Bartschat, B-spline R-matrix-with-pseudostates calculations for electron-impact excitation and ionization of nitrogen, Phys. Rev. A. 89 (2014) 062714. https://doi.org/10.1103/PhysRevA.89.062714.
[105] G. Gousset, C.M. Ferreira, M. Pinheiro, P.A. Sa, M. Touzeau, M. Vialle, J. Loureiro, Electron and heavy-particle kinetics in the low pressure oxygen positive column, J. Phys. Appl. Phys. 24 (1991) 290. https://doi.org/10.1088/0022-3727/24/3/010.
[106] L.L. Alves, P. Coche, M.A. Ridenti, V. Guerra, Electron scattering cross sections for the modelling of oxygen-containing plasmas*, Eur. Phys. J. D. 70 (2016) 124. https://doi.org/10.1140/epjd/e2016-70102-1.
[107] V.O. Klein, S. Rosseland, Uber Zusannnenst61~e zwischen Atomen und freien Elektronen., (n.d.).
[108] M. Foucher, D. Marinov, E. Carbone, P. Chabert, J.-P. Booth, Highly vibrationally excited O2 molecules in low-pressure inductively-coupled plasmas detected by high sensitivity ultra-broad-band optical absorption spectroscopy, Plasma Sources Sci. Technol. 24 (2015) 042001. https://doi.org/10.1088/0963-0252/24/4/042001.
[109] V. Guerra, J. Loureiro, Non-equilibrium coupled kinetics in stationary N2-O2 discharges, J. Phys. Appl. Phys. 28 (1995) 1903. https://doi.org/10.1088/0022-3727/28/9/018.
[110] V. Guerra, J. Loureiro, Self-consistent electron and heavy-particle kinetics in a low-pressure - glow discharge, Plasma Sources Sci. Technol. 6 (1997) 373. https://doi.org/10.1088/0963-0252/6/3/014.
[111] A. Annušová, D. Marinov, J.-P. Booth, N. Sirse, M.L. da Silva, B. Lopez, V. Guerra, Kinetics of highly vibrationally excited O2(X) molecules in inductively-coupled oxygen plasmas, Plasma Sources Sci. Technol. 27 (2018) 045006. https://doi.org/10.1088/1361-6595/aab47d.
[112] M.A. Ridenti, L.L. Alves, V. Guerra, J. Amorim, The role of rotational mechanisms in electron swarm parameters at low reduced electric field in N2, O2 and H2, Plasma Sources Sci. Technol. 24 (2015) 035002. https://doi.org/10.1088/0963-0252/24/3/035002.
[113] D. Marinov, V. Guerra, O. Guaitella, J.-P. Booth, A. Rousseau, Ozone kinetics in low-pressure discharges: vibrationally excited ozone and molecule formation on surfaces, Plasma Sources Sci. Technol. 22 (2013) 055018. https://doi.org/10.1088/0963-0252/22/5/055018.

[114] V. Guerra, P.A. Sá, J. Loureiro, Kinetic modeling of low-pressure nitrogen discharges and post-discharges, Eur. Phys. J. Appl. Phys. 28 (2004) 125–152. https://doi.org/10.1051/epjap:2004188.
[115] V. Guerra, J. Loureiro, Electron and heavy particle kinetics in a low-pressure nitrogen glow discharge, Plasma Sources Sci. Technol. 6 (1997) 361. https://doi.org/10.1088/0963-0252/6/3/013.
[116] O.V. Braginskiy, A.N. Vasilieva, K.S. Klopovskiy, A.S. Kovalev, D.V. Lopaev, O.V. Proshina, T.V. Rakhimova, A.T. Rakhimov, Singlet oxygen generation in O2flow excited by RF discharge: I. Homogeneous discharge mode: $\upalpha$-mode, J. Phys. Appl. Phys. 38 (2005) 3609–3625. https://doi.org/10.1088/0022-3727/38/19/010.
[117] J.P. Booth, A. Chatterjee, O. Guaitella, D. Lopaev, S. Zyryanov, A. Volynets, T. Rakhimova, D. Voloshin, A. Chukalovsky, Y. Mankelevich, V. Guerra, Quenching of O2(b1Σg+) by O(3P) atoms. Effect of gas temperature, Plasma Sources Sci. Technol. 31 (2022) 065012. https://doi.org/10.1088/1361-6595/ac7749.
[118] C.D. Pintassilgo, J. Loureiro, Kinetic study of a N2-CH4 afterglow plasma for production of N-containing hydrocarbon species of Titan's atmosphere, Adv. Space Res. 46 (2010) 657–671. https://doi.org/10.1016/j.asr.2010.04.027.
[119] N.A. Popov, Investigation of the mechanism for rapid heating of nitrogen and air in gas discharges, Plasma Phys. Rep. 27 (2001) 886–896. https://doi.org/10.1134/1.1409722.
[120] R.A. Young, G. Black, T.G. Slanger, Vacuum-Ultraviolet Photolysis of N2O. II. Deactivation of N2(A 3Σu+*rpar; and N2(B 3Πg), J. Chem. Phys. 50 (1969) 303–308. https://doi.org/10.1063/1.1670792.
[121] I. M. Campbell, B. A. Thrush, Behaviour of carbon dioxide and nitrous oxide in active nitrogen, Trans. Faraday Soc. 62 (1966) 3366–3374. https://doi.org/10.1039/TF9666203366.
[122] L.G. Piper, Energy transfer studies on N2(X 1Σ+g,v) and N2(B 3Πg), J. Chem. Phys. 97 (1992) 270–275. https://doi.org/10.1063/1.463625.
[123] J.T. Herron, Evaluated Chemical Kinetics Data for Reactions of N(2D), N(2P), and N2(A 3Σu+) in the Gas Phase, J. Phys. Chem. Ref. Data. 28 (1999) 1453–1483. https://doi.org/10.1063/1.556043.
[124] W. j. Wiegand, W.L. Nighan, Plasma chemistry of CO2 –N2 –He discharges, Appl. Phys. Lett. 22 (1973) 583–586. https://doi.org/10.1063/1.1654516.
[125] J.A. Meyer, D.W. Setser, W.G. Clark, Rate constants for quenching of molecular nitrogen (A3.SIGMA.u+) in active nitrogen, J. Phys. Chem. 76 (1972) 1–9. https://doi.org/10.1021/j100645a001.
[126] D.W. Setser, G.W. Taylor, Comparison of the reactivities of the lowest excited states of nitrogen (A3.SIGMA.u+) and of carbon monoxide (a3.PI.), J. Am. Chem. Soc. 93 (1971) 4930–4932. https://doi.org/10.1021/ja00748a058.
[127] A.B. Callear, I.W.M. Smith, Fluorescence of nitric oxide. Part 4.—Mechanism of deactivation of NO C2Π(v= 0) in nitrogen, Trans. Faraday Soc. 61 (1965) 2383–2394. https://doi.org/10.1039/TF9656102383.
[128] N.A. Popov, Vibrational kinetics of electronically-excited molecules in nitrogen discharge plasma, J. Phys. Appl. Phys. 46 (2013) 355204. https://doi.org/10.1088/0022-3727/46/35/355204.
[129] F. Albugues, A. Birot, D. Blanc, H. Brunet, J. Galy, P. Millet, J.L. Teyssier, Destruction of the levels C3Πu (v′=0, v′=1) of nitrogen by O2,CO2, CH4, and H2O, J. Chem. Phys. 61 (1974) 2695–2699. https://doi.org/10.1063/1.1682401.
[130] L.L. Alves, L. Marques, C.D. Pintassilgo, G. Wattieaux, E. Es-sebbar, J. Berndt, E. Kovacević, N. Carrasco, L. Boufendi, G. Cernogora, Capacitively coupled radio-frequency discharges in nitrogen at low pressures, Plasma Sources Sci. Technol. 21 (2012) 045008. https://doi.org/10.1088/0963-0252/21/4/045008.
[131] M. Capitelli, C. Gorse, G.D. Billing, V—V pumping up in non-equilibrium nitrogen: Effects on the dissoviation rate, Chem. Phys. 52 (1980) 299–304. https://doi.org/10.1016/0301-0104(80)85233-5.
[132] G.D. Billing, E.R. Fisher, VV and VT rate coefficients in N2 by a quantum-classical model, Chem. Phys. 43 (1979) 395–401. https://doi.org/10.1016/0301-0104(79)85207-6.

[133] R.N. Schwartz, Z.I. Slawsky, K.F. Herzfeld, Calculation of Vibrational Relaxation Times in Gases, J. Chem. Phys. 20 (1952) 1591–1599. https://doi.org/10.1063/1.1700221.
[134] R.D. Sharma, C.A. Brau, Near-Resonant Vibrational Energy Transfer in N2-CO2 Mixtures, Phys. Rev. Lett. 19 (1967) 1273–1275. https://doi.org/10.1103/PhysRevLett.19.1273.
[135] R.D. Sharma, C.A. Brau, Energy Transfer in Near-Resonant Molecular Collisions due to Long-Range Forces with Application to Transfer of Vibrational Energy from ν3 Mode of CO2 to N2, J. Chem. Phys. 50 (1969) 924–930. https://doi.org/10.1063/1.1671145.
[136] M. Capitelli, C.M. Ferreira, B.F. Gordiets, A.I. Osipov, Plasma Kinetics in Atmospheric Gases, Springer Science & Business Media, 2013.
[137] M. Lino da Silva, V. Guerra, J. Loureiro, P.A. Sá, Vibrational distributions in N2 with an improved calculation of energy levels using the RKR method, Chem. Phys. 348 (2008) 187–194. https://doi.org/10.1016/j.chemphys.2008.02.048.
[138] A. Chedin, The carbon dioxide molecule, J. Mol. Spectrosc. 76 (1979) 430–491. https://doi.org/10.1016/0022-2852(79)90236-4.
[139] P. Ogloblina, A. Tejero-del-Caz, V. Guerra, L.L. Alves, Electron impact cross sections for carbon monoxide and their importance in the electron kinetics of CO_2–CO mixtures, Plasma Sources Sci. Technol. 29 (2020) 015002. https://doi.org/10.1088/1361-6595/ab4e72.
[140] V. Laporta, C.M. Cassidy, J. Tennyson, R. Celiberto, Electron-impact resonant vibration excitation cross sections and rate coefficients for carbon monoxide, Plasma Sources Sci. Technol. 21 (2012) 045005. https://doi.org/10.1088/0963-0252/21/4/045005.
[141] A.V. Phelps, Rotational and Vibrational Excitation of Molecules by Low-Energy Electrons, Rev. Mod. Phys. 40 (1968) 399–410. https://doi.org/10.1103/RevModPhys.40.399.
[142] G. Colonna, V. Laporta, R. Celiberto, M. Capitelli, J. Tennyson, Non-equilibrium vibrational and electron energy distributions functions in atmospheric nitrogen ns pulsed discharges and $\upmu$s post-discharges: the role of electron molecule vibrational excitation scaling-laws, Plasma Sources Sci. Technol. 24 (2015) 035004. https://doi.org/10.1088/0963-0252/24/3/035004.
[143] A. Bourdon, P. Vervisch, Analytical Models for Electron-Vibration Coupling in Nitrogen Plasma Flows, J. Thermophys. Heat Transf. (2012). https://doi.org/10.2514/2.6571.
[144] G.J. Schulz, Vibrational Excitation of N2, CO and H2 by Electron Impact, Phys. Rev. 135 (1964) A988–A994. https://doi.org/10.1103/PhysRev.135.A988.
[145] H. Ehrhardt, L. Langhans, F. Linder, H.S. Taylor, Resonance Scattering of Slow Electrons from H 2 and CO Angular Distributions, Phys. Rev. 173 (1968) 222–230. https://doi.org/10.1103/PhysRev.173.222.
[146] J.C. Stephenson, R.E. Wood, C.B. Moore, Near-Resonant Energy Transfer between Infrared-Active Vibrations, J. Chem. Phys. 48 (1968) 4790–4791. https://doi.org/10.1063/1.1668068.
[147] E.V. Kustova, E.A. Nagnibeda, I. Armenise, Vibrational-Chemical Kinetics in Mars Entry Problems, Open Plasma Phys. J. 7 (2014) 76–87. https://doi.org/10.2174/1876534301407010076.
[148] J. Blauer, G. Nickerson, A survey of vibrational relaxation rate data for processes importantto CO2-N2-H2O infrared plume radiation, in: 7th Fluid PlasmaDynamics Conf., American Institute of Aeronautics and Astronautics, Palo Alto,CA,U.S.A., 1974. https://doi.org/10.2514/6.1974-536.
[149] R.L. Taylor, M. Camac, R.M. Feinberg, Measurements of vibration-vibration coupling in gas mixtures, Symp. Int. Combust. 11 (1967) 49–65. https://doi.org/10.1016/S0082-0784(67)80133-4.
[150] W.A. Rosser, A.D. Wood, E.T. Gerry, Deactivation of Vibrationally Excited Carbon Dioxide (ν3) by Collisions with Carbon Dioxide or with Nitrogen, J. Chem. Phys. 50 (1969) 4996–5008. https://doi.org/10.1063/1.1670996.
[151] R.L. Taylor, S. Bitterman, Experimental Measurements of the Resonant Vibrational Energy Transfer between Mode v3 of CO2 and N2, J. Chem. Phys. 50 (1969) 1720–1726. https://doi.org/10.1063/1.1671265.
[152] C.B. Moore, R.E. Wood, B. Hu, J.T. Yardley, Vibrational Energy Transfer in CO2 Lasers, J. Chem. Phys. 46 (1967) 4222–4231. https://doi.org/10.1063/1.1840527.

[153] D.F. Starr, J.K. Hancock, Vibrational energy transfer in CO_2 –CO mixtures from 163 to 406 °K, J. Chem. Phys. 63 (1975) 4730–4734. https://doi.org/10.1063/1.431259.
[154] W.A. Rosser, R.D. Sharma, E.T. Gerry, Deactivation of Vibrationally Excited Carbon Dioxide (001) by Collisions with Carbon Monoxide, J. Chem. Phys. 54 (1971) 1196–1205. https://doi.org/10.1063/1.1674955.
[155] R.D. Sharma, Near-resonant vibration-to-vibration energy transfer in the NO+–N2 collisions, J. Chem. Phys. 125 (2006) 114306. https://doi.org/10.1063/1.2348874.
[156] Losev, S. A., Kozlov, P. V., Kuznetsova, L. A., Makarov, V. N., Romanenko, Y. V.,, Romanenko, Y. V. Surzhikov, S. T., Radiation of a Mixture CO2-N2-Ar in Shock Waves: Experiment & Modelling, Aerothermodynamics for space vehicles, Proceedings of the 3rd European Symposium on Aerothermodynamics for space vehicles held at ESTEC, Noordwijk, The Netherlands. (1998) 437.
[157] K.F. Herzfeld, Deactivation of Vibrations by Collision in the Presence of Fermi Resonance, J. Chem. Phys. 47 (1967) 743–752. https://doi.org/10.1063/1.1711947.
[158] A.K. Kurnosov, A.P. Napartovich, S.L. Shnyrev, M. Cacciatore, A database for V–V state-to-state rate constants in N2–N2 and N2–CO collisions in a wide temperature range: dynamical calculations and analytical approximations, Plasma Sources Sci. Technol. 19 (2010) 045015. https://doi.org/10.1088/0963-0252/19/4/045015.
[159] D.C. Allen, C.J.S.M. Simpson, Vibrational energy exchange between CO and the isotopes of N2 between 300 K and 80 K, Chem. Phys. 45 (1980) 203–211. https://doi.org/10.1016/0301-0104(80)85068-3.
[160] G. Mastrocinque, A. Chakroun, L. Doyennette, H. Gueguen, M. Margottin-Maclou, L. Henry, Vibrational energy transfer from the υ = 1 level of carbon monoxide to the υ = 1 level of the two isotopic species of nitrogen: 14N2 and 15N2, Chem. Phys. Lett. 39 (1976) 347–349. https://doi.org/10.1016/0009-2614(76)80092-9.
[161] Q. Hong, M. Bartolomei, C. Coletti, A. Lombardi, Q. Sun, F. Pirani, Vibrational Energy Transfer in CO+N2 Collisions: A Database for V–V and V–T/R Quantum-Classical Rate Coefficients, Molecules. 26 (2021) 7152. https://doi.org/10.3390/molecules26237152.
[162] Y. Sato, S. Tsuchiya, K. Kuratani, Shock-Wave Study of Vibrational Energy Exchange between Diatomic Molecules, J. Chem. Phys. 50 (1969) 1911–1919. https://doi.org/10.1063/1.1671306.
[163] H.K. Shin, Vibration-to-vibration energy transfer in near-resonant collisions, J. Chem. Phys. 60 (1974) 1064–1070. https://doi.org/10.1063/1.1681114.
[164] P.F. Zittel, C.B. Moore, Vibration-to-vibration energy transfer in N2–CO, Appl. Phys. Lett. 21 (1972) 81–83. https://doi.org/10.1063/1.1654298.
[165] J.C. Stephenson, E.R. Mosburg, Vibrational energy transfer in CO from 100 to 300 °K, J. Chem. Phys. 60 (1974) 3562–3566. https://doi.org/10.1063/1.1681574.
[166] D.F. Starr, J.K. Hancock, W.H. Green, Vibrational deactivation of carbon monoxide by hydrogen and nitrogen from 100 to 650 °K, J. Chem. Phys. 61 (1974) 5421–5425. https://doi.org/10.1063/1.1681897.
[167] W.H. Green, J.K. Hancock, Measurement of CO(ν = 1) vibrational energy transfer rates using a frequency-doubled CO2 laser, J. Chem. Phys. 59 (1973) 4326–4335. https://doi.org/10.1063/1.1680629.
[168] E. Plönjes, P. Palm, W. Lee, M. D. Chidley, I.V. Adamovich, W. R. Lempert, J.W. Rich, Vibrational energy storage in high pressure mixtures of diatomic molecules, Chem. Phys. 260 (2000) 353–366. https://doi.org/10.1016/S0301-0104(00)00257-3.
[169] M. Capitelli, M. Dilonardo, E. Molinari, A theoretical calculation of dissociation rates of molecular hydrogen in electrical discharges, Chem. Phys. 20 (1977) 417–429. https://doi.org/10.1016/0301-0104(77)87030-4.
[170] M. Capitelli, Nonequilibrium Vibrational Kinetics, Springer-Verlag, Berlin, New York, 1986.
[171] R. J. Kee, F. M. Rupley, J. A. Miller, M. E. Coltrin, J. F. Grcar, E. Meeks, H. K. Moffat, A. E. Lutz, G. DixonLewis, M. D. Smooke, J. Warnatz, G. H. Evans, R. S. Larson, R. E. Mitchell, L. R. Petzold, W. C. Reynolds, M. Caracotsios, W. E. Stewart, P. Glarborg, C. Wang, and O. Adigun, CHEMKIN Collection, Release 3.6, San Digeo, CA, 2000.
[172] L. Terraz, T. Silva, A. Morillo-Candas, O. Guaitella, A. Tejero-del-Caz, L.L. Alves, V. Guerra, Influence of N2 on the CO2 vibrational distribution function and dissociation yield in non-

equilibrium plasmas, J. Phys. Appl. Phys. 53 (2019) 094002. https://doi.org/10.1088/1361-6463/ab55fb.
[173] G. Black, H. Wise, S. Schechter, R.L. Sharpless, Measurements of vibrationally excited molecules by Raman scattering. II. Surface deactivation of vibrationally excited N_2, J. Chem. Phys. 60 (1974) 3526–3536. https://doi.org/10.1063/1.1681570.
[174] D. Marinov, D. Lopatik, O. Guaitella, M. Hübner, Y. Ionikh, J. Röpcke, A. Rousseau, Surface vibrational relaxation of N_2 studied by CO_2 titration with time-resolved quantum cascade laser absorption spectroscopy, J. Phys. Appl. Phys. 45 (2012) 175201. https://doi.org/10.1088/0022-3727/45/17/175201.
[175] P. Ogloblina, In situ resource utilization on Mars using non-equilibrium plasmas, (2020) 139.
[176] J.P. Booth, O. Guaitella, A. Chatterjee, C. Drag, V. Guerra, D. Lopaev, S. Zyryanov, T. Rakhimova, D. Voloshin, Y. Mankelevich, Oxygen (3P) atom recombination on a Pyrex surface in an O2 plasma, Plasma Sources Sci. Technol. 28 (2019) 055005. https://doi.org/10.1088/1361-6595/ab13e8.
[177] A. Cenian, A. Chernukho, V. Borodin, G. Śliwiński, Modeling of Plasma-Chemical Reactions in Gas Mixture of CO2 Lasers I. Gas Decomposition in Pure CO2 Glow Discharge, Contrib. Plasma Phys. 34 (1994) 25–37. https://doi.org/10.1002/ctpp.2150340105.
[178] A.S. Kovalev, D.V. Lopaev, Y.A. Mankelevich, N.A. Popov, T.V. Rakhimova, A.Y. Poroykov, D.L. Carroll, Kinetics of in oxygen RF discharges, J. Phys. Appl. Phys. 38 (2005) 2360–2370. https://doi.org/10.1088/0022-3727/38/14/010.
[179] V.V. Ivanov, K.S. Klopovskii, D.V. Lopaev, A.T. Rakhimov, T.V. Rakhimova, Nonlocal nature of the electron energy spectrum in a glow discharge in pure O2: I. Nonlocal character of the electron distribution function, Plasma Phys. Rep. 26 (2000) 972–979. https://doi.org/10.1134/1.1323562.
[180] L.S. Polak, D.I. Slovetsky, Electron impact induced electronic excitation and molecular dissociation, Int. J. Radiat. Phys. Chem. 8 (1976) 257–282. https://doi.org/10.1016/0020-7055(76)90070-X.
[181] J. Levaton, A.N. Klein, J. Amorim, Kinetic investigation of N2 flowing DC discharges, Phys. Plasmas. 27 (2020) 063503. https://doi.org/10.1063/1.5144467.
[182] A.F. Silva, A.S. Morillo-Candás, A. Tejero-del-Caz, L.L. Alves, O. Guaitella, V. Guerra, A reaction mechanism for vibrationally-cold low-pressure CO2 plasmas, Plasma Sources Sci. Technol. 29 (2020) 125020. https://doi.org/10.1088/1361-6595/abc818.
[183] R. Snoeckx, S. Heijkers, K.V. Wesenbeeck, S. Lenaerts, A. Bogaerts, CO2 conversion in a dielectric barrier discharge plasma: N2 in the mix as a helping hand or problematic impurity?, Energy Environ. Sci. 9 (2016) 999–1011. https://doi.org/10.1039/C5EE03304G.
[184] A.S. Morillo-Candas, V. Guerra, O. Guaitella, Time Evolution of the Dissociation Fraction in rf CO2 Plasmas: Impact and Nature of Back-Reaction Mechanisms, J. Phys. Chem. C. 124 (2020) 17459–17475. https://doi.org/10.1021/acs.jpcc.0c03354.
[185] T. Silva, A.S. Morillo-Candas, O. Guaitella, V. Guerra, Modeling the time evolution of the dissociation fraction in low-pressure CO2 plasmas, J. CO2 Util. 53 (2021) 101719. https://doi.org/10.1016/j.jcou.2021.101719.
[186] S. Xu, J.C. Whitehead, P.A. Martin, CO2 conversion in a non-thermal, barium titanate packed bed plasma reactor: The effect of dilution by Ar and N2, Chem. Eng. J. 327 (2017) 764–773. https://doi.org/10.1016/j.cej.2017.06.090.
[187] M. Ramakers, I. Michielsen, R. Aerts, V. Meynen, A. Bogaerts, Effect of Argon or Helium on the CO2 Conversion in a Dielectric Barrier Discharge, Plasma Process. Polym. 12 (2015) 755–763. https://doi.org/10.1002/ppap.201400213.
[188] A. Ozkan, T. Dufour, G. Arnoult, P. De Keyzer, A. Bogaerts, F. Reniers, CO2–CH4 conversion and syngas formation at atmospheric pressure using a multi-electrode dielectric barrier discharge, J. CO2 Util. 9 (2015) 74–81. https://doi.org/10.1016/j.jcou.2015.01.002.
[189] World Health Organization, WHO global air quality guidelines: particulate matter (PM2.5 and PM10), ozone, nitrogen dioxide, sulfur dioxide and carbon monoxide, World Health Organization, 2021. https://apps.who.int/iris/handle/10665/345329 (accessed November 28, 2022).

[190] Directive 2008/50/EC of the European Parliament and of the Council on ambient air quality and cleaner air for Europe., (2008). https://www.ecolex.org/details/legislation/directive-200850ec-of-the-european-parliament-and-of-the-council-on-ambient-air-quality-and-cleaner-air-for-europe-lex-faoc080016/ (accessed November 28, 2022).
[191] B.F. Gordiets, C.M. Ferreira, V.L. Guerra, J.M.A.H. Loureiro, J. Nahorny, D. Pagnon, M. Touzeau, M. Vialle, Kinetic model of a low-pressure N/sub 2/-O/sub 2/ flowing glow discharge, IEEE Trans. Plasma Sci. 23 (1995) 750–768. https://doi.org/10.1109/27.467998.
[192] P. Coche, V. Guerra, L.L. Alves, Microwave air plasmas in capillaries at low pressure I. Self-consistent modeling, J. Phys. Appl. Phys. 49 (2016) 235207. https://doi.org/10.1088/0022-3727/49/23/235207.
[193] C.D. Pintassilgo, J. Loureiro, V. Guerra, Modelling of a N2–O2 flowing afterglow for plasma sterilization, J. Phys. Appl. Phys. 38 (2005) 417. https://doi.org/10.1088/0022-3727/38/3/011.
[194] B.F. Gordiets, C.M. Ferreira, Self-Consistent Modeling of Volume and Surface Processes in Air Plasma, AIAA J. 36 (1998) 1643–1651. https://doi.org/10.2514/2.566.
[195] A.S. Morillo-Candas, B.L.M. Klarenaar, C. Amoedo, V. Guerra, O. Guaitella, Effect of oxygen atoms on the vibrational kinetics of CO_2 and CO revealed by the use of a large surface area material, J. Phys. Appl. Phys. 54 (2021) 095208. https://doi.org/10.1088/1361-6463/abc992.
[196] R. Vertongen, G. Trenchev, R. Van Loenhout, A. Bogaerts, Enhancing CO2 conversion with plasma reactors in series and O2 removal, J. CO2 Util. 66 (2022) 102252. https://doi.org/10.1016/j.jcou.2022.102252.

Supporting Information

Validation of non-equilibrium kinetics in CO_2-N_2 plasmas

C. Fromentin[1], T. Silva[1], T. C. Dias[1], E. Baratte[2], O. Guaitella[2] and V. Guerra[1]

[1] Instituto de Plasmas e Fusão Nuclear, Instituto Superior Técnico, Universidade de Lisboa, Portugal

[2] Laboratoire de Physique des Plasmas (UMR 7648), CNRS, Univ. Paris Saclay, Sorbonne Université, École Polytechnique, France

A. Rate coefficients of some V-V processes included in the model

i. N_2-CO V-V:

The process:

$N_2(v) + CO(w) \leftrightarrow N_2(v') + CO(w')$ | nitrogenCO2VV| a, b, c |

has a rate coefficient of $k = 1{,}66 \cdot 10^{-30} \cdot \exp\left(a + b \cdot T^{-1/3} + c \cdot T^{-2/3}\right)$ in m^3s^{-1}, with T the gas temperature.

N2(X,v=1) + CO(X,v=0) ↔ N2(X,v=0) + CO(X,v=1) | nitrogenCO2VV| 26.3332, -28.231, 36.2268|

N2(X,v=2) + CO(X,v=0) ↔ N2(X,v=1) + CO(X,v=1) | nitrogenCO2VV| 20.3092, 68.1801, -287.656|

N2(X,v=3) + CO(X,v=0) ↔ N2(X,v=2) + CO(X,v=1) | nitrogenCO2VV| 22.0824, 44.2821, -175.498|

N2(X,v=4) + CO(X,v=0) ↔ N2(X,v=3) + CO(X,v=1) | nitrogenCO2VV| 24.0239, 18.1109, -65.108|

N2(X,v=5) + CO(X,v=0) ↔ N2(X,v=4) + CO(X,v=1) | nitrogenCO2VV| 25.8676, -6.42702, 32.3927|

N2(X,v=6) + CO(X,v=0) ↔ N2(X,v=5) + CO(X,v=1) | nitrogenCO2VV| 27.7473, -31.3048, 125.122|

N2(X,v=7) + CO(X,v=0) ↔ N2(X,v=6) + CO(X,v=1) | nitrogenCO2VV| 29.5121, -54.0773, 203.928|

N2(X,v=8) + CO(X,v=0) ↔ N2(X,v=7) + CO(X,v=1) | nitrogenCO2VV| 30.0891, -58.7989, 212.465|

N2(X,v=9) + CO(X,v=0) ↔ N2(X,v=8) + CO(X,v=1) | nitrogenCO2VV| 30.881, -69.8849, 256.471|

N2(X,v=10) + CO(X,v=0) ↔ N2(X,v=9) + CO(X,v=1) | nitrogenCO2VV| 29.5312, -45.2338, 149.915|

N2(X,v=11) + CO(X,v=0) ↔ N2(X,v=10) + CO(X,v=1) | nitrogenCO2VV| 29.5352, -42.901, 129.101|

N2(X,v=12) + CO(X,v=0) ↔ N2(X,v=11) + CO(X,v=1) | nitrogenCO2VV| 29.8874, -45.2534, 120.008|

N2(X,v=13) + CO(X,v=0) ↔ N2(X,v=12) + CO(X,v=1) | nitrogenCO2VV| 29.9643, -42.9403, 89.0297|

N2(X,v=14) + CO(X,v=0) ↔ N2(X,v=13) + CO(X,v=1) | nitrogenCO2VV| 29.3396, -29.103, 9.7148|

N2(X,v=15) + CO(X,v=0) ↔ N2(X,v=14) + CO(X,v=1) | nitrogenCO2VV| 27.8155, -0.646867, -129.407|

N2(X,v=16) + CO(X,v=0) ↔ N2(X,v=15) + CO(X,v=1) | nitrogenCO2VV| 27.1068, 12.9426, -203.402|

N2(X,v=17) + CO(X,v=0) ↔ N2(X,v=16) + CO(X,v=1) | nitrogenCO2VV| 28.6016, -12.1581, -111.344|

N2(X,v=18) + CO(X,v=0) ↔ N2(X,v=17) + CO(X,v=1) | nitrogenCO2VV| 29.7772, -30.2926, -58.3128|

N2(X,v=19) + CO(X,v=0) ↔ N2(X,v=18) + CO(X,v=1) | nitrogenCO2VV| 29.17, -17.065, -143.787|

N2(X,v=20) + CO(X,v=0) ↔ N2(X,v=19) + CO(X,v=1) | nitrogenCO2VV| 34.6908, -104.556, 179.69|

N2(X,v=21) + CO(X,v=0) ↔ N2(X,v=20) + CO(X,v=1) | nitrogenCO2VV| 32.109, -54.5671, -74.0396|

N2(X,v=22) + CO(X,v=0) ↔ N2(X,v=21) + CO(X,v=1) | nitrogenCO2VV| 24.7211, 79.8345, -695.697|

N2(X,v=23) + CO(X,v=0) ↔ N2(X,v=22) + CO(X,v=1) | nitrogenCO2VV| 24.9209, 73.9707, -674.065|

N2(X,v=24) + CO(X,v=0) ↔ N2(X,v=23) + CO(X,v=1) | nitrogenCO2VV| 28.5622, 5.81752, -373.63|

N2(X,v=25) + CO(X,v=0) ↔ N2(X,v=24) + CO(X,v=1) | nitrogenCO2VV| 31.154, -41.5012, -176.977|

N2(X,v=26) + CO(X,v=0) ↔ N2(X,v=25) + CO(X,v=1) | nitrogenCO2VV| 32.2306, -60.632, -111.204|

N2(X,v=27) + CO(X,v=0) ↔ N2(X,v=26) + CO(X,v=1) | nitrogenCO2VV| 33.0182, -74.8529, -65.8755|

N2(X,v=28) + CO(X,v=0) ↔ N2(X,v=27) + CO(X,v=1) | nitrogenCO2VV| 33.9564, -91.9747, -6.32267|

N2(X,v=29) + CO(X,v=0) ↔ N2(X,v=28) + CO(X,v=1) | nitrogenCO2VV| 43.4796, -254.273, 663.788|

N2(X,v=30) + CO(X,v=0) ↔ N2(X,v=29) + CO(X,v=1) | nitrogenCO2VV| 30.564, -17.9899, -424.744|

N2(X,v=31) + CO(X,v=0) ↔ N2(X,v=30) + CO(X,v=1) | nitrogenCO2VV| 27.7379, 28.5226, -625.886|

N2(X,v=32) + CO(X,v=0) ↔ N2(X,v=31) + CO(X,v=1) | nitrogenCO2VV| 30.829, -33.3464, -334.196|

N2(X,v=33) + CO(X,v=0) ↔ N2(X,v=32) + CO(X,v=1) | nitrogenCO2VV| 33.6843, -88.9491, -81.1479|

N2(X,v=34) + CO(X,v=0) ↔ N2(X,v=33) + CO(X,v=1) | nitrogenCO2VV| 34.7668, -110.18, 5.64985|

N2(X,v=35) + CO(X,v=0) ↔ N2(X,v=34) + CO(X,v=1) | nitrogenCO2VV| 34.8102, -111.565, -1.97593|

N2(X,v=36) + CO(X,v=0) ↔ N2(X,v=35) + CO(X,v=1) | nitrogenCO2VV| 34.7416, -110.751, -20.2669|

N2(X,v=37) + CO(X,v=0) ↔ N2(X,v=36) + CO(X,v=1) | nitrogenCO2VV| 34.4341, -105.579, -58.3648|

N2(X,v=38) + CO(X,v=0) ↔ N2(X,v=37) + CO(X,v=1) | nitrogenCO2VV| 45.5932, -299.167, 761.766|

N2(X,v=39) + CO(X,v=0) ↔ N2(X,v=38) + CO(X,v=1) | nitrogenCO2VV| 26.2462, 59.0595, -902.365|

N2(X,v=40) + CO(X,v=0) ↔ N2(X,v=39) + CO(X,v=1) | nitrogenCO2VV| 27.0993, 36.8597, -782.868|

N2(X,v=41) + CO(X,v=0) ↔ N2(X,v=40) + CO(X,v=1) | nitrogenCO2VV| 31.73, -54.0204, -354.017|

N2(X,v=42) + CO(X,v=0) ↔ N2(X,v=41) + CO(X,v=1) | nitrogenCO2VV| 34.2438, -102.633, -136.098|

N2(X,v=43) + CO(X,v=0) ↔ N2(X,v=42) + CO(X,v=1) | nitrogenCO2VV| 34.5945, -109.5, -119.431|

N2(X,v=44) + CO(X,v=0) ↔ N2(X,v=43) + CO(X,v=1) | nitrogenCO2VV| 34.6051, -109.844, -134.055|

N2(X,v=45) + CO(X,v=0) ↔ N2(X,v=44) + CO(X,v=1) | nitrogenCO2VV| 34.6302, -110.461, -147.463|

N2(X,v=46) + CO(X,v=0) ↔ N2(X,v=45) + CO(X,v=1) | nitrogenCO2VV| 34.4717, -107.741, -176.064|

N2(X,v=47) + CO(X,v=0) ↔ N2(X,v=46) + CO(X,v=1) | nitrogenCO2VV| 48.1873, -349.272, 867.79|

N2(X,v=48) + CO(X,v=0) ↔ N2(X,v=47) + CO(X,v=1) | nitrogenCO2VV| 22.0091, 138.858, -1412.78|

N2(X,v=49) + CO(X,v=0) ↔ N2(X,v=48) + CO(X,v=1) | nitrogenCO2VV| 27.3199, 31.3902, -886.6|

N2(X,v=50) + CO(X,v=0) ↔ N2(X,v=49) + CO(X,v=1) | nitrogenCO2VV| 33.2078, -83.5415, -343.361|

N2(X,v=51) + CO(X,v=0) ↔ N2(X,v=50) + CO(X,v=1) | nitrogenCO2VV| 34.7509, -113.508, -215.362|

N2(X,v=52) + CO(X,v=0) ↔ N2(X,v=51) + CO(X,v=1) | nitrogenCO2VV| 34.8601, -115.775, -221.044|

N2(X,v=53) + CO(X,v=0) ↔ N2(X,v=52) + CO(X,v=1) | nitrogenCO2VV| 34.8929, -116.58, -233.768|

N2(X,v=54) + CO(X,v=0) ↔ N2(X,v=53) + CO(X,v=1) | nitrogenCO2VV| 34.9307, -117.489, -245.996|

N2(X,v=55) + CO(X,v=0) ↔ N2(X,v=54) + CO(X,v=1) | nitrogenCO2VV| 34.7726, -114.8, -274.767|

N2(X,v=56) + CO(X,v=0) ↔ N2(X,v=55) + CO(X,v=1) | nitrogenCO2VV| 50.7052, -398.104, 965.111|

N2(X,v=57) + CO(X,v=0) ↔ N2(X,v=56) + CO(X,v=1) | nitrogenCO2VV| 19.6094, 183.904, -1763.|

N2(X,v=58) + CO(X,v=0) ↔ N2(X,v=57) + CO(X,v=1) | nitrogenCO2VV| 28.7204, 2.91625, -881.976|

N2(X,v=59) + CO(X,v=0) ↔ N2(X,v=58) + CO(X,v=1) | nitrogenCO2VV| 34.3987, -107.96, -358.729|

N2(X,v=1) + CO(X,v=1) ↔ N2(X,v=0) + CO(X,v=2) | nitrogenCO2VV| 26.981, -26.0999, 7.89671|

N2(X,v=2) + CO(X,v=1) ↔ N2(X,v=1) + CO(X,v=2) | nitrogenCO2VV| 19.4259, 95.0473, -412.61|

N2(X,v=3) + CO(X,v=1) ↔ N2(X,v=2) + CO(X,v=2) | nitrogenCO2VV| 21.9281, 58.5236, -244.966|

N2(X,v=4) + CO(X,v=1) ↔ N2(X,v=3) + CO(X,v=2) | nitrogenCO2VV| 24.1953, 26.5833, -107.814|

N2(X,v=5) + CO(X,v=1) ↔ N2(X,v=4) + CO(X,v=2) | nitrogenCO2VV| 26.2081, -1.14478, 6.12999|

N2(X,v=6) + CO(X,v=1) ↔ N2(X,v=5) + CO(X,v=2) | nitrogenCO2VV| 28.2131, -28.4666, 112.38|

N2(X,v=7) + CO(X,v=1) ↔ N2(X,v=6) + CO(X,v=2) | nitrogenCO2VV| 30.1963, -55.0413, 209.764|

N2(X,v=8) + CO(X,v=1) ↔ N2(X,v=7) + CO(X,v=2) | nitrogenCO2VV| 31.1801, -65.8525, 243.291|

N2(X,v=9) + CO(X,v=1) ↔ N2(X,v=8) + CO(X,v=2) | nitrogenCO2VV| 31.6112, -70.6277, 262.664|

N2(X,v=10) + CO(X,v=1) ↔ N2(X,v=9) + CO(X,v=2) | nitrogenCO2VV| 30.3535, -47.7734, 166.84|

N2(X,v=11) + CO(X,v=1) ↔ N2(X,v=10) + CO(X,v=2) | nitrogenCO2VV| 30.0098, -40.4913, 132.572|

N2(X,v=12) + CO(X,v=1) ↔ N2(X,v=11) + CO(X,v=2) | nitrogenCO2VV| 30.4767, -44.8218, 134.47|

N2(X,v=13) + CO(X,v=1) ↔ N2(X,v=12) + CO(X,v=2) | nitrogenCO2VV| 30.6932, -45.0098, 116.586|

N2(X,v=14) + CO(X,v=1) ↔ N2(X,v=13) + CO(X,v=2) | nitrogenCO2VV| 30.3889, -36.6968, 62.4105|

N2(X,v=15) + CO(X,v=1) ↔ N2(X,v=14) + CO(X,v=2) | nitrogenCO2VV| 29.2469, -14.809, -47.3793|

N2(X,v=16) + CO(X,v=1) ↔ N2(X,v=15) + CO(X,v=2) | nitrogenCO2VV| 28.1446, 5.66111, -149.719|

N2(X,v=17) + CO(X,v=1) ↔ N2(X,v=16) + CO(X,v=2) | nitrogenCO2VV| 28.9285, -6.99532, -110.216|

N2(X,v=18) + CO(X,v=1) ↔ N2(X,v=17) + CO(X,v=2) | nitrogenCO2VV| 30.6683, -35.2702, -10.7146|

N2(X,v=19) + CO(X,v=1) ↔ N2(X,v=18) + CO(X,v=2) | nitrogenCO2VV| 29.8027, -17.6694, -113.42|

N2(X,v=20) + CO(X,v=1) ↔ N2(X,v=19) + CO(X,v=2) | nitrogenCO2VV| 34.4967, -90.5394, 146.727|

N2(X,v=21) + CO(X,v=1) ↔ N2(X,v=20) + CO(X,v=2) | nitrogenCO2VV| 32.998, -59.8838, -20.9005|

N2(X,v=22) + CO(X,v=1) ↔ N2(X,v=21) + CO(X,v=2) | nitrogenCO2VV| 26.3412, 61.4596, -584.133|

N2(X,v=23) + CO(X,v=1) ↔ N2(X,v=22) + CO(X,v=2) | nitrogenCO2VV| 25.2668, 79.482, -673.535|

N2(X,v=24) + CO(X,v=1) ↔ N2(X,v=23) + CO(X,v=2) | nitrogenCO2VV| 28.4635, 19.8308, -413.254|

N2(X,v=25) + CO(X,v=1) ↔ N2(X,v=24) + CO(X,v=2) | nitrogenCO2VV| 31.2705, -31.1343, -201.283|

N2(X,v=26) + CO(X,v=1) ↔ N2(X,v=25) + CO(X,v=2) | nitrogenCO2VV| 32.3347, -49.5656, -141.075|

N2(X,v=27) + CO(X,v=1) ↔ N2(X,v=26) + CO(X,v=2) | nitrogenCO2VV| 33.133, -63.5476, -99.1671|

N2(X,v=28) + CO(X,v=1) ↔ N2(X,v=27) + CO(X,v=2) | nitrogenCO2VV| 34.1563, -81.8531, -36.3461|

N2(X,v=29) + CO(X,v=1) ↔ N2(X,v=28) + CO(X,v=2) | nitrogenCO2VV| 43.6842, -243.848, 630.203|

N2(X,v=30) + CO(X,v=1) ↔ N2(X,v=29) + CO(X,v=2) | nitrogenCO2VV| 31.3319, -17.9028, -411.373|

N2(X,v=31) + CO(X,v=1) ↔ N2(X,v=30) + CO(X,v=2) | nitrogenCO2VV| 28.0961, 36.2131, -647.92|

N2(X,v=32) + CO(X,v=1) ↔ N2(X,v=31) + CO(X,v=2) | nitrogenCO2VV| 31.2603, -26.9969, -350.44|

N2(X,v=33) + CO(X,v=1) ↔ N2(X,v=32) + CO(X,v=2) | nitrogenCO2VV| 34.1982, -84.1272, -90.6923|

N2(X,v=34) + CO(X,v=1) ↔ N2(X,v=33) + CO(X,v=2) | nitrogenCO2VV| 35.4413, -108.427, 10.453|

N2(X,v=35) + CO(X,v=1) ↔ N2(X,v=34) + CO(X,v=2) | nitrogenCO2VV| 35.5695, -111.486, 10.8357|

N2(X,v=36) + CO(X,v=1) ↔ N2(X,v=35) + CO(X,v=2) | nitrogenCO2VV| 35.5216, -111.153, -4.9239|

N2(X,v=37) + CO(X,v=1) ↔ N2(X,v=36) + CO(X,v=2) | nitrogenCO2VV| 35.231, -106.389, -40.79|

N2(X,v=38) + CO(X,v=1) ↔ N2(X,v=37) + CO(X,v=2) | nitrogenCO2VV| 46.1449, -295.323, 757.31|

N2(X,v=39) + CO(X,v=1) ↔ N2(X,v=38) + CO(X,v=2) | nitrogenCO2VV| 27.5905, 47.765, -834.771|

N2(X,v=40) + CO(X,v=1) ↔ N2(X,v=39) + CO(X,v=2) | nitrogenCO2VV| 27.916, 35.5083, -762.061|

N2(X,v=41) + CO(X,v=1) ↔ N2(X,v=40) + CO(X,v=2) | nitrogenCO2VV| 32.3243, -51.1791, -352.959|

N2(X,v=42) + CO(X,v=1) ↔ N2(X,v=41) + CO(X,v=2) | nitrogenCO2VV| 34.9206, -101.417, -127.061|

N2(X,v=43) + CO(X,v=1) ↔ N2(X,v=42) + CO(X,v=2) | nitrogenCO2VV| 35.3166, -109.18, -105.987|

N2(X,v=44) + CO(X,v=1) ↔ N2(X,v=43) + CO(X,v=2) | nitrogenCO2VV| 35.3177, -109.364, -121.263|

N2(X,v=45) + CO(X,v=1) ↔ N2(X,v=44) + CO(X,v=2) | nitrogenCO2VV| 35.3346, -109.84, -135.264|

N2(X,v=46) + CO(X,v=1) ↔ N2(X,v=45) + CO(X,v=2) | nitrogenCO2VV| 35.1675, -106.973, -164.474|

N2(X,v=47) + CO(X,v=1) ↔ N2(X,v=46) + CO(X,v=2) | nitrogenCO2VV| 48.6326, -343.759, 856.996|

N2(X,v=48) + CO(X,v=1) ↔ N2(X,v=47) + CO(X,v=2) | nitrogenCO2VV| 23.0774, 132.474, -1366.88|

N2(X,v=49) + CO(X,v=1) ↔ N2(X,v=48) + CO(X,v=2) | nitrogenCO2VV| 27.9304, 33.803, -882.896|

N2(X,v=50) + CO(X,v=1) ↔ N2(X,v=49) + CO(X,v=2) | nitrogenCO2VV| 33.7625, -80.0616, -344.732|

N2(X,v=51) + CO(X,v=1) ↔ N2(X,v=50) + CO(X,v=2) | nitrogenCO2VV| 35.4266, -112.355, -205.541|

N2(X,v=52) + CO(X,v=1) ↔ N2(X,v=51) + CO(X,v=2) | nitrogenCO2VV| 35.5522, -114.938, -209.702|

N2(X,v=53) + CO(X,v=1) ↔ N2(X,v=52) + CO(X,v=2) | nitrogenCO2VV| 35.5844, -115.731, -222.468|

N2(X,v=54) + CO(X,v=1) ↔ N2(X,v=53) + CO(X,v=2) | nitrogenCO2VV| 35.6222, -116.641, -234.682|

N2(X,v=55) + CO(X,v=1) ↔ N2(X,v=54) + CO(X,v=2) | nitrogenCO2VV| 35.4659, -113.988, -263.261|

N2(X,v=56) + CO(X,v=1) ↔ N2(X,v=55) + CO(X,v=2) | nitrogenCO2VV| 51.1906, -393.34, 957.882|

N2(X,v=57) + CO(X,v=1) ↔ N2(X,v=56) + CO(X,v=2) | nitrogenCO2VV| 20.5333, 180.254, -1729.91|

N2(X,v=58) + CO(X,v=1) ↔ N2(X,v=57) + CO(X,v=2) | nitrogenCO2VV| 29.2418, 7.06244, -886.597|

N2(X,v=59) + CO(X,v=1) ↔ N2(X,v=58) + CO(X,v=2) | nitrogenCO2VV| 35.0137, -105.633, -354.509|

N2(X,v=1) + CO(X,v=2) ↔ N2(X,v=0) + CO(X,v=3) | nitrogenCO2VV| 27.4833, -26.3038, -12.1825|

N2(X,v=2) + CO(X,v=2) ↔ N2(X,v=1) + CO(X,v=3) | nitrogenCO2VV| 17.3403, 137.944, -608.467|

N2(X,v=3) + CO(X,v=2) ↔ N2(X,v=2) + CO(X,v=3) | nitrogenCO2VV| 21.2886, 76.4103, -332.498|

N2(X,v=4) + CO(X,v=2) ↔ N2(X,v=3) + CO(X,v=3) | nitrogenCO2VV| 24.0462, 35.9698, -157.594|

N2(X,v=5) + CO(X,v=2) ↔ N2(X,v=4) + CO(X,v=3) | nitrogenCO2VV| 26.2951, 4.01149, -23.4525|

N2(X,v=6) + CO(X,v=2) ↔ N2(X,v=5) + CO(X,v=3) | nitrogenCO2VV| 28.4639, -26.3416, 98.2404|

N2(X,v=7) + CO(X,v=2) ↔ N2(X,v=6) + CO(X,v=3) | nitrogenCO2VV| 30.624, -56.0838, 211.466|

N2(X,v=8) + CO(X,v=2) ↔ N2(X,v=7) + CO(X,v=3) | nitrogenCO2VV| 31.9653, -72.7365, 270.594|

N2(X,v=9) + CO(X,v=2) ↔ N2(X,v=8) + CO(X,v=3) | nitrogenCO2VV| 31.9634, -69.7467, 259.35|

N2(X,v=10) + CO(X,v=2) ↔ N2(X,v=9) + CO(X,v=3) | nitrogenCO2VV| 30.8039, -48.7856, 174.562|

N2(X,v=11) + CO(X,v=2) ↔ N2(X,v=10) + CO(X,v=3) | nitrogenCO2VV| 30.3042, -39.6059, 137.909|

N2(X,v=12) + CO(X,v=2) ↔ N2(X,v=11) + CO(X,v=3) | nitrogenCO2VV| 30.5861, -41.4426, 135.187|

N2(X,v=13) + CO(X,v=2) ↔ N2(X,v=12) + CO(X,v=3) | nitrogenCO2VV| 31.0533, -45.6196, 135.52|

N2(X,v=14) + CO(X,v=2) ↔ N2(X,v=13) + CO(X,v=3) | nitrogenCO2VV| 31.0201, -41.895, 102.467|

N2(X,v=15) + CO(X,v=2) ↔ N2(X,v=14) + CO(X,v=3) | nitrogenCO2VV| 30.2641, -26.5553, 21.6727|

N2(X,v=16) + CO(X,v=2) ↔ N2(X,v=15) + CO(X,v=3) | nitrogenCO2VV| 29.0803, -4.68498, -85.0465|

N2(X,v=17) + CO(X,v=2) ↔ N2(X,v=16) + CO(X,v=3) | nitrogenCO2VV| 29.1216, -4.43065, -99.578|

N2(X,v=18) + CO(X,v=2) ↔ N2(X,v=17) + CO(X,v=3) | nitrogenCO2VV| 31.3302, -41.1274, 38.8394|

N2(X,v=19) + CO(X,v=2) ↔ N2(X,v=18) + CO(X,v=3) | nitrogenCO2VV| 30.217, -19.4877, -78.8056|

N2(X,v=20) + CO(X,v=2) ↔ N2(X,v=19) + CO(X,v=3) | nitrogenCO2VV| 34.1178, -78.5852, 123.126|

N2(X,v=21) + CO(X,v=2) ↔ N2(X,v=20) + CO(X,v=3) | nitrogenCO2VV| 33.4137, -62.0127, 18.0351|

N2(X,v=22) + CO(X,v=2) ↔ N2(X,v=21) + CO(X,v=3) | nitrogenCO2VV| 27.9888, 37.15, -445.385|

N2(X,v=23) + CO(X,v=2) ↔ N2(X,v=22) + CO(X,v=3) | nitrogenCO2VV| 25.6785, 78.1875, -640.839|

N2(X,v=24) + CO(X,v=2) ↔ N2(X,v=23) + CO(X,v=3) | nitrogenCO2VV| 28.1667, 31.8651, -442.514|

N2(X,v=25) + CO(X,v=2) ↔ N2(X,v=24) + CO(X,v=3) | nitrogenCO2VV| 31.136, -21.8395, -218.864|

N2(X,v=26) + CO(X,v=2) ↔ N2(X,v=25) + CO(X,v=3) | nitrogenCO2VV| 32.2214, -40.2223, -160.912|

N2(X,v=27) + CO(X,v=2) ↔ N2(X,v=26) + CO(X,v=3) | nitrogenCO2VV| 32.9528, -52.5048, -129.149|

N2(X,v=28) + CO(X,v=2) ↔ N2(X,v=27) + CO(X,v=3) | nitrogenCO2VV| 33.9497, -69.923, -72.576|

N2(X,v=29) + CO(X,v=2) ↔ N2(X,v=28) + CO(X,v=3) | nitrogenCO2VV| 43.4483, -230.927, 587.018|

N2(X,v=30) + CO(X,v=2) ↔ N2(X,v=29) + CO(X,v=3) | nitrogenCO2VV| 31.7653, -17.1373, -399.931|

N2(X,v=31) + CO(X,v=2) ↔ N2(X,v=30) + CO(X,v=3) | nitrogenCO2VV| 28.0068, 46.7731, -682.424|

N2(X,v=32) + CO(X,v=2) ↔ N2(X,v=31) + CO(X,v=3) | nitrogenCO2VV| 31.2746, -18.3129, -376.844|

N2(X,v=33) + CO(X,v=2) ↔ N2(X,v=32) + CO(X,v=3) | nitrogenCO2VV| 34.335, -77.6478, -107.59|

N2(X,v=34) + CO(X,v=2) ↔ N2(X,v=33) + CO(X,v=3) | nitrogenCO2VV| 35.7497, -105.163, 8.2543|

N2(X,v=35) + CO(X,v=2) ↔ N2(X,v=34) + CO(X,v=3) | nitrogenCO2VV| 35.9973, -110.513, 19.3345|

N2(X,v=36) + CO(X,v=2) ↔ N2(X,v=35) + CO(X,v=3) | nitrogenCO2VV| 35.994, -111.097, 8.02783|

N2(X,v=37) + CO(X,v=2) ↔ N2(X,v=36) + CO(X,v=3) | nitrogenCO2VV| 35.7519, -107.318, -23.0184|

N2(X,v=38) + CO(X,v=2) ↔ N2(X,v=37) + CO(X,v=3) | nitrogenCO2VV| 46.4312, -291.792, 753.901|

N2(X,v=39) + CO(X,v=2) ↔ N2(X,v=38) + CO(X,v=3) | nitrogenCO2VV| 28.6614, 36.2975, -766.758|

N2(X,v=40) + CO(X,v=2) ↔ N2(X,v=39) + CO(X,v=3) | nitrogenCO2VV| 28.4726, 33.6972, -739.334|

N2(X,v=41) + CO(X,v=2) ↔ N2(X,v=40) + CO(X,v=3) | nitrogenCO2VV| 32.6487, -48.6264, -350.742|

N2(X,v=42) + CO(X,v=2) ↔ N2(X,v=41) + CO(X,v=3) | nitrogenCO2VV| 35.3147, -100.26, -117.921|

N2(X,v=43) + CO(X,v=2) ↔ N2(X,v=42) + CO(X,v=3) | nitrogenCO2VV| 35.762, -109.041, -91.8179|

N2(X,v=44) + CO(X,v=2) ↔ N2(X,v=43) + CO(X,v=3) | nitrogenCO2VV| 35.7518, -109.04, -107.828|

N2(X,v=45) + CO(X,v=2) ↔ N2(X,v=44) + CO(X,v=3) | nitrogenCO2VV| 35.7581, -109.334, -122.586|

N2(X,v=46) + CO(X,v=2) ↔ N2(X,v=45) + CO(X,v=3) | nitrogenCO2VV| 35.5787, -106.254, -152.683|

N2(X,v=47) + CO(X,v=2) ↔ N2(X,v=46) + CO(X,v=3) | nitrogenCO2VV| 48.7883, -338.208, 845.993|

N2(X,v=48) + CO(X,v=2) ↔ N2(X,v=47) + CO(X,v=3) | nitrogenCO2VV| 23.884, 125.604, -1318.74|

N2(X,v=49) + CO(X,v=2) ↔ N2(X,v=48) + CO(X,v=3) | nitrogenCO2VV| 28.2683, 35.9281, -877.83|

N2(X,v=50) + CO(X,v=2) ↔ N2(X,v=49) + CO(X,v=3) | nitrogenCO2VV| 34.0246, -76.4881, -346.563|

N2(X,v=51) + CO(X,v=2) ↔ N2(X,v=50) + CO(X,v=3) | nitrogenCO2VV| 35.8121, -111.155, -195.96|

N2(X,v=52) + CO(X,v=2) ↔ N2(X,v=51) + CO(X,v=3) | nitrogenCO2VV| 35.9568, -114.104, -198.354|

N2(X,v=53) + CO(X,v=2) ↔ N2(X,v=52) + CO(X,v=3) | nitrogenCO2VV| 35.9882, -114.882, -211.178|

N2(X,v=54) + CO(X,v=2) ↔ N2(X,v=53) + CO(X,v=3) | nitrogenCO2VV| 36.026, -115.791, -223.388|

N2(X,v=55) + CO(X,v=2) ↔ N2(X,v=54) + CO(X,v=3) | nitrogenCO2VV| 35.8714, -113.171, -251.782|

N2(X,v=56) + CO(X,v=2) ↔ N2(X,v=55) + CO(X,v=3) | nitrogenCO2VV| 51.3828, -388.47, 950.152|

N2(X,v=57) + CO(X,v=2) ↔ N2(X,v=56) + CO(X,v=3) | nitrogenCO2VV| 21.1819, 176.366, -1695.69|

N2(X,v=58) + CO(X,v=2) ↔ N2(X,v=57) + CO(X,v=3) | nitrogenCO2VV| 29.4826, 11.0718, -890.557|

N2(X,v=59) + CO(X,v=2) ↔ N2(X,v=58) + CO(X,v=3) | nitrogenCO2VV| 35.3341, -103.171, -350.943|

N2(X,v=1) + CO(X,v=3) ↔ N2(X,v=0) + CO(X,v=4) | nitrogenCO2VV| 28.0399, -29.5167, -20.2133|

N2(X,v=2) + CO(X,v=3) ↔ N2(X,v=1) + CO(X,v=4) | nitrogenCO2VV| 13.8918, 203.073, -904.017|

N2(X,v=3) + CO(X,v=3) ↔ N2(X,v=2) + CO(X,v=4) | nitrogenCO2VV| 20.2934, 98.6659, -441.184|

N2(X,v=4) + CO(X,v=3) ↔ N2(X,v=3) + CO(X,v=4) | nitrogenCO2VV| 23.7898, 45.528, -211.175|

N2(X,v=5) + CO(X,v=3) ↔ N2(X,v=4) + CO(X,v=4) | nitrogenCO2VV| 26.3439, 8.28304, -53.105|

N2(X,v=6) + CO(X,v=3) ↔ N2(X,v=5) + CO(X,v=4) | nitrogenCO2VV| 28.7007, -25.4209, 84.7976|

N2(X,v=7) + CO(X,v=3) ↔ N2(X,v=6) + CO(X,v=4) | nitrogenCO2VV| 30.9861, -57.514, 210.531|

N2(X,v=8) + CO(X,v=3) ↔ N2(X,v=7) + CO(X,v=4) | nitrogenCO2VV| 32.5146, -77.4178, 285.439|

N2(X,v=9) + CO(X,v=3) ↔ N2(X,v=8) + CO(X,v=4) | nitrogenCO2VV| 32.1491, -68.2122, 250.454|

N2(X,v=10) + CO(X,v=3) ↔ N2(X,v=9) + CO(X,v=4) | nitrogenCO2VV| 31.0571, -48.1596, 172.47|

N2(X,v=11) + CO(X,v=3) ↔ N2(X,v=10) + CO(X,v=4) | nitrogenCO2VV| 30.5592, -39.6642, 142.824|

N2(X,v=12) + CO(X,v=3) ↔ N2(X,v=11) + CO(X,v=4) | nitrogenCO2VV| 30.5894, -38.1716, 132.761|

N2(X,v=13) + CO(X,v=3) ↔ N2(X,v=12) + CO(X,v=4) | nitrogenCO2VV| 31.0996, -43.231, 140.519|

N2(X,v=14) + CO(X,v=3) ↔ N2(X,v=13) + CO(X,v=4) | nitrogenCO2VV| 31.4071, -44.8769, 130.811|

N2(X,v=15) + CO(X,v=3) ↔ N2(X,v=14) + CO(X,v=4) | nitrogenCO2VV| 31.019, -35.6442, 76.8818|

N2(X,v=16) + CO(X,v=3) ↔ N2(X,v=15) + CO(X,v=4) | nitrogenCO2VV| 29.9767, -16.1616, -18.1923|

N2(X,v=17) + CO(X,v=3) ↔ N2(X,v=16) + CO(X,v=4) | nitrogenCO2VV| 29.4407, -5.96878, -73.3649|

N2(X,v=18) + CO(X,v=3) ↔ N2(X,v=17) + CO(X,v=4) | nitrogenCO2VV| 31.9056, -47.3071, 87.4179|

N2(X,v=19) + CO(X,v=3) ↔ N2(X,v=18) + CO(X,v=4) | nitrogenCO2VV| 30.5841, -22.437, -40.94|

N2(X,v=20) + CO(X,v=3) ↔ N2(X,v=19) + CO(X,v=4) | nitrogenCO2VV| 33.7437, -68.9434, 109.336|

N2(X,v=21) + CO(X,v=3) ↔ N2(X,v=20) + CO(X,v=4) | nitrogenCO2VV| 33.5605, -61.5366, 45.0187|

N2(X,v=22) + CO(X,v=3) ↔ N2(X,v=21) + CO(X,v=4) | nitrogenCO2VV| 29.6205, 10.961, -298.823|

N2(X,v=23) + CO(X,v=3) ↔ N2(X,v=22) + CO(X,v=4) | nitrogenCO2VV| 26.3567, 69.6395, -574.67|

N2(X,v=24) + CO(X,v=3) ↔ N2(X,v=23) + CO(X,v=4) | nitrogenCO2VV| 27.9109, 40.7174, -456.41|

N2(X,v=25) + CO(X,v=3) ↔ N2(X,v=24) + CO(X,v=4) | nitrogenCO2VV| 30.9008, -13.1942, -232.125|

N2(X,v=26) + CO(X,v=3) ↔ N2(X,v=25) + CO(X,v=4) | nitrogenCO2VV| 32.1043, -33.3844, -167.386|

N2(X,v=27) + CO(X,v=3) ↔ N2(X,v=26) + CO(X,v=4) | nitrogenCO2VV| 32.7013, -42.7386, -151.171|

N2(X,v=28) + CO(X,v=3) ↔ N2(X,v=27) + CO(X,v=4) | nitrogenCO2VV| 33.5599, -57.2306, -109.976|

N2(X,v=29) + CO(X,v=3) ↔ N2(X,v=28) + CO(X,v=4) | nitrogenCO2VV| 42.9428, -215.624, 535.166|

N2(X,v=30) + CO(X,v=3) ↔ N2(X,v=29) + CO(X,v=4) | nitrogenCO2VV| 32.1047, -17.1061, -383.413|

N2(X,v=31) + CO(X,v=3) ↔ N2(X,v=30) + CO(X,v=4) | nitrogenCO2VV| 27.6726, 59.5068, -725.782|

N2(X,v=32) + CO(X,v=3) ↔ N2(X,v=31) + CO(X,v=4) | nitrogenCO2VV| 31.0242, -7.03326, -414.264|

N2(X,v=33) + CO(X,v=3) ↔ N2(X,v=32) + CO(X,v=4) | nitrogenCO2VV| 34.2496, -69.2999, -132.463|

N2(X,v=34) + CO(X,v=3) ↔ N2(X,v=33) + CO(X,v=4) | nitrogenCO2VV| 35.8407, -100.041, -2.28859|

N2(X,v=35) + CO(X,v=3) ↔ N2(X,v=34) + CO(X,v=4) | nitrogenCO2VV| 36.2392, -108.222, 21.7098|

N2(X,v=36) + CO(X,v=3) ↔ N2(X,v=35) + CO(X,v=4) | nitrogenCO2VV| 36.3094, -110.233, 17.0567|

N2(X,v=37) + CO(X,v=3) ↔ N2(X,v=36) + CO(X,v=4) | nitrogenCO2VV| 36.1555, -108.154, -6.02542|

N2(X,v=38) + CO(X,v=3) ↔ N2(X,v=37) + CO(X,v=4) | nitrogenCO2VV| 46.6161, -288.454, 750.973|

N2(X,v=39) + CO(X,v=3) ↔ N2(X,v=38) + CO(X,v=4) | nitrogenCO2VV| 29.6106, 25.0124, -700.032|

N2(X,v=40) + CO(X,v=3) ↔ N2(X,v=39) + CO(X,v=4) | nitrogenCO2VV| 28.9312, 31.5849, -715.466|

N2(X,v=41) + CO(X,v=3) ↔ N2(X,v=40) + CO(X,v=4) | nitrogenCO2VV| 32.8731, -46.3516, -347.456|

N2(X,v=42) + CO(X,v=3) ↔ N2(X,v=41) + CO(X,v=4) | nitrogenCO2VV| 35.5957, -99.1396, -108.816|

N2(X,v=43) + CO(X,v=3) ↔ N2(X,v=42) + CO(X,v=4) | nitrogenCO2VV| 36.102, -109.098, -76.8904|

N2(X,v=44) + CO(X,v=3) ↔ N2(X,v=43) + CO(X,v=4) | nitrogenCO2VV| 36.0795, -108.904, -93.6271|

N2(X,v=45) + CO(X,v=3) ↔ N2(X,v=44) + CO(X,v=4) | nitrogenCO2VV| 36.0726, -108.976, -109.297|

N2(X,v=46) + CO(X,v=3) ↔ N2(X,v=45) + CO(X,v=4) | nitrogenCO2VV| 35.8766, -105.614, -140.58|

N2(X,v=47) + CO(X,v=3) ↔ N2(X,v=46) + CO(X,v=4) | nitrogenCO2VV| 48.8266, -332.654, 834.931|

N2(X,v=48) + CO(X,v=3) ↔ N2(X,v=47) + CO(X,v=4) | nitrogenCO2VV| 24.6019, 118.195, -1268.11|

N2(X,v=49) + CO(X,v=3) ↔ N2(X,v=48) + CO(X,v=4) | nitrogenCO2VV| 28.5052, 37.735, -871.265|

N2(X,v=50) + CO(X,v=3) ↔ N2(X,v=49) + CO(X,v=4) | nitrogenCO2VV| 34.1655, -72.8472, -348.735|

N2(X,v=51) + CO(X,v=3) ↔ N2(X,v=50) + CO(X,v=4) | nitrogenCO2VV| 36.0776, -109.909, -186.621|

N2(X,v=52) + CO(X,v=3) ↔ N2(X,v=51) + CO(X,v=4) | nitrogenCO2VV| 36.2442, -113.279, -186.977|

N2(X,v=53) + CO(X,v=3) ↔ N2(X,v=52) + CO(X,v=4) | nitrogenCO2VV| 36.2745, -114.036, -199.883|

N2(X,v=54) + CO(X,v=3) ↔ N2(X,v=53) + CO(X,v=4) | nitrogenCO2VV| 36.312, -114.94, -212.107|

N2(X,v=55) + CO(X,v=3) ↔ N2(X,v=54) + CO(X,v=4) | nitrogenCO2VV| 36.1588, -112.35, -240.332|

N2(X,v=56) + CO(X,v=3) ↔ N2(X,v=55) + CO(X,v=4) | nitrogenCO2VV| 51.4514, -383.492, 941.914|

N2(X,v=57) + CO(X,v=3) ↔ N2(X,v=56) + CO(X,v=4) | nitrogenCO2VV| 21.7262, 172.225, -1660.27|

N2(X,v=58) + CO(X,v=3) ↔ N2(X,v=57) + CO(X,v=4) | nitrogenCO2VV| 29.6133, 14.9291, -893.783|

N2(X,v=59) + CO(X,v=3) ↔ N2(X,v=58) + CO(X,v=4) | nitrogenCO2VV| 35.5294, -100.57, -348.055|

N2(X,v=1) + CO(X,v=4) ↔ N2(X,v=0) + CO(X,v=5) | nitrogenCO2VV| 28.7124, -36.0457, -13.9044|

N2(X,v=2) + CO(X,v=4) ↔ N2(X,v=1) + CO(X,v=5) | nitrogenCO2VV| 9.96555, 276.42, -1240.94|

N2(X,v=3) + CO(X,v=4) ↔ N2(X,v=2) + CO(X,v=5) | nitrogenCO2VV| 19.0126, 125.06, -570.169|

N2(X,v=4) + CO(X,v=4) ↔ N2(X,v=3) + CO(X,v=5) | nitrogenCO2VV| 23.5601, 53.8472, -262.334|

N2(X,v=5) + CO(X,v=4) ↔ N2(X,v=4) + CO(X,v=5) | nitrogenCO2VV| 26.4837, 10.3646, -77.186|

N2(X,v=6) + CO(X,v=4) ↔ N2(X,v=5) + CO(X,v=5) | nitrogenCO2VV| 29.0255, -26.5243, 75.5598|

N2(X,v=7) + CO(X,v=4) ↔ N2(X,v=6) + CO(X,v=5) | nitrogenCO2VV| 31.3554, -59.646, 208.363|

N2(X,v=8) + CO(X,v=4) ↔ N2(X,v=7) + CO(X,v=5) | nitrogenCO2VV| 32.9103, -80.3156, 289.647|

N2(X,v=9) + CO(X,v=4) ↔ N2(X,v=8) + CO(X,v=5) | nitrogenCO2VV| 32.2215, -65.6863, 234.278|

N2(X,v=10) + CO(X,v=4) ↔ N2(X,v=9) + CO(X,v=5) | nitrogenCO2VV| 31.1683, -46.4548, 163.069|

N2(X,v=11) + CO(X,v=4) ↔ N2(X,v=10) + CO(X,v=5) | nitrogenCO2VV| 30.3445, -33.2697, 120.98|

N2(X,v=12) + CO(X,v=4) ↔ N2(X,v=11) + CO(X,v=5) | nitrogenCO2VV| 30.8673, -39.6111, 142.913|

N2(X,v=13) + CO(X,v=4) ↔ N2(X,v=12) + CO(X,v=5) | nitrogenCO2VV| 30.9429, -38.807, 134.935|

N2(X,v=14) + CO(X,v=4) ↔ N2(X,v=13) + CO(X,v=5) | nitrogenCO2VV| 31.536, -44.8697, 145.124|

N2(X,v=15) + CO(X,v=4) ↔ N2(X,v=14) + CO(X,v=5) | nitrogenCO2VV| 31.5625, -42.1543, 118.813|

N2(X,v=16) + CO(X,v=4) ↔ N2(X,v=15) + CO(X,v=5) | nitrogenCO2VV| 30.7966, -27.205, 43.9881|

N2(X,v=17) + CO(X,v=4) ↔ N2(X,v=16) + CO(X,v=5) | nitrogenCO2VV| 29.9453, -11.6386, -31.9725|

N2(X,v=18) + CO(X,v=4) ↔ N2(X,v=17) + CO(X,v=5) | nitrogenCO2VV| 32.4229, -53.3216, 132.543|

N2(X,v=19) + CO(X,v=4) ↔ N2(X,v=18) + CO(X,v=5) | nitrogenCO2VV| 30.9588, -26.4456, -0.733776|

N2(X,v=20) + CO(X,v=4) ↔ N2(X,v=19) + CO(X,v=5) | nitrogenCO2VV| 33.4465, -61.8396, 105.668|

N2(X,v=21) + CO(X,v=4) ↔ N2(X,v=20) + CO(X,v=5) | nitrogenCO2VV| 33.5614, -59.6581, 65.0434|

N2(X,v=22) + CO(X,v=4) ↔ N2(X,v=21) + CO(X,v=5) | nitrogenCO2VV| 31.0166, -12.0466, -167.913|

N2(X,v=23) + CO(X,v=4) ↔ N2(X,v=22) + CO(X,v=5) | nitrogenCO2VV| 27.3369, 54.3095, -478.07|

N2(X,v=24) + CO(X,v=4) ↔ N2(X,v=23) + CO(X,v=5) | nitrogenCO2VV| 27.8215, 45.1497, -449.872|

N2(X,v=25) + CO(X,v=4) ↔ N2(X,v=24) + CO(X,v=5) | nitrogenCO2VV| 30.601, -4.80598, -243.414|

N2(X,v=26) + CO(X,v=4) ↔ N2(X,v=25) + CO(X,v=5) | nitrogenCO2VV| 32.0497, -29.2349, -160.124|

N2(X,v=27) + CO(X,v=4) ↔ N2(X,v=26) + CO(X,v=5) | nitrogenCO2VV| 32.4764, -35.0556, -161.759|

N2(X,v=28) + CO(X,v=4) ↔ N2(X,v=27) + CO(X,v=5) | nitrogenCO2VV| 33.1095, -45.0786, -142.571|

N2(X,v=29) + CO(X,v=4) ↔ N2(X,v=28) + CO(X,v=5) | nitrogenCO2VV| 42.2409, -198.377, 476.918|

N2(X,v=30) + CO(X,v=4) ↔ N2(X,v=29) + CO(X,v=5) | nitrogenCO2VV| 32.4783, -19.2927, -354.594|

N2(X,v=31) + CO(X,v=4) ↔ N2(X,v=30) + CO(X,v=5) | nitrogenCO2VV| 27.2177, 73.0085, -771.099|

N2(X,v=32) + CO(X,v=4) ↔ N2(X,v=31) + CO(X,v=5) | nitrogenCO2VV| 30.5627, 6.75581, -461.952|

N2(X,v=33) + CO(X,v=4) ↔ N2(X,v=32) + CO(X,v=5) | nitrogenCO2VV| 33.9878, -59.0261, -165.177|

N2(X,v=34) + CO(X,v=4) ↔ N2(X,v=33) + CO(X,v=5) | nitrogenCO2VV| 35.7541, -92.8773, -21.6812|

N2(X,v=35) + CO(X,v=4) ↔ N2(X,v=34) + CO(X,v=5) | nitrogenCO2VV| 36.3242, -104.205, 16.3304|

N2(X,v=36) + CO(X,v=4) ↔ N2(X,v=35) + CO(X,v=5) | nitrogenCO2VV| 36.4985, -108.17, 20.504|

N2(X,v=37) + CO(X,v=4) ↔ N2(X,v=36) + CO(X,v=5) | nitrogenCO2VV| 36.4777, -108.577, 8.76549|

N2(X,v=38) + CO(X,v=4) ↔ N2(X,v=37) + CO(X,v=5) | nitrogenCO2VV| 46.7419, -285.105, 747.615|

N2(X,v=39) + CO(X,v=4) ↔ N2(X,v=38) + CO(X,v=5) | nitrogenCO2VV| 30.4683, 14.3525, -636.677|

N2(X,v=40) + CO(X,v=4) ↔ N2(X,v=39) + CO(X,v=5) | nitrogenCO2VV| 29.3312, 29.4419, -691.741|

N2(X,v=41) + CO(X,v=4) ↔ N2(X,v=40) + CO(X,v=5) | nitrogenCO2VV| 33.0479, -44.2884, -343.437|

N2(X,v=42) + CO(X,v=4) ↔ N2(X,v=41) + CO(X,v=5) | nitrogenCO2VV| 35.8143, -97.9997, -100.055|

N2(X,v=43) + CO(X,v=4) ↔ N2(X,v=42) + CO(X,v=5) | nitrogenCO2VV| 36.3897, -109.339, -61.2993|

N2(X,v=44) + CO(X,v=4) ↔ N2(X,v=43) + CO(X,v=5) | nitrogenCO2VV| 36.3557, -108.98, -78.5912|

N2(X,v=45) + CO(X,v=4) ↔ N2(X,v=44) + CO(X,v=5) | nitrogenCO2VV| 36.3334, -108.799, -95.2798|

N2(X,v=46) + CO(X,v=4) ↔ N2(X,v=45) + CO(X,v=5) | nitrogenCO2VV| 36.1168, -105.086, -128.024|

N2(X,v=47) + CO(X,v=4) ↔ N2(X,v=46) + CO(X,v=5) | nitrogenCO2VV| 48.8035, -327.144, 824.006|

N2(X,v=48) + CO(X,v=4) ↔ N2(X,v=47) + CO(X,v=5) | nitrogenCO2VV| 25.2874, 110.195, -1214.76|

N2(X,v=49) + CO(X,v=4) ↔ N2(X,v=48) + CO(X,v=5) | nitrogenCO2VV| 28.6964, 39.1873, -863.042|

N2(X,v=50) + CO(X,v=4) ↔ N2(X,v=49) + CO(X,v=5) | nitrogenCO2VV| 34.2404, -69.1724, -351.095|

N2(X,v=51) + CO(X,v=4) ↔ N2(X,v=50) + CO(X,v=5) | nitrogenCO2VV| 36.2763, -108.619, -177.511|

N2(X,v=52) + CO(X,v=4) ↔ N2(X,v=51) + CO(X,v=5) | nitrogenCO2VV| 36.468, -112.471, -175.537|

N2(X,v=53) + CO(X,v=4) ↔ N2(X,v=52) + CO(X,v=5) | nitrogenCO2VV| 36.4968, -113.2, -188.558|

N2(X,v=54) + CO(X,v=4) ↔ N2(X,v=53) + CO(X,v=5) | nitrogenCO2VV| 36.5336, -114.091, -200.825|

N2(X,v=55) + CO(X,v=4) ↔ N2(X,v=54) + CO(X,v=5) | nitrogenCO2VV| 36.3815, -111.526, -228.909|

N2(X,v=56) + CO(X,v=4) ↔ N2(X,v=55) + CO(X,v=5) | nitrogenCO2VV| 51.4497, -378.406, 933.164|

N2(X,v=57) + CO(X,v=4) ↔ N2(X,v=56) + CO(X,v=5) | nitrogenCO2VV| 22.2202, 167.809, -1623.57|

N2(X,v=58) + CO(X,v=4) ↔ N2(X,v=57) + CO(X,v=5) | nitrogenCO2VV| 29.6881, 18.6193, -896.203|

N2(X,v=59) + CO(X,v=4) ↔ N2(X,v=58) + CO(X,v=5) | nitrogenCO2VV| 35.6527, -97.8252, -345.861|

N2(X,v=1) + CO(X,v=5) ↔ N2(X,v=0) + CO(X,v=6) | nitrogenCO2VV| 29.5142, -45.8604, 7.53336|

N2(X,v=2) + CO(X,v=5) ↔ N2(X,v=1) + CO(X,v=6) | nitrogenCO2VV| 6.01693, 350.254, -1584.71|

N2(X,v=3) + CO(X,v=5) ↔ N2(X,v=2) + CO(X,v=6) | nitrogenCO2VV| 17.6738, 152.078, -704.339|

N2(X,v=4) + CO(X,v=5) ↔ N2(X,v=3) + CO(X,v=6) | nitrogenCO2VV| 23.4978, 58.8402, -301.726|

N2(X,v=5) + CO(X,v=5) ↔ N2(X,v=4) + CO(X,v=6) | nitrogenCO2VV| 26.8328, 8.57754, -88.2173|

N2(X,v=6) + CO(X,v=5) ↔ N2(X,v=5) + CO(X,v=6) | nitrogenCO2VV| 29.5105, -30.5336, 74.581|

N2(X,v=7) + CO(X,v=5) ↔ N2(X,v=6) + CO(X,v=6) | nitrogenCO2VV| 31.7628, -62.6401, 205.957|

N2(X,v=8) + CO(X,v=5) ↔ N2(X,v=7) + CO(X,v=6) | nitrogenCO2VV| 33.1834, -81.5264, 283.71|

N2(X,v=9) + CO(X,v=5) ↔ N2(X,v=8) + CO(X,v=6) | nitrogenCO2VV| 32.2106, -62.1688, 210.767|

N2(X,v=10) + CO(X,v=5) ↔ N2(X,v=9) + CO(X,v=6) | nitrogenCO2VV| 31.1889, -43.7306, 146.179|

N2(X,v=11) + CO(X,v=5) ↔ N2(X,v=10) + CO(X,v=6) | nitrogenCO2VV| 30.1934, -28.4173, 100.894|

N2(X,v=12) + CO(X,v=5) ↔ N2(X,v=11) + CO(X,v=6) | nitrogenCO2VV| 30.4178, -30.5468, 112.43|

N2(X,v=13) + CO(X,v=5) ↔ N2(X,v=12) + CO(X,v=6) | nitrogenCO2VV| 31.3229, -42.3498, 152.611|

N2(X,v=14) + CO(X,v=5) ↔ N2(X,v=13) + CO(X,v=6) | nitrogenCO2VV| 31.349, -40.9694, 142.642|

N2(X,v=15) + CO(X,v=5) ↔ N2(X,v=14) + CO(X,v=6) | nitrogenCO2VV| 31.8887, -45.8982, 147.361|

N2(X,v=16) + CO(X,v=5) ↔ N2(X,v=15) + CO(X,v=6) | nitrogenCO2VV| 31.508, -36.9472, 97.9109|

N2(X,v=17) + CO(X,v=5) ↔ N2(X,v=16) + CO(X,v=6) | nitrogenCO2VV| 30.5881, -20.1511, 18.6202|

N2(X,v=18) + CO(X,v=5) ↔ N2(X,v=17) + CO(X,v=6) | nitrogenCO2VV| 32.8848, -58.7855, 172.331|

N2(X,v=19) + CO(X,v=5) ↔ N2(X,v=18) + CO(X,v=6) | nitrogenCO2VV| 31.3515, -31.1981, 39.9442|

N2(X,v=20) + CO(X,v=5) ↔ N2(X,v=19) + CO(X,v=6) | nitrogenCO2VV| 33.2572, -57.285, 111.454|

N2(X,v=21) + CO(X,v=5) ↔ N2(X,v=20) + CO(X,v=6) | nitrogenCO2VV| 33.5127, -57.6153, 83.1573|

N2(X,v=22) + CO(X,v=5) ↔ N2(X,v=21) + CO(X,v=6) | nitrogenCO2VV| 32.0087, -28.4057, -68.2942|

N2(X,v=23) + CO(X,v=5) ↔ N2(X,v=22) + CO(X,v=6) | nitrogenCO2VV| 28.5656, 33.7739, -359.147|

N2(X,v=24) + CO(X,v=5) ↔ N2(X,v=23) + CO(X,v=6) | nitrogenCO2VV| 27.9806, 44.1908, -419.117|

N2(X,v=25) + CO(X,v=5) ↔ N2(X,v=24) + CO(X,v=6) | nitrogenCO2VV| 30.2715, 3.2029, -252.75|

N2(X,v=26) + CO(X,v=5) ↔ N2(X,v=25) + CO(X,v=6) | nitrogenCO2VV| 32.0498, -27.1048, -142.78|

N2(X,v=27) + CO(X,v=5) ↔ N2(X,v=26) + CO(X,v=6) | nitrogenCO2VV| 32.33, -29.924, -159.196|

N2(X,v=28) + CO(X,v=5) ↔ N2(X,v=27) + CO(X,v=6) | nitrogenCO2VV| 32.6899, -34.6917, -165.003|

N2(X,v=29) + CO(X,v=5) ↔ N2(X,v=28) + CO(X,v=6) | nitrogenCO2VV| 41.4027, -179.9, 415.623|

N2(X,v=30) + CO(X,v=5) ↔ N2(X,v=29) + CO(X,v=6) | nitrogenCO2VV| 32.9607, -24.6947, -308.695|

N2(X,v=31) + CO(X,v=5) ↔ N2(X,v=30) + CO(X,v=6) | nitrogenCO2VV| 26.7718, 85.2295, -808.576|

N2(X,v=32) + CO(X,v=5) ↔ N2(X,v=31) + CO(X,v=6) | nitrogenCO2VV| 29.9399, 22.4977, -517.029|

N2(X,v=33) + CO(X,v=5) ↔ N2(X,v=32) + CO(X,v=6) | nitrogenCO2VV| 33.5765, -46.9662, -204.696|

N2(X,v=34) + CO(X,v=5) ↔ N2(X,v=33) + CO(X,v=6) | nitrogenCO2VV| 35.5135, -83.7479, -49.1636|

N2(X,v=35) + CO(X,v=5) ↔ N2(X,v=34) + CO(X,v=6) | nitrogenCO2VV| 36.2572, -98.173, 2.18915|

N2(X,v=36) + CO(X,v=5) ↔ N2(X,v=35) + CO(X,v=6) | nitrogenCO2VV| 36.5624, -104.525, 16.8451|

N2(X,v=37) + CO(X,v=5) ↔ N2(X,v=36) + CO(X,v=6) | nitrogenCO2VV| 36.7179, -108.158, 19.524|

N2(X,v=38) + CO(X,v=5) ↔ N2(X,v=37) + CO(X,v=6) | nitrogenCO2VV| 46.8157, -281.452, 742.575|

N2(X,v=39) + CO(X,v=5) ↔ N2(X,v=38) + CO(X,v=6) | nitrogenCO2VV| 31.2319, 4.81176, -578.966|

N2(X,v=40) + CO(X,v=5) ↔ N2(X,v=39) + CO(X,v=6) | nitrogenCO2VV| 29.6753, 27.667, -670.008|

N2(X,v=41) + CO(X,v=5) ↔ N2(X,v=40) + CO(X,v=6) | nitrogenCO2VV| 33.1897, -42.2954, -339.355|

N2(X,v=42) + CO(X,v=5) ↔ N2(X,v=41) + CO(X,v=6) | nitrogenCO2VV| 35.9893, -96.735, -92.1615|

N2(X,v=43) + CO(X,v=5) ↔ N2(X,v=42) + CO(X,v=6) | nitrogenCO2VV| 36.6468, -109.711, -45.3402|

N2(X,v=44) + CO(X,v=5) ↔ N2(X,v=43) + CO(X,v=6) | nitrogenCO2VV| 36.6049, -109.269, -62.7512|

N2(X,v=45) + CO(X,v=5) ↔ N2(X,v=44) + CO(X,v=6) | nitrogenCO2VV| 36.566, -108.824, -80.4649|

N2(X,v=46) + CO(X,v=5) ↔ N2(X,v=45) + CO(X,v=6) | nitrogenCO2VV| 36.3256, -104.713, -114.849|

N2(X,v=47) + CO(X,v=5) ↔ N2(X,v=46) + CO(X,v=6) | nitrogenCO2VV| 48.7461, -321.736, 813.453|

N2(X,v=48) + CO(X,v=5) ↔ N2(X,v=47) + CO(X,v=6) | nitrogenCO2VV| 25.9671, 101.551, -1158.5|

N2(X,v=49) + CO(X,v=5) ↔ N2(X,v=48) + CO(X,v=6) | nitrogenCO2VV| 28.868, 40.2428, -852.982|

N2(X,v=50) + CO(X,v=5) ↔ N2(X,v=49) + CO(X,v=6) | nitrogenCO2VV| 34.2751, -65.5053, -353.456|

N2(X,v=51) + CO(X,v=5) ↔ N2(X,v=50) + CO(X,v=6) | nitrogenCO2VV| 36.4327, -107.294, -168.597|

N2(X,v=52) + CO(X,v=5) ↔ N2(X,v=51) + CO(X,v=6) | nitrogenCO2VV| 36.6527, -111.693, -163.981|

N2(X,v=53) + CO(X,v=5) ↔ N2(X,v=52) + CO(X,v=6) | nitrogenCO2VV| 36.6792, -112.382, -177.168|

N2(X,v=54) + CO(X,v=5) ↔ N2(X,v=53) + CO(X,v=6) | nitrogenCO2VV| 36.7149, -113.251, -189.519|

N2(X,v=55) + CO(X,v=5) ↔ N2(X,v=54) + CO(X,v=6) | nitrogenCO2VV| 36.5633, -110.7, -217.507|

N2(X,v=56) + CO(X,v=5) ↔ N2(X,v=55) + CO(X,v=6) | nitrogenCO2VV| 51.4013, -373.211, 923.903|

N2(X,v=57) + CO(X,v=5) ↔ N2(X,v=56) + CO(X,v=6) | nitrogenCO2VV| 22.6891, 163.1, -1585.49|

N2(X,v=58) + CO(X,v=5) ↔ N2(X,v=57) + CO(X,v=6) | nitrogenCO2VV| 29.7315, 22.1274, -897.746|

N2(X,v=59) + CO(X,v=5) ↔ N2(X,v=58) + CO(X,v=6) | nitrogenCO2VV| 35.7277, -94.9358, -344.367|

N2(X,v=1) + CO(X,v=6) ↔ N2(X,v=0) + CO(X,v=7) | nitrogenCO2VV| 30.4277, -58.554, 43.123|

N2(X,v=2) + CO(X,v=6) ↔ N2(X,v=1) + CO(X,v=7) | nitrogenCO2VV| 2.225, 421.313, -1919.33|

N2(X,v=3) + CO(X,v=6) ↔ N2(X,v=2) + CO(X,v=7) | nitrogenCO2VV| 16.604, 174.121, -818.798|

N2(X,v=4) + CO(X,v=6) ↔ N2(X,v=3) + CO(X,v=7) | nitrogenCO2VV| 23.7337, 58.3391, -319.318|

N2(X,v=5) + CO(X,v=6) ↔ N2(X,v=4) + CO(X,v=7) | nitrogenCO2VV| 27.4781, 1.50919, -79.4283|

N2(X,v=6) + CO(X,v=6) ↔ N2(X,v=5) + CO(X,v=7) | nitrogenCO2VV| 30.1914, -37.9909, 84.9749|

N2(X,v=7) + CO(X,v=6) ↔ N2(X,v=6) + CO(X,v=7) | nitrogenCO2VV| 32.2119, -66.4584, 203.827|

N2(X,v=8) + CO(X,v=6) ↔ N2(X,v=7) + CO(X,v=7) | nitrogenCO2VV| 33.3528, -81.1625, 268.278|

N2(X,v=9) + CO(X,v=6) ↔ N2(X,v=8) + CO(X,v=7) | nitrogenCO2VV| 32.1412, -57.8323, 180.698|

N2(X,v=10) + CO(X,v=6) ↔ N2(X,v=9) + CO(X,v=7) | nitrogenCO2VV| 31.1498, -40.177, 122.496|

N2(X,v=11) + CO(X,v=6) ↔ N2(X,v=10) + CO(X,v=7) | nitrogenCO2VV| 29.9809, -22.7362, 73.7917|

N2(X,v=12) + CO(X,v=6) ↔ N2(X,v=11) + CO(X,v=7) | nitrogenCO2VV| 30.1567, -24.6314, 89.1957|

N2(X,v=13) + CO(X,v=6) ↔ N2(X,v=12) + CO(X,v=7) | nitrogenCO2VV| 30.7599, -32.2445, 119.402|

N2(X,v=14) + CO(X,v=6) ↔ N2(X,v=13) + CO(X,v=7) | nitrogenCO2VV| 31.8423, -46.4704, 166.942|

N2(X,v=15) + CO(X,v=6) ↔ N2(X,v=14) + CO(X,v=7) | nitrogenCO2VV| 31.8545, -45.2031, 157.911|

N2(X,v=16) + CO(X,v=6) ↔ N2(X,v=15) + CO(X,v=7) | nitrogenCO2VV| 32.0918, -45.0987, 142.771|

N2(X,v=17) + CO(X,v=6) ↔ N2(X,v=16) + CO(X,v=7) | nitrogenCO2VV| 31.2948, -30.0207, 71.8323|

N2(X,v=18) + CO(X,v=6) ↔ N2(X,v=17) + CO(X,v=7) | nitrogenCO2VV| 33.2876, -63.4307, 205.534|

N2(X,v=19) + CO(X,v=6) ↔ N2(X,v=18) + CO(X,v=7) | nitrogenCO2VV| 31.7481, -36.1841, 78.553|

N2(X,v=20) + CO(X,v=6) ↔ N2(X,v=19) + CO(X,v=7) | nitrogenCO2VV| 33.1728, -54.891, 124.322|

N2(X,v=21) + CO(X,v=6) ↔ N2(X,v=20) + CO(X,v=7) | nitrogenCO2VV| 33.4772, -56.2233, 102.442|

N2(X,v=22) + CO(X,v=6) ↔ N2(X,v=21) + CO(X,v=7) | nitrogenCO2VV| 32.6263, -38.4704, 1.79401|

N2(X,v=23) + CO(X,v=6) ↔ N2(X,v=22) + CO(X,v=7) | nitrogenCO2VV| 29.8937, 11.108, -232.591|

N2(X,v=24) + CO(X,v=6) ↔ N2(X,v=23) + CO(X,v=7) | nitrogenCO2VV| 28.4263, 37.4974, -363.3|

N2(X,v=25) + CO(X,v=6) ↔ N2(X,v=24) + CO(X,v=7) | nitrogenCO2VV| 29.9746, 10.0087, -256.959|

N2(X,v=26) + CO(X,v=6) ↔ N2(X,v=25) + CO(X,v=7) | nitrogenCO2VV| 32.0364, -25.4241, -123.112|

N2(X,v=27) + CO(X,v=6) ↔ N2(X,v=26) + CO(X,v=7) | nitrogenCO2VV| 32.2862, -27.4687, -143.492|

N2(X,v=28) + CO(X,v=6) ↔ N2(X,v=27) + CO(X,v=7) | nitrogenCO2VV| 32.3621, -26.8957, -173.96|

N2(X,v=29) + CO(X,v=6) ↔ N2(X,v=28) + CO(X,v=7) | nitrogenCO2VV| 40.4871, -161.043, 355.045|

N2(X,v=30) + CO(X,v=6) ↔ N2(X,v=29) + CO(X,v=7) | nitrogenCO2VV| 33.5615, -33.2699, -245.985|

N2(X,v=31) + CO(X,v=6) ↔ N2(X,v=30) + CO(X,v=7) | nitrogenCO2VV| 26.4747, 93.7493, -826.846|

N2(X,v=32) + CO(X,v=6) ↔ N2(X,v=31) + CO(X,v=7) | nitrogenCO2VV| 29.2236, 39.1121, -574.291|

N2(X,v=33) + CO(X,v=6) ↔ N2(X,v=32) + CO(X,v=7) | nitrogenCO2VV| 33.0423, -33.4572, -249.135|

N2(X,v=34) + CO(X,v=6) ↔ N2(X,v=33) + CO(X,v=7) | nitrogenCO2VV| 35.1482, -73.0539, -82.4635|

N2(X,v=35) + CO(X,v=6) ↔ N2(X,v=34) + CO(X,v=7) | nitrogenCO2VV| 36.0438, -90.0706, -20.5866|

N2(X,v=36) + CO(X,v=6) ↔ N2(X,v=35) + CO(X,v=7) | nitrogenCO2VV| 36.495, -99.0088, 5.06243|

N2(X,v=37) + CO(X,v=6) ↔ N2(X,v=36) + CO(X,v=7) | nitrogenCO2VV| 36.8595, -106.396, 24.1797|

N2(X,v=38) + CO(X,v=6) ↔ N2(X,v=37) + CO(X,v=7) | nitrogenCO2VV| 46.8282, -277.12, 734.321|

N2(X,v=39) + CO(X,v=6) ↔ N2(X,v=38) + CO(X,v=7) | nitrogenCO2VV| 31.8877, -3.12846, -529.045|

N2(X,v=40) + CO(X,v=6) ↔ N2(X,v=39) + CO(X,v=7) | nitrogenCO2VV| 29.9481, 26.7825, -652.65|

N2(X,v=41) + CO(X,v=6) ↔ N2(X,v=40) + CO(X,v=7) | nitrogenCO2VV| 33.2985, -40.1377, -336.278|

N2(X,v=42) + CO(X,v=6) ↔ N2(X,v=41) + CO(X,v=7) | nitrogenCO2VV| 36.1251, -95.1832, -85.9054|

N2(X,v=43) + CO(X,v=6) ↔ N2(X,v=42) + CO(X,v=7) | nitrogenCO2VV| 36.8802, -110.098, -29.5854|

N2(X,v=44) + CO(X,v=6) ↔ N2(X,v=43) + CO(X,v=7) | nitrogenCO2VV| 36.8386, -109.739, -46.3032|

N2(X,v=45) + CO(X,v=6) ↔ N2(X,v=44) + CO(X,v=7) | nitrogenCO2VV| 36.7837, -109.055, -64.8792|

N2(X,v=46) + CO(X,v=6) ↔ N2(X,v=45) + CO(X,v=7) | nitrogenCO2VV| 36.5184, -104.538, -100.884|

N2(X,v=47) + CO(X,v=6) ↔ N2(X,v=46) + CO(X,v=7) | nitrogenCO2VV| 48.6711, -316.493, 803.532|

N2(X,v=48) + CO(X,v=6) ↔ N2(X,v=47) + CO(X,v=7) | nitrogenCO2VV| 26.6562, 92.2293, -1099.18|

N2(X,v=49) + CO(X,v=6) ↔ N2(X,v=48) + CO(X,v=7) | nitrogenCO2VV| 29.0355, 40.8556, -840.891|

N2(X,v=50) + CO(X,v=6) ↔ N2(X,v=49) + CO(X,v=7) | nitrogenCO2VV| 34.2851, -61.8945, -355.602|

N2(X,v=51) + CO(X,v=6) ↔ N2(X,v=50) + CO(X,v=7) | nitrogenCO2VV| 36.5601, -105.948, -159.832|

N2(X,v=52) + CO(X,v=6) ↔ N2(X,v=51) + CO(X,v=7) | nitrogenCO2VV| 36.8119, -110.96, -152.24|

N2(X,v=53) + CO(X,v=6) ↔ N2(X,v=52) + CO(X,v=7) | nitrogenCO2VV| 36.8352, -111.593, -165.661|

N2(X,v=54) + CO(X,v=6) ↔ N2(X,v=53) + CO(X,v=7) | nitrogenCO2VV| 36.8689, -112.427, -178.155|

N2(X,v=55) + CO(X,v=6) ↔ N2(X,v=54) + CO(X,v=7) | nitrogenCO2VV| 36.717, -109.873, -206.119|

N2(X,v=56) + CO(X,v=6) ↔ N2(X,v=55) + CO(X,v=7) | nitrogenCO2VV| 51.3191, -367.91, 914.139|

N2(X,v=57) + CO(X,v=6) ↔ N2(X,v=56) + CO(X,v=7) | nitrogenCO2VV| 23.1465, 158.071, -1545.9|

N2(X,v=58) + CO(X,v=6) ↔ N2(X,v=57) + CO(X,v=7) | nitrogenCO2VV| 29.7568, 25.4383, -898.339|

N2(X,v=59) + CO(X,v=6) ↔ N2(X,v=58) + CO(X,v=7) | nitrogenCO2VV| 35.767, -91.902, -343.573|

N2(X,v=1) + CO(X,v=7) ↔ N2(X,v=0) + CO(X,v=8) | nitrogenCO2VV| 31.403, -73.1946, 89.3921|

N2(X,v=2) + CO(X,v=7) ↔ N2(X,v=1) + CO(X,v=8) | nitrogenCO2VV| -1.09366, 483.763, -2217.19|

N2(X,v=3) + CO(X,v=7) ↔ N2(X,v=2) + CO(X,v=8) | nitrogenCO2VV| 15.9983, 187.669, -896.943|

N2(X,v=4) + CO(X,v=7) ↔ N2(X,v=3) + CO(X,v=8) | nitrogenCO2VV| 24.3359, 51.1143, -308.805|

N2(X,v=5) + CO(X,v=7) ↔ N2(X,v=4) + CO(X,v=8) | nitrogenCO2VV| 28.4318, -11.1314, -48.3867|

N2(X,v=6) + CO(X,v=7) ↔ N2(X,v=5) + CO(X,v=8) | nitrogenCO2VV| 31.0518, -48.7321, 107.383|

N2(X,v=7) + CO(X,v=7) ↔ N2(X,v=6) + CO(X,v=8) | nitrogenCO2VV| 32.6924, -70.9723, 202.432|

N2(X,v=8) + CO(X,v=7) ↔ N2(X,v=7) + CO(X,v=8) | nitrogenCO2VV| 33.4399, -79.4918, 244.777|

N2(X,v=9) + CO(X,v=7) ↔ N2(X,v=8) + CO(X,v=8) | nitrogenCO2VV| 32.0391, -52.9934, 145.584|

N2(X,v=10) + CO(X,v=7) ↔ N2(X,v=9) + CO(X,v=8) | nitrogenCO2VV| 31.0821, -36.1486, 93.5398|

N2(X,v=11) + CO(X,v=7) ↔ N2(X,v=10) + CO(X,v=8) | nitrogenCO2VV| 29.6858, -15.7056, 37.761|

N2(X,v=12) + CO(X,v=7) ↔ N2(X,v=11) + CO(X,v=8) | nitrogenCO2VV| 29.8717, -18.3125, 60.406|

N2(X,v=13) + CO(X,v=7) ↔ N2(X,v=12) + CO(X,v=8) | nitrogenCO2VV| 30.4619, -26.2484, 96.5757|

N2(X,v=14) + CO(X,v=7) ↔ N2(X,v=13) + CO(X,v=8) | nitrogenCO2VV| 31.2853, -37.0287, 137.264|

N2(X,v=15) + CO(X,v=7) ↔ N2(X,v=14) + CO(X,v=8) | nitrogenCO2VV| 32.4019, -51.4844, 184.048|

N2(X,v=16) + CO(X,v=7) ↔ N2(X,v=15) + CO(X,v=8) | nitrogenCO2VV| 32.4456, -51.1992, 179.52|

N2(X,v=17) + CO(X,v=7) ↔ N2(X,v=16) + CO(X,v=8) | nitrogenCO2VV| 32.0192, -40.4821, 124.433|

N2(X,v=18) + CO(X,v=7) ↔ N2(X,v=17) + CO(X,v=8) | nitrogenCO2VV| 33.628, -67.1309, 231.619|

N2(X,v=19) + CO(X,v=7) ↔ N2(X,v=18) + CO(X,v=8) | nitrogenCO2VV| 32.1268, -40.8926, 112.737|

N2(X,v=20) + CO(X,v=7) ↔ N2(X,v=19) + CO(X,v=8) | nitrogenCO2VV| 33.1611, -53.886, 140.427|

N2(X,v=21) + CO(X,v=7) ↔ N2(X,v=20) + CO(X,v=8) | nitrogenCO2VV| 33.477, -55.6677, 123.2|

N2(X,v=22) + CO(X,v=7) ↔ N2(X,v=21) + CO(X,v=8) | nitrogenCO2VV| 33.0088, -44.6233, 52.9067|

N2(X,v=23) + CO(X,v=7) ↔ N2(X,v=22) + CO(X,v=8) | nitrogenCO2VV| 31.091, -9.35236, -118.151|

N2(X,v=24) + CO(X,v=7) ↔ N2(X,v=23) + CO(X,v=8) | nitrogenCO2VV| 29.1411, 25.6512, -285.811|

N2(X,v=25) + CO(X,v=7) ↔ N2(X,v=24) + CO(X,v=8) | nitrogenCO2VV| 29.7958, 14.281, -250.581|

N2(X,v=26) + CO(X,v=7) ↔ N2(X,v=25) + CO(X,v=8) | nitrogenCO2VV| 31.9249, -22.4412, -109.584|

N2(X,v=27) + CO(X,v=7) ↔ N2(X,v=26) + CO(X,v=8) | nitrogenCO2VV| 32.3506, -27.5512, -115.949|

N2(X,v=28) + CO(X,v=7) ↔ N2(X,v=27) + CO(X,v=8) | nitrogenCO2VV| 32.1526, -21.9488, -168.877|

N2(X,v=29) + CO(X,v=7) ↔ N2(X,v=28) + CO(X,v=8) | nitrogenCO2VV| 39.5474, -142.616, 298.567|

N2(X,v=30) + CO(X,v=7) ↔ N2(X,v=29) + CO(X,v=8) | nitrogenCO2VV| 34.2218, -43.754, -172.586|

N2(X,v=31) + CO(X,v=7) ↔ N2(X,v=30) + CO(X,v=8) | nitrogenCO2VV| 26.4597, 96.2157, -815.085|

N2(X,v=32) + CO(X,v=7) ↔ N2(X,v=31) + CO(X,v=8) | nitrogenCO2VV| 28.5025, 55.0507, -626.504|

N2(X,v=33) + CO(X,v=7) ↔ N2(X,v=32) + CO(X,v=8) | nitrogenCO2VV| 32.4165, -18.9942, -296.016|

N2(X,v=34) + CO(X,v=7) ↔ N2(X,v=33) + CO(X,v=8) | nitrogenCO2VV| 34.6992, -61.4968, -117.97|

N2(X,v=35) + CO(X,v=7) ↔ N2(X,v=34) + CO(X,v=8) | nitrogenCO2VV| 35.7018, -80.1762, -50.3015|

N2(X,v=36) + CO(X,v=7) ↔ N2(X,v=35) + CO(X,v=8) | nitrogenCO2VV| 36.2946, -91.526, -14.9103|

N2(X,v=37) + CO(X,v=7) ↔ N2(X,v=36) + CO(X,v=8) | nitrogenCO2VV| 36.8791, -102.784, 20.7499|

N2(X,v=38) + CO(X,v=7) ↔ N2(X,v=37) + CO(X,v=8) | nitrogenCO2VV| 46.7606, -271.676, 721.151|

N2(X,v=39) + CO(X,v=7) ↔ N2(X,v=38) + CO(X,v=8) | nitrogenCO2VV| 32.4215, -9.09216, -488.489|

N2(X,v=40) + CO(X,v=7) ↔ N2(X,v=39) + CO(X,v=8) | nitrogenCO2VV| 30.1236, 27.3981, -642.395|

N2(X,v=41) + CO(X,v=7) ↔ N2(X,v=40) + CO(X,v=8) | nitrogenCO2VV| 33.3636, -37.4769, -335.703|

N2(X,v=42) + CO(X,v=7) ↔ N2(X,v=41) + CO(X,v=8) | nitrogenCO2VV| 36.2177, -93.123, -82.2962|

N2(X,v=43) + CO(X,v=7) ↔ N2(X,v=42) + CO(X,v=8) | nitrogenCO2VV| 37.0878, -110.31, -14.9449|

N2(X,v=44) + CO(X,v=7) ↔ N2(X,v=43) + CO(X,v=8) | nitrogenCO2VV| 37.0604, -110.303, -29.6788|

N2(X,v=45) + CO(X,v=7) ↔ N2(X,v=44) + CO(X,v=8) | nitrogenCO2VV| 36.9931, -109.461, -48.7041|

N2(X,v=46) + CO(X,v=7) ↔ N2(X,v=45) + CO(X,v=8) | nitrogenCO2VV| 36.7056, -104.603, -85.9879|

N2(X,v=47) + CO(X,v=7) ↔ N2(X,v=46) + CO(X,v=8) | nitrogenCO2VV| 48.5902, -311.483, 794.502|

N2(X,v=48) + CO(X,v=7) ↔ N2(X,v=47) + CO(X,v=8) | nitrogenCO2VV| 27.3632, 82.2188, -1036.81|

N2(X,v=49) + CO(X,v=7) ↔ N2(X,v=48) + CO(X,v=8) | nitrogenCO2VV| 29.2092, 40.9804, -826.585|

N2(X,v=50) + CO(X,v=7) ↔ N2(X,v=49) + CO(X,v=8) | nitrogenCO2VV| 34.2811, -58.3949, -357.294|

N2(X,v=51) + CO(X,v=7) ↔ N2(X,v=50) + CO(X,v=8) | nitrogenCO2VV| 36.6672, -104.596, -151.149|

N2(X,v=52) + CO(X,v=7) ↔ N2(X,v=51) + CO(X,v=8) | nitrogenCO2VV| 36.9543, -110.294, -140.223|

N2(X,v=53) + CO(X,v=7) ↔ N2(X,v=52) + CO(X,v=8) | nitrogenCO2VV| 36.9733, -110.85, -153.964|

N2(X,v=54) + CO(X,v=7) ↔ N2(X,v=53) + CO(X,v=8) | nitrogenCO2VV| 37.0039, -111.629, -166.685|

N2(X,v=55) + CO(X,v=7) ↔ N2(X,v=54) + CO(X,v=8) | nitrogenCO2VV| 36.8502, -109.049, -194.728|

N2(X,v=56) + CO(X,v=7) ↔ N2(X,v=55) + CO(X,v=8) | nitrogenCO2VV| 51.2108, -362.507, 903.89|

N2(X,v=57) + CO(X,v=7) ↔ N2(X,v=56) + CO(X,v=8) | nitrogenCO2VV| 23.6017, 152.696, -1504.7|

N2(X,v=58) + CO(X,v=7) ↔ N2(X,v=57) + CO(X,v=8) | nitrogenCO2VV| 29.7725, 28.5361, -897.909|

N2(X,v=59) + CO(X,v=7) ↔ N2(X,v=58) + CO(X,v=8) | nitrogenCO2VV| 35.7783, -88.7268, -343.463|

N2(X,v=1) + CO(X,v=8) ↔ N2(X,v=0) + CO(X,v=9) | nitrogenCO2VV| 32.3618, -88.3454, 140.387|

N2(X,v=2) + CO(X,v=8) ↔ N2(X,v=1) + CO(X,v=9) | nitrogenCO2VV| -3.73436, 533.706, -2459.22|

N2(X,v=3) + CO(X,v=8) ↔ N2(X,v=2) + CO(X,v=9) | nitrogenCO2VV| 15.912, 191.598, -932.546|

N2(X,v=4) + CO(X,v=8) ↔ N2(X,v=3) + CO(X,v=9) | nitrogenCO2VV| 25.2813, 37.4707, -270.39|

N2(X,v=5) + CO(X,v=8) ↔ N2(X,v=4) + CO(X,v=9) | nitrogenCO2VV| 29.6215, -28.2553, 1.66105|

N2(X,v=6) + CO(X,v=8) ↔ N2(X,v=5) + CO(X,v=9) | nitrogenCO2VV| 32.032, -61.9251, 139.847|

N2(X,v=7) + CO(X,v=8) ↔ N2(X,v=6) + CO(X,v=9) | nitrogenCO2VV| 33.1967, -76.1716, 202.899|

N2(X,v=8) + CO(X,v=8) ↔ N2(X,v=7) + CO(X,v=9) | nitrogenCO2VV| 33.4787, -77.0806, 216.061|

N2(X,v=9) + CO(X,v=8) ↔ N2(X,v=8) + CO(X,v=9) | nitrogenCO2VV| 31.9344, -48.1254, 107.766|

N2(X,v=10) + CO(X,v=8) ↔ N2(X,v=9) + CO(X,v=9) | nitrogenCO2VV| 31.0228, -32.201, 61.8396|

N2(X,v=11) + CO(X,v=8) ↔ N2(X,v=10) + CO(X,v=9) | nitrogenCO2VV| 29.3031, -7.14863, -7.77146|

N2(X,v=12) + CO(X,v=8) ↔ N2(X,v=11) + CO(X,v=9) | nitrogenCO2VV| 29.5279, -10.9223, 23.6776|

N2(X,v=13) + CO(X,v=8) ↔ N2(X,v=12) + CO(X,v=9) | nitrogenCO2VV| 30.1699, -20.215, 69.4873|

N2(X,v=14) + CO(X,v=8) ↔ N2(X,v=13) + CO(X,v=9) | nitrogenCO2VV| 31.0208, -31.9396, 118.412|

N2(X,v=15) + CO(X,v=8) ↔ N2(X,v=14) + CO(X,v=9) | nitrogenCO2VV| 32.0295, -45.3682, 167.699|

N2(X,v=16) + CO(X,v=8) ↔ N2(X,v=15) + CO(X,v=9) | nitrogenCO2VV| 32.8678, -55.2454, 196.072|

N2(X,v=17) + CO(X,v=8) ↔ N2(X,v=16) + CO(X,v=9) | nitrogenCO2VV| 32.8027, -53.8685, 188.364|

N2(X,v=18) + CO(X,v=8) ↔ N2(X,v=17) + CO(X,v=9) | nitrogenCO2VV| 33.9073, -69.9873, 251.113|

N2(X,v=19) + CO(X,v=8) ↔ N2(X,v=18) + CO(X,v=9) | nitrogenCO2VV| 32.4666, -44.9351, 140.834|

N2(X,v=20) + CO(X,v=8) ↔ N2(X,v=19) + CO(X,v=9) | nitrogenCO2VV| 33.1698, -53.2823, 155.337|

N2(X,v=21) + CO(X,v=8) ↔ N2(X,v=20) + CO(X,v=9) | nitrogenCO2VV| 33.4986, -55.5803, 143.452|

N2(X,v=22) + CO(X,v=8) ↔ N2(X,v=21) + CO(X,v=9) | nitrogenCO2VV| 33.2677, -48.7401, 93.0705|

N2(X,v=23) + CO(X,v=8) ↔ N2(X,v=22) + CO(X,v=9) | nitrogenCO2VV| 32.0049, -24.8499, -27.8647|

N2(X,v=24) + CO(X,v=8) ↔ N2(X,v=23) + CO(X,v=9) | nitrogenCO2VV| 30.042, 10.3659, -195.065|

N2(X,v=25) + CO(X,v=8) ↔ N2(X,v=24) + CO(X,v=9) | nitrogenCO2VV| 29.8201, 14.6561, -228.041|

N2(X,v=26) + CO(X,v=8) ↔ N2(X,v=25) + CO(X,v=9) | nitrogenCO2VV| 31.6916, -17.5779, -105.225|

N2(X,v=27) + CO(X,v=8) ↔ N2(X,v=26) + CO(X,v=9) | nitrogenCO2VV| 32.517, -29.8576, -78.6974|

N2(X,v=28) + CO(X,v=8) ↔ N2(X,v=27) + CO(X,v=9) | nitrogenCO2VV| 32.0567, -19.5722, -151.69|

N2(X,v=29) + CO(X,v=8) ↔ N2(X,v=28) + CO(X,v=9) | nitrogenCO2VV| 38.6269, -125.262, 248.641|

N2(X,v=30) + CO(X,v=8) ↔ N2(X,v=29) + CO(X,v=9) | nitrogenCO2VV| 34.8377, -54.0826, -98.4217|

N2(X,v=31) + CO(X,v=8) ↔ N2(X,v=30) + CO(X,v=9) | nitrogenCO2VV| 26.8297, 90.8501, -765.404|

N2(X,v=32) + CO(X,v=8) ↔ N2(X,v=31) + CO(X,v=9) | nitrogenCO2VV| 27.8804, 68.4718, -665.245|

N2(X,v=33) + CO(X,v=8) ↔ N2(X,v=32) + CO(X,v=9) | nitrogenCO2VV| 31.7351, -4.18328, -342.516|

N2(X,v=34) + CO(X,v=8) ↔ N2(X,v=33) + CO(X,v=9) | nitrogenCO2VV| 34.2136, -49.9261, -151.515|

N2(X,v=35) + CO(X,v=8) ↔ N2(X,v=34) + CO(X,v=9) | nitrogenCO2VV| 35.2671, -69.1465, -83.5518|

N2(X,v=36) + CO(X,v=8) ↔ N2(X,v=35) + CO(X,v=9) | nitrogenCO2VV| 35.972, -82.2682, -41.7865|

N2(X,v=37) + CO(X,v=8) ↔ N2(X,v=36) + CO(X,v=9) | nitrogenCO2VV| 36.7554, -96.9259, 7.83565|

N2(X,v=38) + CO(X,v=8) ↔ N2(X,v=37) + CO(X,v=9) | nitrogenCO2VV| 46.5894, -264.667, 701.364|

N2(X,v=39) + CO(X,v=8) ↔ N2(X,v=38) + CO(X,v=9) | nitrogenCO2VV| 32.8274, -12.9261, -457.74|

N2(X,v=40) + CO(X,v=8) ↔ N2(X,v=39) + CO(X,v=9) | nitrogenCO2VV| 30.1723, 30.1307, -641.936|

N2(X,v=41) + CO(X,v=8) ↔ N2(X,v=40) + CO(X,v=9) | nitrogenCO2VV| 33.3654, -33.8782, -339.516|

N2(X,v=42) + CO(X,v=8) ↔ N2(X,v=41) + CO(X,v=9) | nitrogenCO2VV| 36.2567, -90.28, -82.5366|

N2(X,v=43) + CO(X,v=8) ↔ N2(X,v=42) + CO(X,v=9) | nitrogenCO2VV| 37.2602, -110.071, -2.68413|

N2(X,v=44) + CO(X,v=8) ↔ N2(X,v=43) + CO(X,v=9) | nitrogenCO2VV| 37.2675, -110.81, -13.6114|

N2(X,v=45) + CO(X,v=8) ↔ N2(X,v=44) + CO(X,v=9) | nitrogenCO2VV| 37.1955, -109.964, -32.3401|

N2(X,v=46) + CO(X,v=8) ↔ N2(X,v=45) + CO(X,v=9) | nitrogenCO2VV| 36.8942, -104.931, -70.0985|

N2(X,v=47) + CO(X,v=8) ↔ N2(X,v=46) + CO(X,v=9) | nitrogenCO2VV| 48.5121, -306.762, 786.572|

N2(X,v=48) + CO(X,v=8) ↔ N2(X,v=47) + CO(X,v=9) | nitrogenCO2VV| 28.0918, 71.5555, -971.601|

N2(X,v=49) + CO(X,v=8) ↔ N2(X,v=48) + CO(X,v=9) | nitrogenCO2VV| 29.3963, 40.5812, -809.933|

N2(X,v=50) + CO(X,v=8) ↔ N2(X,v=49) + CO(X,v=9) | nitrogenCO2VV| 34.2713, -55.0634, -358.291|

N2(X,v=51) + CO(X,v=8) ↔ N2(X,v=50) + CO(X,v=9) | nitrogenCO2VV| 36.7601, -103.258, -142.477|

N2(X,v=52) + CO(X,v=8) ↔ N2(X,v=51) + CO(X,v=9) | nitrogenCO2VV| 37.0864, -109.721, -127.82|

N2(X,v=53) + CO(X,v=8) ↔ N2(X,v=52) + CO(X,v=9) | nitrogenCO2VV| 37.0995, -110.175, -141.985|

N2(X,v=54) + CO(X,v=8) ↔ N2(X,v=53) + CO(X,v=9) | nitrogenCO2VV| 37.1256, -110.875, -155.04|

N2(X,v=55) + CO(X,v=8) ↔ N2(X,v=54) + CO(X,v=9) | nitrogenCO2VV| 36.9683, -108.236, -183.307|

N2(X,v=56) + CO(X,v=8) ↔ N2(X,v=55) + CO(X,v=9) | nitrogenCO2VV| 51.0817, -357.009, 893.191|

N2(X,v=57) + CO(X,v=8) ↔ N2(X,v=56) + CO(X,v=9) | nitrogenCO2VV| 24.0612, 146.943, -1461.72|

N2(X,v=58) + CO(X,v=8) ↔ N2(X,v=57) + CO(X,v=9) | nitrogenCO2VV| 29.7843, 31.4039, -896.377|

N2(X,v=59) + CO(X,v=8) ↔ N2(X,v=58) + CO(X,v=9) | nitrogenCO2VV| 35.7668, -85.4168, -344.006|

N2(X,v=1) + CO(X,v=9) ↔ N2(X,v=0) + CO(X,v=10) | nitrogenCO2VV| 33.2204, -102.447, 189.316|

N2(X,v=2) + CO(X,v=9) ↔ N2(X,v=1) + CO(X,v=10) | nitrogenCO2VV| -5.6317, 569.782, -2637.94|

N2(X,v=3) + CO(X,v=9) ↔ N2(X,v=2) + CO(X,v=10) | nitrogenCO2VV| 16.3071, 186.471, -927.03|

N2(X,v=4) + CO(X,v=9) ↔ N2(X,v=3) + CO(X,v=10) | nitrogenCO2VV| 26.4668, 19.1097, -210.435|

N2(X,v=5) + CO(X,v=9) ↔ N2(X,v=4) + CO(X,v=10) | nitrogenCO2VV| 30.9276, -47.9501, 63.8296|

N2(X,v=6) + CO(X,v=9) ↔ N2(X,v=5) + CO(X,v=10) | nitrogenCO2VV| 33.0599, -76.5064, 179.239|

N2(X,v=7) + CO(X,v=9) ↔ N2(X,v=6) + CO(X,v=10) | nitrogenCO2VV| 33.7306, -82.2853, 207.325|

N2(X,v=8) + CO(X,v=9) ↔ N2(X,v=7) + CO(X,v=10) | nitrogenCO2VV| 33.523, -74.9006, 186.907|

N2(X,v=9) + CO(X,v=9) ↔ N2(X,v=8) + CO(X,v=10) | nitrogenCO2VV| 31.8635, -43.8771, 70.5171|

N2(X,v=10) + CO(X,v=9) ↔ N2(X,v=9) + CO(X,v=10) | nitrogenCO2VV| 31.018, -29.1196, 31.0993|

N2(X,v=11) + CO(X,v=9) ↔ N2(X,v=10) + CO(X,v=10) | nitrogenCO2VV| 28.8321, 2.99391, -62.8544|

N2(X,v=12) + CO(X,v=9) ↔ N2(X,v=11) + CO(X,v=10) | nitrogenCO2VV| 29.1205, -2.32015, -21.3736|

N2(X,v=13) + CO(X,v=9) ↔ N2(X,v=12) + CO(X,v=10) | nitrogenCO2VV| 29.8514, -13.5554, 36.1305|

N2(X,v=14) + CO(X,v=9) ↔ N2(X,v=13) + CO(X,v=10) | nitrogenCO2VV| 30.7857, -27.1095, 96.3588|

N2(X,v=15) + CO(X,v=9) ↔ N2(X,v=14) + CO(X,v=10) | nitrogenCO2VV| 31.8973, -42.6205, 157.965|

N2(X,v=16) + CO(X,v=9) ↔ N2(X,v=15) + CO(X,v=10) | nitrogenCO2VV| 32.9819, -56.9686, 209.272|

N2(X,v=17) + CO(X,v=9) ↔ N2(X,v=16) + CO(X,v=10) | nitrogenCO2VV| 33.1225, -56.1964, 198.935|

N2(X,v=18) + CO(X,v=9) ↔ N2(X,v=17) + CO(X,v=10) | nitrogenCO2VV| 34.1266, -72.9717, 269.1|

N2(X,v=19) + CO(X,v=9) ↔ N2(X,v=18) + CO(X,v=10) | nitrogenCO2VV| 32.7486, -48.0928, 162.049|

N2(X,v=20) + CO(X,v=9) ↔ N2(X,v=19) + CO(X,v=10) | nitrogenCO2VV| 33.1203, -51.818, 164.014|

N2(X,v=21) + CO(X,v=9) ↔ N2(X,v=20) + CO(X,v=10) | nitrogenCO2VV| 33.5025, -55.2404, 159.984|

N2(X,v=22) + CO(X,v=9) ↔ N2(X,v=21) + CO(X,v=10) | nitrogenCO2VV| 33.4518, -51.6074, 125.475|

N2(X,v=23) + CO(X,v=9) ↔ N2(X,v=22) + CO(X,v=10) | nitrogenCO2VV| 32.6541, -35.7329, 40.0799|

N2(X,v=24) + CO(X,v=9) ↔ N2(X,v=23) + CO(X,v=10) | nitrogenCO2VV| 30.9868, -5.67572, -103.473|

N2(X,v=25) + CO(X,v=9) ↔ N2(X,v=24) + CO(X,v=10) | nitrogenCO2VV| 30.0975, 10.3894, -186.584|

N2(X,v=26) + CO(X,v=9) ↔ N2(X,v=25) + CO(X,v=10) | nitrogenCO2VV| 31.4012, -11.8884, -105.723|

N2(X,v=27) + CO(X,v=9) ↔ N2(X,v=26) + CO(X,v=10) | nitrogenCO2VV| 32.7705, -33.9485, -34.4103|

N2(X,v=28) + CO(X,v=9) ↔ N2(X,v=27) + CO(X,v=10) | nitrogenCO2VV| 32.0509, -19.1746, -125.744|

N2(X,v=29) + CO(X,v=9) ↔ N2(X,v=28) + CO(X,v=10) | nitrogenCO2VV| 37.7578, -109.427, 206.721|

N2(X,v=30) + CO(X,v=9) ↔ N2(X,v=29) + CO(X,v=10) | nitrogenCO2VV| 35.3059, -62.2261, -33.2488|

N2(X,v=31) + CO(X,v=9) ↔ N2(X,v=30) + CO(X,v=10) | nitrogenCO2VV| 27.6315, 76.9357, -675.108|

N2(X,v=32) + CO(X,v=9) ↔ N2(X,v=31) + CO(X,v=10) | nitrogenCO2VV| 27.4622, 77.5115, -682.173|

N2(X,v=33) + CO(X,v=9) ↔ N2(X,v=32) + CO(X,v=10) | nitrogenCO2VV| 31.0404, 10.261, -385.5|

N2(X,v=34) + CO(X,v=9) ↔ N2(X,v=33) + CO(X,v=10) | nitrogenCO2VV| 33.7322, -39.0703, -179.677|

N2(X,v=35) + CO(X,v=9) ↔ N2(X,v=34) + CO(X,v=10) | nitrogenCO2VV| 34.7918, -57.9553, -115.578|

N2(X,v=36) + CO(X,v=9) ↔ N2(X,v=35) + CO(X,v=10) | nitrogenCO2VV| 35.5545, -71.7656, -72.7516|

N2(X,v=37) + CO(X,v=9) ↔ N2(X,v=36) + CO(X,v=10) | nitrogenCO2VV| 36.4783, -88.6724, -14.7636|

N2(X,v=38) + CO(X,v=9) ↔ N2(X,v=37) + CO(X,v=10) | nitrogenCO2VV| 46.2905, -255.678, 673.509|

N2(X,v=39) + CO(X,v=9) ↔ N2(X,v=38) + CO(X,v=10) | nitrogenCO2VV| 33.1156, -14.8287, -435.521|

N2(X,v=40) + CO(X,v=9) ↔ N2(X,v=39) + CO(X,v=10) | nitrogenCO2VV| 30.0684, 35.4771, -653.336|

N2(X,v=41) + CO(X,v=9) ↔ N2(X,v=40) + CO(X,v=10) | nitrogenCO2VV| 33.2786, -28.8421, -349.83|

N2(X,v=42) + CO(X,v=9) ↔ N2(X,v=41) + CO(X,v=10) | nitrogenCO2VV| 36.228, -86.3459, -87.9188|

N2(X,v=43) + CO(X,v=9) ↔ N2(X,v=42) + CO(X,v=10) | nitrogenCO2VV| 37.3816, -109.034, 5.63488|

N2(X,v=44) + CO(X,v=9) ↔ N2(X,v=43) + CO(X,v=10) | nitrogenCO2VV| 37.4509, -111.026, 0.820871|

N2(X,v=45) + CO(X,v=9) ↔ N2(X,v=44) + CO(X,v=10) | nitrogenCO2VV| 37.3873, -110.424, -16.465|

N2(X,v=46) + CO(X,v=9) ↔ N2(X,v=45) + CO(X,v=10) | nitrogenCO2VV| 37.0877, -105.513, -53.3103|

N2(X,v=47) + CO(X,v=9) ↔ N2(X,v=46) + CO(X,v=10) | nitrogenCO2VV| 48.4428, -302.366, 779.847|

N2(X,v=48) + CO(X,v=9) ↔ N2(X,v=47) + CO(X,v=10) | nitrogenCO2VV| 28.8408, 60.34, -904.086|

N2(X,v=49) + CO(X,v=9) ↔ N2(X,v=48) + CO(X,v=10) | nitrogenCO2VV| 29.6015, 39.645, -790.914|

N2(X,v=50) + CO(X,v=9) ↔ N2(X,v=49) + CO(X,v=10) | nitrogenCO2VV| 34.2623, -51.9532, -358.373|

N2(X,v=51) + CO(X,v=9) ↔ N2(X,v=50) + CO(X,v=10) | nitrogenCO2VV| 36.8435, -101.954, -133.755|

N2(X,v=52) + CO(X,v=9) ↔ N2(X,v=51) + CO(X,v=10) | nitrogenCO2VV| 37.2134, -109.272, -114.909|

N2(X,v=53) + CO(X,v=9) ↔ N2(X,v=52) + CO(X,v=10) | nitrogenCO2VV| 37.2188, -109.595, -129.61|

N2(X,v=54) + CO(X,v=9) ↔ N2(X,v=53) + CO(X,v=10) | nitrogenCO2VV| 37.2385, -110.184, -143.131|

N2(X,v=55) + CO(X,v=9) ↔ N2(X,v=54) + CO(X,v=10) | nitrogenCO2VV| 37.0752, -107.442, -171.815|

N2(X,v=56) + CO(X,v=9) ↔ N2(X,v=55) + CO(X,v=10) | nitrogenCO2VV| 50.9359, -351.43, 882.095|

N2(X,v=57) + CO(X,v=9) ↔ N2(X,v=56) + CO(X,v=10) | nitrogenCO2VV| 24.5304, 140.774, -1416.81|

N2(X,v=58) + CO(X,v=9) ↔ N2(X,v=57) + CO(X,v=10) | nitrogenCO2VV| 29.7967, 34.0224, -893.654|

N2(X,v=59) + CO(X,v=9) ↔ N2(X,v=58) + CO(X,v=10) | nitrogenCO2VV| 35.7364, -81.9823, -345.153|

ii. N_2-CO_2 V-V:

The process:

$CO_2(00^0v_i1) + N_2(w_i) \leftrightarrow CO_2(00^0v_f1) + N_2(w_f)$ | KustovaScaling_CO2v3_N2 | v_i*w_f | has a rate coefficient of $k = v_i \cdot w_f \cdot 1.66 \cdot 10^{-30} \cdot \exp\left(27.221 + 10.8178 \cdot T^{-1/3} - 224.158 \cdot T^{-2/3}\right)$ in m^3s^{-1}.

CO2(X,v=00011) + N2(X,v=0) ↔ CO2(X,v=00001) + N2(X,v=1) | nitrogenCO2VV | 43.8, -306, 1288 | %k=k0*(v3+1)(w+1)

CO2(X,v=00011) + N2(X,v=1) ↔ CO2(X,v=00021) + N2(X,v=0) | nitrogenCO2VV | 46.953, -349.851, 1482|

CO2(X,v=00021) + N2(X,v=1) ↔ CO2(X,v=00031) + N2(X,v=0) | nitrogenCO2VV | 41.6815, -239.359, 944.929 |

CO2(X,v=00031) + N2(X,v=1) ↔ CO2(X,v=00041) + N2(X,v=0) | KustovaScaling_CO2v3_N2 | 4 |

CO2(X,v=00041) + N2(X,v=1) ↔ CO2(X,v=00051) + N2(X,v=0) | KustovaScaling_CO2v3_N2 | 5 |

CO2(X,v=00011) + N2(X,v=1) ↔ CO2(X,v=00001) + N2(X,v=2) | nitrogenCO2VV | 35.8752, -138.147, 471.585 |

CO2(X,v=00021) + N2(X,v=1) ↔ CO2(X,v=00011) + N2(X,v=2) | nitrogenCO2VV | 44.8346, -294.813, 1213.08 |

CO2(X,v=00021) + N2(X,v=2) ↔ CO2(X,v=00031) + N2(X,v=1) | nitrogenCO2VV | 48.0886, -350.201, 1481.91 |

CO2(X,v=00031) + N2(X,v=2) ↔ CO2(X,v=00041) + N2(X,v=1) | nitrogenCO2VV | 44.0283, -265.507, 1069.99 |

CO2(X,v=00041) + N2(X,v=2) ↔ CO2(X,v=00051) + N2(X,v=1) | KustovaScaling_CO2v3_N2 | 10 |

CO2(X,v=00011) + N2(X,v=2) ↔ CO2(X,v=00001) + N2(X,v=3) | KustovaScaling_CO2v3_N2 | 3 |

CO2(X,v=00021) + N2(X,v=2) ↔ CO2(X,v=00011) + N2(X,v=3) | KustovaScaling_CO2v3_N2 | 6 |

CO2(X,v=00031) + N2(X,v=2) ↔ CO2(X,v=00021) + N2(X,v=3) | nitrogenCO2VV | 45.2075, -286.167, 1170.46 |

CO2(X,v=00041) + N2(X,v=2) ↔ CO2(X,v=00031) + N2(X,v=3) | nitrogenCO2VV | 48.6965, -348.305, 1471.57 |

CO2(X,v=00041) + N2(X,v=3) ↔ CO2(X,v=00051) + N2(X,v=2) | nitrogenCO2VV | 45.8051, -287.873, 1178.84 |

CO2(X,v=00011) + N2(X,v=3) ↔ CO2(X,v=00001) + N2(X,v=4) | KustovaScaling_CO2v3_N2 | 4 |

CO2(X,v=00021) + N2(X,v=3) ↔ CO2(X,v=00011) + N2(X,v=4) | KustovaScaling_CO2v3_N2 | 8 |

CO2(X,v=00031) + N2(X,v=3) ↔ CO2(X,v=00021) + N2(X,v=4) | KustovaScaling_CO2v3_N2 | 12 |

CO2(X,v=00041) + N2(X,v=3) ↔ CO2(X,v=00031) + N2(X,v=4) | nitrogenCO2VV | 44.6275, -263.695, 1061.25 |

CO2(X,v=00051) + N2(X,v=3) ↔ CO2(X,v=00041) + N2(X,v=4) | nitrogenCO2VV | 49.2916, -350.245, 1482.44 |

CO2(X,v=00011) + N2(X,v=4) ↔ CO2(X,v=00001) + N2(X,v=5) | KustovaScaling_CO2v3_N2 | 5 |

CO2(X,v=00021) + N2(X,v=4) ↔ CO2(X,v=00011) + N2(X,v=5) | KustovaScaling_CO2v3_N2 | 10 |

CO2(X,v=00031) + N2(X,v=4) ↔ CO2(X,v=00021) + N2(X,v=5) | KustovaScaling_CO2v3_N2 | 15 |

CO2(X,v=00041) + N2(X,v=4) ↔ CO2(X,v=00031) + N2(X,v=5) | KustovaScaling_CO2v3_N2 | 20 |

CO2(X,v=00051) + N2(X,v=4) ↔ CO2(X,v=00041) + N2(X,v=5) | nitrogenCO2VV | 43.6765, -236.98, 933.642 |

CO2(X,v=00011) + N2(X,v=5) ↔ CO2(X,v=00001) + N2(X,v=6) | KustovaScaling_CO2v3_N2 | 6 |

CO2(X,v=00021) + N2(X,v=5) ↔ CO2(X,v=00011) + N2(X,v=6) | KustovaScaling_CO2v3_N2 | 12 |

CO2(X,v=00031) + N2(X,v=5) ↔ CO2(X,v=00021) + N2(X,v=6) | KustovaScaling_CO2v3_N2 | 18 |

CO2(X,v=00041) + N2(X,v=5) ↔ CO2(X,v=00031) + N2(X,v=6) | KustovaScaling_CO2v3_N2 | 24 |

CO2(X,v=00051) + N2(X,v=5) ↔ CO2(X,v=00041) + N2(X,v=6) | KustovaScaling_CO2v3_N2 | 30 |

CO2(X,v=00011) + N2(X,v=6) ↔ CO2(X,v=00001) + N2(X,v=7) | KustovaScaling_CO2v3_N2 | 7 |

CO2(X,v=00021) + N2(X,v=6) ↔ CO2(X,v=00011) + N2(X,v=7) | KustovaScaling_CO2v3_N2 | 14 |

CO2(X,v=00031) + N2(X,v=6) ↔ CO2(X,v=00021) + N2(X,v=7) | KustovaScaling_CO2v3_N2 | 21 |

CO2(X,v=00041) + N2(X,v=6) ↔ CO2(X,v=00031) + N2(X,v=7) | KustovaScaling_CO2v3_N2 | 28 |

CO2(X,v=00051) + N2(X,v=6) ↔ CO2(X,v=00041) + N2(X,v=7) | KustovaScaling_CO2v3_N2 | 35 |

CO2(X,v=00011) + N2(X,v=7) ↔ CO2(X,v=00001) + N2(X,v=8) | KustovaScaling_CO2v3_N2 | 8 |

CO2(X,v=00021) + N2(X,v=7) ↔ CO2(X,v=00011) + N2(X,v=8) | KustovaScaling_CO2v3_N2 | 16 |

CO2(X,v=00031) + N2(X,v=7) ↔ CO2(X,v=00021) + N2(X,v=8) | KustovaScaling_CO2v3_N2 | 24 |

CO2(X,v=00041) + N2(X,v=7) ↔ CO2(X,v=00031) + N2(X,v=8) | KustovaScaling_CO2v3_N2 | 32 |

CO2(X,v=00051) + N2(X,v=7) ↔ CO2(X,v=00041) + N2(X,v=8) | KustovaScaling_CO2v3_N2 | 40 |

CO2(X,v=00011) + N2(X,v=8) ↔ CO2(X,v=00001) + N2(X,v=9) | KustovaScaling_CO2v3_N2 | 9 |

CO2(X,v=00021) + N2(X,v=8) ↔ CO2(X,v=00011) + N2(X,v=9) | KustovaScaling_CO2v3_N2 | 18 |

CO2(X,v=00031) + N2(X,v=8) ↔ CO2(X,v=00021) + N2(X,v=9) | KustovaScaling_CO2v3_N2 | 27 |

CO2(X,v=00041) + N2(X,v=8) ↔ CO2(X,v=00031) + N2(X,v=9) | KustovaScaling_CO2v3_N2 | 36 |

CO2(X,v=00051) + N2(X,v=8) ↔ CO2(X,v=00041) + N2(X,v=9) | KustovaScaling_CO2v3_N2 | 45 |

CO2(X,v=00011) + N2(X,v=9) ↔ CO2(X,v=00001) + N2(X,v=10) | KustovaScaling_CO2v3_N2 | 10 |

CO2(X,v=00021) + N2(X,v=9) ↔ CO2(X,v=00011) + N2(X,v=10) | KustovaScaling_CO2v3_N2 | 20 |

CO2(X,v=00031) + N2(X,v=9) ↔ CO2(X,v=00021) + N2(X,v=10) | KustovaScaling_CO2v3_N2 | 30 |

CO2(X,v=00041) + N2(X,v=9) ↔ CO2(X,v=00031) + N2(X,v=10) | KustovaScaling_CO2v3_N2 | 40 |

CO2(X,v=00051) + N2(X,v=9) ↔ CO2(X,v=00041) + N2(X,v=10) | KustovaScaling_CO2v3_N2 | 50 |

CO2(X,v=00011) + N2(X,v=10) ↔ CO2(X,v=00001) + N2(X,v=11) | KustovaScaling_CO2v3_N2 | 11 |

CO2(X,v=00021) + N2(X,v=10) ↔ CO2(X,v=00011) + N2(X,v=11) | KustovaScaling_CO2v3_N2 | 22 |

CO2(X,v=00031) + N2(X,v=10) ↔ CO2(X,v=00021) + N2(X,v=11) | KustovaScaling_CO2v3_N2 | 33 |

CO2(X,v=00041) + N2(X,v=10) ↔ CO2(X,v=00031) + N2(X,v=11) | KustovaScaling_CO2v3_N2 | 44 |

CO2(X,v=00051) + N2(X,v=10) ↔ CO2(X,v=00041) + N2(X,v=11) | KustovaScaling_CO2v3_N2 | 55 |

CO2(X,v=00011) + N2(X,v=11) ↔ CO2(X,v=00001) + N2(X,v=12) | KustovaScaling_CO2v3_N2 | 12 |

CO2(X,v=00021) + N2(X,v=11) ↔ CO2(X,v=00011) + N2(X,v=12) | KustovaScaling_CO2v3_N2 | 24 |

CO2(X,v=00031) + N2(X,v=11) ↔ CO2(X,v=00021) + N2(X,v=12) | KustovaScaling_CO2v3_N2 | 36 |

CO2(X,v=00041) + N2(X,v=11) ↔ CO2(X,v=00031) + N2(X,v=12) | KustovaScaling_CO2v3_N2 | 48 |

CO2(X,v=00051) + N2(X,v=11) ↔ CO2(X,v=00041) + N2(X,v=12) | KustovaScaling_CO2v3_N2 | 60 |

CO2(X,v=00011) + N2(X,v=12) ↔ CO2(X,v=00001) + N2(X,v=13) | KustovaScaling_CO2v3_N2 | 13 |

CO2(X,v=00021) + N2(X,v=12) ↔ CO2(X,v=00011) + N2(X,v=13) | KustovaScaling_CO2v3_N2 | 26 |

CO2(X,v=00031) + N2(X,v=12) ↔ CO2(X,v=00021) + N2(X,v=13) | KustovaScaling_CO2v3_N2 | 39 |

CO2(X,v=00041) + N2(X,v=12) ↔ CO2(X,v=00031) + N2(X,v=13) | KustovaScaling_CO2v3_N2 | 52 |

CO2(X,v=00051) + N2(X,v=12) ↔ CO2(X,v=00041) + N2(X,v=13) | KustovaScaling_CO2v3_N2 | 65 |

CO2(X,v=00011) + N2(X,v=13) ↔ CO2(X,v=00001) + N2(X,v=14) | KustovaScaling_CO2v3_N2 | 14 |

CO2(X,v=00021) + N2(X,v=13) ↔ CO2(X,v=00011) + N2(X,v=14) | KustovaScaling_CO2v3_N2 | 28 |

CO2(X,v=00031) + N2(X,v=13) ↔ CO2(X,v=00021) + N2(X,v=14) | KustovaScaling_CO2v3_N2 | 42 |

CO2(X,v=00041) + N2(X,v=13) ↔ CO2(X,v=00031) + N2(X,v=14) | KustovaScaling_CO2v3_N2 | 56 |

CO2(X,v=00051) + N2(X,v=13) ↔ CO2(X,v=00041) + N2(X,v=14) | KustovaScaling_CO2v3_N2 | 70 |

CO2(X,v=00011) + N2(X,v=14) ↔ CO2(X,v=00001) + N2(X,v=15) | KustovaScaling_CO2v3_N2 | 15 |

CO2(X,v=00021) + N2(X,v=14) ↔ CO2(X,v=00011) + N2(X,v=15) | KustovaScaling_CO2v3_N2 | 30 |

CO2(X,v=00031) + N2(X,v=14) ↔ CO2(X,v=00021) + N2(X,v=15) | KustovaScaling_CO2v3_N2 | 45 |

CO2(X,v=00041) + N2(X,v=14) ↔ CO2(X,v=00031) + N2(X,v=15) | KustovaScaling_CO2v3_N2 | 60 |

CO2(X,v=00051) + N2(X,v=14) ↔ CO2(X,v=00041) + N2(X,v=15) | KustovaScaling_CO2v3_N2 | 75 |

CO2(X,v=00011) + N2(X,v=15) ↔ CO2(X,v=00001) + N2(X,v=16) | KustovaScaling_CO2v3_N2 | 16 |

CO2(X,v=00021) + N2(X,v=15) ↔ CO2(X,v=00011) + N2(X,v=16) | KustovaScaling_CO2v3_N2 | 32 |

CO2(X,v=00031) + N2(X,v=15) ↔ CO2(X,v=00021) + N2(X,v=16) | KustovaScaling_CO2v3_N2 | 48 |

CO2(X,v=00041) + N2(X,v=15) ↔ CO2(X,v=00031) + N2(X,v=16) | KustovaScaling_CO2v3_N2 | 64 |

CO2(X,v=00051) + N2(X,v=15) ↔ CO2(X,v=00041) + N2(X,v=16) | KustovaScaling_CO2v3_N2 | 80 |

CO2(X,v=00011) + N2(X,v=16) ↔ CO2(X,v=00001) + N2(X,v=17) | KustovaScaling_CO2v3_N2 | 17 |

CO2(X,v=00021) + N2(X,v=16) ↔ CO2(X,v=00011) + N2(X,v=17) | KustovaScaling_CO2v3_N2 | 34 |

CO2(X,v=00031) + N2(X,v=16) ↔ CO2(X,v=00021) + N2(X,v=17) | KustovaScaling_CO2v3_N2 | 51 |

CO2(X,v=00041) + N2(X,v=16) ↔ CO2(X,v=00031) + N2(X,v=17) | KustovaScaling_CO2v3_N2 | 68 |

CO2(X,v=00051) + N2(X,v=16) ↔ CO2(X,v=00041) + N2(X,v=17) | KustovaScaling_CO2v3_N2 | 85 |

CO2(X,v=00011) + N2(X,v=17) ↔ CO2(X,v=00001) + N2(X,v=18) | KustovaScaling_CO2v3_N2 | 18 |

CO2(X,v=00021) + N2(X,v=17) ↔ CO2(X,v=00011) + N2(X,v=18) | KustovaScaling_CO2v3_N2 | 36 |

CO2(X,v=00031) + N2(X,v=17) ↔ CO2(X,v=00021) + N2(X,v=18) | KustovaScaling_CO2v3_N2 | 54 |

CO2(X,v=00041) + N2(X,v=17) ↔ CO2(X,v=00031) + N2(X,v=18) | KustovaScaling_CO2v3_N2 | 72 |

CO2(X,v=00051) + N2(X,v=17) ↔ CO2(X,v=00041) + N2(X,v=18) | KustovaScaling_CO2v3_N2 | 90 |

CO2(X,v=00011) + N2(X,v=18) ↔ CO2(X,v=00001) + N2(X,v=19) | KustovaScaling_CO2v3_N2 | 19 |

CO2(X,v=00021) + N2(X,v=18) ↔ CO2(X,v=00011) + N2(X,v=19) | KustovaScaling_CO2v3_N2 | 38 |

CO2(X,v=00031) + N2(X,v=18) ↔ CO2(X,v=00021) + N2(X,v=19) | KustovaScaling_CO2v3_N2 | 57 |

CO2(X,v=00041) + N2(X,v=18) ↔ CO2(X,v=00031) + N2(X,v=19) | KustovaScaling_CO2v3_N2 | 76 |

CO2(X,v=00051) + N2(X,v=18) ↔ CO2(X,v=00041) + N2(X,v=19) | KustovaScaling_CO2v3_N2 | 95 |

CO2(X,v=00011) + N2(X,v=19) ↔ CO2(X,v=00001) + N2(X,v=20) | KustovaScaling_CO2v3_N2 | 20 |

CO2(X,v=00021) + N2(X,v=19) ↔ CO2(X,v=00011) + N2(X,v=20) | KustovaScaling_CO2v3_N2 | 40 |

CO2(X,v=00031) + N2(X,v=19) ↔ CO2(X,v=00021) + N2(X,v=20) | KustovaScaling_CO2v3_N2 | 60 |

CO2(X,v=00041) + N2(X,v=19) ↔ CO2(X,v=00031) + N2(X,v=20) | KustovaScaling_CO2v3_N2 | 80 |

CO2(X,v=00051) + N2(X,v=19) ↔ CO2(X,v=00041) + N2(X,v=20) | KustovaScaling_CO2v3_N2 | 100 |

CO2(X,v=00011) + N2(X,v=20) ↔ CO2(X,v=00001) + N2(X,v=21) | KustovaScaling_CO2v3_N2 | 21 |

CO2(X,v=00021) + N2(X,v=20) ↔ CO2(X,v=00011) + N2(X,v=21) | KustovaScaling_CO2v3_N2 | 42 |

CO2(X,v=00031) + N2(X,v=20) ↔ CO2(X,v=00021) + N2(X,v=21) | KustovaScaling_CO2v3_N2 | 63 |

CO2(X,v=00041) + N2(X,v=20) ↔ CO2(X,v=00031) + N2(X,v=21) | KustovaScaling_CO2v3_N2 | 84 |

CO2(X,v=00051) + N2(X,v=20) ↔ CO2(X,v=00041) + N2(X,v=21) | KustovaScaling_CO2v3_N2 | 105 |

CO2(X,v=00011) + N2(X,v=21) ↔ CO2(X,v=00001) + N2(X,v=22) | KustovaScaling_CO2v3_N2 | 22 |

CO2(X,v=00021) + N2(X,v=21) ↔ CO2(X,v=00011) + N2(X,v=22) | KustovaScaling_CO2v3_N2 | 44 |

CO2(X,v=00031) + N2(X,v=21) ↔ CO2(X,v=00021) + N2(X,v=22) | KustovaScaling_CO2v3_N2 | 66 |

CO2(X,v=00041) + N2(X,v=21) ↔ CO2(X,v=00031) + N2(X,v=22) | KustovaScaling_CO2v3_N2 | 88 |

CO2(X,v=00051) + N2(X,v=21) ↔ CO2(X,v=00041) + N2(X,v=22) | KustovaScaling_CO2v3_N2 | 110 |

CO2(X,v=00011) + N2(X,v=22) ↔ CO2(X,v=00001) + N2(X,v=23) | KustovaScaling_CO2v3_N2 | 43 |

CO2(X,v=00021) + N2(X,v=22) ↔ CO2(X,v=00021) + N2(X,v=23) | KustovaScaling_CO2v3_N2 | 46 |

CO2(X,v=00031) + N2(X,v=22) ↔ CO2(X,v=00021) + N2(X,v=23) | KustovaScaling_CO2v3_N2 | 69 |

CO2(X,v=00041) + N2(X,v=22) ↔ CO2(X,v=00031) + N2(X,v=23) | KustovaScaling_CO2v3_N2 | 92 |

CO2(X,v=00051) + N2(X,v=22) ↔ CO2(X,v=00041) + N2(X,v=23) | KustovaScaling_CO2v3_N2 | 115 |

CO2(X,v=00011) + N2(X,v=23) ↔ CO2(X,v=00001) + N2(X,v=24) | KustovaScaling_CO2v3_N2 | 24 |

CO2(X,v=00021) + N2(X,v=23) ↔ CO2(X,v=00011) + N2(X,v=24) | KustovaScaling_CO2v3_N2 | 48 |

CO2(X,v=00031) + N2(X,v=23) ↔ CO2(X,v=00021) + N2(X,v=24) | KustovaScaling_CO2v3_N2 | 72 |

CO2(X,v=00041) + N2(X,v=23) ↔ CO2(X,v=00031) + N2(X,v=24) | KustovaScaling_CO2v3_N2 | 96 |

CO2(X,v=00051) + N2(X,v=23) ↔ CO2(X,v=00041) + N2(X,v=24) | KustovaScaling_CO2v3_N2 | 120 |

CO2(X,v=00011) + N2(X,v=24) ↔ CO2(X,v=00001) + N2(X,v=25) | KustovaScaling_CO2v3_N2 | 25 |

CO2(X,v=00021) + N2(X,v=24) ↔ CO2(X,v=00011) + N2(X,v=25) | KustovaScaling_CO2v3_N2 | 50 |

CO2(X,v=00031) + N2(X,v=24) ↔ CO2(X,v=00021) + N2(X,v=25) | KustovaScaling_CO2v3_N2 | 75 |

CO2(X,v=00041) + N2(X,v=24) ↔ CO2(X,v=00031) + N2(X,v=25) | KustovaScaling_CO2v3_N2 | 100 |

CO2(X,v=00051) + N2(X,v=24) ↔ CO2(X,v=00041) + N2(X,v=25) | KustovaScaling_CO2v3_N2 | 125 |

CO2(X,v=00011) + N2(X,v=25) ↔ CO2(X,v=00001) + N2(X,v=26) | KustovaScaling_CO2v3_N2 | 26 |

CO2(X,v=00021) + N2(X,v=25) ↔ CO2(X,v=00011) + N2(X,v=26) | KustovaScaling_CO2v3_N2 | 52 |

CO2(X,v=00031) + N2(X,v=25) ↔ CO2(X,v=00021) + N2(X,v=26) | KustovaScaling_CO2v3_N2 | 78 |

CO2(X,v=00041) + N2(X,v=25) ↔ CO2(X,v=00031) + N2(X,v=26) | KustovaScaling_CO2v3_N2 | 104 |

CO2(X,v=00051) + N2(X,v=25) ↔ CO2(X,v=00041) + N2(X,v=26) | KustovaScaling_CO2v3_N2 | 130 |

CO2(X,v=00011) + N2(X,v=26) ↔ CO2(X,v=00001) + N2(X,v=27) | KustovaScaling_CO2v3_N2 | 27 |

CO2(X,v=00021) + N2(X,v=26) ↔ CO2(X,v=00011) + N2(X,v=27) | KustovaScaling_CO2v3_N2 | 54 |

CO2(X,v=00031) + N2(X,v=26) ↔ CO2(X,v=00021) + N2(X,v=27) | KustovaScaling_CO2v3_N2 | 81 |

CO2(X,v=00041) + N2(X,v=26) ↔ CO2(X,v=00031) + N2(X,v=27) | KustovaScaling_CO2v3_N2 | 108 |

CO2(X,v=00051) + N2(X,v=26) ↔ CO2(X,v=00041) + N2(X,v=27) | KustovaScaling_CO2v3_N2 | 135 |

CO2(X,v=00011) + N2(X,v=27) ↔ CO2(X,v=00001) + N2(X,v=28) | KustovaScaling_CO2v3_N2 | 28 |

CO2(X,v=00021) + N2(X,v=27) ↔ CO2(X,v=00011) + N2(X,v=28) | KustovaScaling_CO2v3_N2 | 56 |

CO2(X,v=00031) + N2(X,v=27) ↔ CO2(X,v=00021) + N2(X,v=28) | KustovaScaling_CO2v3_N2 | 84 |

CO2(X,v=00041) + N2(X,v=27) ↔ CO2(X,v=00031) + N2(X,v=28) | KustovaScaling_CO2v3_N2 | 112 |

CO2(X,v=00051) + N2(X,v=27) ↔ CO2(X,v=00041) + N2(X,v=28) | KustovaScaling_CO2v3_N2 | 140 |

CO2(X,v=00011) + N2(X,v=28) ↔ CO2(X,v=00001) + N2(X,v=29) | KustovaScaling_CO2v3_N2 | 29 |

CO2(X,v=00021) + N2(X,v=28) ↔ CO2(X,v=00011) + N2(X,v=29) | KustovaScaling_CO2v3_N2 | 58 |

CO2(X,v=00031) + N2(X,v=28) ↔ CO2(X,v=00021) + N2(X,v=29) | KustovaScaling_CO2v3_N2 | 87 |

CO2(X,v=00041) + N2(X,v=28) ↔ CO2(X,v=00031) + N2(X,v=29) | KustovaScaling_CO2v3_N2 | 116 |

CO2(X,v=00051) + N2(X,v=28) ↔ CO2(X,v=00041) + N2(X,v=29) | KustovaScaling_CO2v3_N2 | 145 |

CO2(X,v=00011) + N2(X,v=29) ↔ CO2(X,v=00001) + N2(X,v=30) | KustovaScaling_CO2v3_N2 | 30 |

CO2(X,v=00021) + N2(X,v=29) ↔ CO2(X,v=00011) + N2(X,v=30) | KustovaScaling_CO2v3_N2 | 60 |

CO2(X,v=00031) + N2(X,v=29) ↔ CO2(X,v=00021) + N2(X,v=30) | KustovaScaling_CO2v3_N2 | 90 |

CO2(X,v=00041) + N2(X,v=29) ↔ CO2(X,v=00031) + N2(X,v=30) | KustovaScaling_CO2v3_N2 | 120 |

CO2(X,v=00051) + N2(X,v=29) ↔ CO2(X,v=00041) + N2(X,v=30) | KustovaScaling_CO2v3_N2 | 150 |

CO2(X,v=00011) + N2(X,v=30) ↔ CO2(X,v=00001) + N2(X,v=31) | KustovaScaling_CO2v3_N2 | 31 |

CO2(X,v=00021) + N2(X,v=30) ↔ CO2(X,v=00011) + N2(X,v=31) | KustovaScaling_CO2v3_N2 | 62 |

CO2(X,v=00031) + N2(X,v=30) ↔ CO2(X,v=00021) + N2(X,v=31) | KustovaScaling_CO2v3_N2 | 93 |

CO2(X,v=00041) + N2(X,v=30) ↔ CO2(X,v=00031) + N2(X,v=31) | KustovaScaling_CO2v3_N2 | 124 |

CO2(X,v=00051) + N2(X,v=30) ↔ CO2(X,v=00041) + N2(X,v=31) | KustovaScaling_CO2v3_N2 | 155 |

CO2(X,v=00011) + N2(X,v=31) ↔ CO2(X,v=00001) + N2(X,v=32) | KustovaScaling_CO2v3_N2 | 32 |

CO2(X,v=00021) + N2(X,v=31) ↔ CO2(X,v=00011) + N2(X,v=32) | KustovaScaling_CO2v3_N2 | 64 |

CO2(X,v=00031) + N2(X,v=31) ↔ CO2(X,v=00021) + N2(X,v=32) | KustovaScaling_CO2v3_N2 | 96 |

CO2(X,v=00041) + N2(X,v=31) ↔ CO2(X,v=00031) + N2(X,v=32) | KustovaScaling_CO2v3_N2 | 128 |

CO2(X,v=00051) + N2(X,v=31) ↔ CO2(X,v=00041) + N2(X,v=32) | KustovaScaling_CO2v3_N2 | 160 |

CO2(X,v=00011) + N2(X,v=32) ↔ CO2(X,v=00001) + N2(X,v=33) | KustovaScaling_CO2v3_N2 | 33 |

CO2(X,v=00021) + N2(X,v=32) ↔ CO2(X,v=00001) + N2(X,v=33) | KustovaScaling_CO2v3_N2 | 66 |

CO2(X,v=00031) + N2(X,v=32) ↔ CO2(X,v=00021) + N2(X,v=33) | KustovaScaling_CO2v3_N2 | 99 |

CO2(X,v=00041) + N2(X,v=32) ↔ CO2(X,v=00031) + N2(X,v=33) | KustovaScaling_CO2v3_N2 | 132 |

CO2(X,v=00051) + N2(X,v=32) ↔ CO2(X,v=00041) + N2(X,v=33) | KustovaScaling_CO2v3_N2 | 165 |

CO2(X,v=00011) + N2(X,v=33) ↔ CO2(X,v=00001) + N2(X,v=34) | KustovaScaling_CO2v3_N2 | 34 |

CO2(X,v=00021) + N2(X,v=33) ↔ CO2(X,v=00011) + N2(X,v=34) | KustovaScaling_CO2v3_N2 | 68 |

CO2(X,v=00031) + N2(X,v=33) ↔ CO2(X,v=00021) + N2(X,v=34) | KustovaScaling_CO2v3_N2 | 102 |

CO2(X,v=00041) + N2(X,v=33) ↔ CO2(X,v=00031) + N2(X,v=34) | KustovaScaling_CO2v3_N2 | 136 |

CO2(X,v=00051) + N2(X,v=33) ↔ CO2(X,v=00041) + N2(X,v=34) | KustovaScaling_CO2v3_N2 | 170 |

CO2(X,v=00011) + N2(X,v=34) ↔ CO2(X,v=00001) + N2(X,v=35) | KustovaScaling_CO2v3_N2 | 35 |

CO2(X,v=00021) + N2(X,v=34) ↔ CO2(X,v=00011) + N2(X,v=35) | KustovaScaling_CO2v3_N2 | 70 |

CO2(X,v=00031) + N2(X,v=34) ↔ CO2(X,v=00021) + N2(X,v=35) | KustovaScaling_CO2v3_N2 | 105 |

CO2(X,v=00041) + N2(X,v=34) ↔ CO2(X,v=00031) + N2(X,v=35) | KustovaScaling_CO2v3_N2 | 140 |

CO2(X,v=00051) + N2(X,v=34) ↔ CO2(X,v=00041) + N2(X,v=35) | KustovaScaling_CO2v3_N2 | 175 |

CO2(X,v=00011) + N2(X,v=35) ↔ CO2(X,v=00001) + N2(X,v=36) | KustovaScaling_CO2v3_N2 | 36 |

CO2(X,v=00021) + N2(X,v=35) ↔ CO2(X,v=00011) + N2(X,v=36) | KustovaScaling_CO2v3_N2 | 72 |

CO2(X,v=00031) + N2(X,v=35) ↔ CO2(X,v=00021) + N2(X,v=36) | KustovaScaling_CO2v3_N2 | 108 |

CO2(X,v=00041) + N2(X,v=35) ↔ CO2(X,v=00031) + N2(X,v=36) | KustovaScaling_CO2v3_N2 | 144 |

CO2(X,v=00051) + N2(X,v=35) ↔ CO2(X,v=00041) + N2(X,v=36) | KustovaScaling_CO2v3_N2 | 180 |

CO2(X,v=00011) + N2(X,v=36) ↔ CO2(X,v=00001) + N2(X,v=37) | KustovaScaling_CO2v3_N2 | 37 |

CO2(X,v=00021) + N2(X,v=36) ↔ CO2(X,v=00011) + N2(X,v=37) | KustovaScaling_CO2v3_N2 | 74 |

CO2(X,v=00031) + N2(X,v=36) ↔ CO2(X,v=00021) + N2(X,v=37) | KustovaScaling_CO2v3_N2 | 111 |

CO2(X,v=00041) + N2(X,v=36) ↔ CO2(X,v=00031) + N2(X,v=37) | KustovaScaling_CO2v3_N2 | 148 |

CO2(X,v=00051) + N2(X,v=36) ↔ CO2(X,v=00041) + N2(X,v=37) | KustovaScaling_CO2v3_N2 | 185 |

CO2(X,v=00011) + N2(X,v=37) ↔ CO2(X,v=00001) + N2(X,v=38) | KustovaScaling_CO2v3_N2 | 38 |

CO2(X,v=00021) + N2(X,v=37) ↔ CO2(X,v=00011) + N2(X,v=38) | KustovaScaling_CO2v3_N2 | 76 |

CO2(X,v=00031) + N2(X,v=37) ↔ CO2(X,v=00021) + N2(X,v=38) | KustovaScaling_CO2v3_N2 | 114 |

CO2(X,v=00041) + N2(X,v=37) ↔ CO2(X,v=00031) + N2(X,v=38) | KustovaScaling_CO2v3_N2 | 152 |

CO2(X,v=00051) + N2(X,v=37) ↔ CO2(X,v=00041) + N2(X,v=38) | KustovaScaling_CO2v3_N2 | 190 |

CO2(X,v=00011) + N2(X,v=38) ↔ CO2(X,v=00001) + N2(X,v=39) | KustovaScaling_CO2v3_N2 | 39 |

CO2(X,v=00021) + N2(X,v=38) ↔ CO2(X,v=00011) + N2(X,v=39) | KustovaScaling_CO2v3_N2 | 78 |

CO2(X,v=00031) + N2(X,v=38) ↔ CO2(X,v=00021) + N2(X,v=39) | KustovaScaling_CO2v3_N2 | 117 |

CO2(X,v=00041) + N2(X,v=38) ↔ CO2(X,v=00031) + N2(X,v=39) | KustovaScaling_CO2v3_N2 | 156 |

CO2(X,v=00051) + N2(X,v=38) ↔ CO2(X,v=00041) + N2(X,v=39) | KustovaScaling_CO2v3_N2 | 195 |

CO2(X,v=00011) + N2(X,v=39) ↔ CO2(X,v=00001) + N2(X,v=40) | KustovaScaling_CO2v3_N2 | 40 |

CO2(X,v=00021) + N2(X,v=39) ↔ CO2(X,v=00011) + N2(X,v=40) | KustovaScaling_CO2v3_N2 | 80 |

CO2(X,v=00031) + N2(X,v=39) ↔ CO2(X,v=00021) + N2(X,v=40) | KustovaScaling_CO2v3_N2 | 120 |

CO2(X,v=00041) + N2(X,v=39) ↔ CO2(X,v=00031) + N2(X,v=40) | KustovaScaling_CO2v3_N2 | 160 |

CO2(X,v=00051) + N2(X,v=39) ↔ CO2(X,v=00041) + N2(X,v=40) | KustovaScaling_CO2v3_N2 | 200 |

CO2(X,v=00011) + N2(X,v=40) ↔ CO2(X,v=00001) + N2(X,v=41) | KustovaScaling_CO2v3_N2 | 41 |

CO2(X,v=00021) + N2(X,v=40) ↔ CO2(X,v=00011) + N2(X,v=41) | KustovaScaling_CO2v3_N2 | 82 |

CO2(X,v=00031) + N2(X,v=40) ↔ CO2(X,v=00021) + N2(X,v=41) | KustovaScaling_CO2v3_N2 | 123 |

CO2(X,v=00041) + N2(X,v=40) ↔ CO2(X,v=00031) + N2(X,v=41) | KustovaScaling_CO2v3_N2 | 164 |

CO2(X,v=00051) + N2(X,v=40) ↔ CO2(X,v=00041) + N2(X,v=41) | KustovaScaling_CO2v3_N2 | 205 |

CO2(X,v=00011) + N2(X,v=41) ↔ CO2(X,v=00001) + N2(X,v=42) | KustovaScaling_CO2v3_N2 | 42 |

CO2(X,v=00021) + N2(X,v=41) ↔ CO2(X,v=00011) + N2(X,v=42) | KustovaScaling_CO2v3_N2 | 84 |

CO2(X,v=00031) + N2(X,v=41) ↔ CO2(X,v=00021) + N2(X,v=42) | KustovaScaling_CO2v3_N2 | 126 |

CO2(X,v=00041) + N2(X,v=41) ↔ CO2(X,v=00031) + N2(X,v=42) | KustovaScaling_CO2v3_N2 | 168 |

CO2(X,v=00051) + N2(X,v=41) ↔ CO2(X,v=00041) + N2(X,v=42) | KustovaScaling_CO2v3_N2 | 210 |

CO2(X,v=00011) + N2(X,v=42) ↔ CO2(X,v=00001) + N2(X,v=43) | KustovaScaling_CO2v3_N2 | 43 |

CO2(X,v=00021) + N2(X,v=42) ↔ CO2(X,v=00011) + N2(X,v=43) | KustovaScaling_CO2v3_N2 | 86 |

CO2(X,v=00031) + N2(X,v=42) ↔ CO2(X,v=00021) + N2(X,v=43) | KustovaScaling_CO2v3_N2 | 129 |

CO2(X,v=00041) + N2(X,v=42) ↔ CO2(X,v=00031) + N2(X,v=43) | KustovaScaling_CO2v3_N2 | 172 |

CO2(X,v=00051) + N2(X,v=42) ↔ CO2(X,v=00041) + N2(X,v=43) | KustovaScaling_CO2v3_N2 | 215 |

CO2(X,v=00011) + N2(X,v=43) ↔ CO2(X,v=00001) + N2(X,v=44) | KustovaScaling_CO2v3_N2 | 44 |

CO2(X,v=00021) + N2(X,v=43) ↔ CO2(X,v=00011) + N2(X,v=44) | KustovaScaling_CO2v3_N2 | 88 |

CO2(X,v=00031) + N2(X,v=43) ↔ CO2(X,v=00021) + N2(X,v=44) | KustovaScaling_CO2v3_N2 | 132 |

CO2(X,v=00041) + N2(X,v=43) ↔ CO2(X,v=00031) + N2(X,v=44) | KustovaScaling_CO2v3_N2 | 176 |

CO2(X,v=00051) + N2(X,v=43) ↔ CO2(X,v=00041) + N2(X,v=44) | KustovaScaling_CO2v3_N2 | 220 |

CO2(X,v=00011) + N2(X,v=44) ↔ CO2(X,v=00001) + N2(X,v=45) | KustovaScaling_CO2v3_N2 | 45 |

CO2(X,v=00021) + N2(X,v=44) ↔ CO2(X,v=00011) + N2(X,v=45) | KustovaScaling_CO2v3_N2 | 90 |

CO2(X,v=00031) + N2(X,v=44) ↔ CO2(X,v=00021) + N2(X,v=45) | KustovaScaling_CO2v3_N2 | 135 |

CO2(X,v=00041) + N2(X,v=44) ↔ CO2(X,v=00031) + N2(X,v=45) | KustovaScaling_CO2v3_N2 | 180 |

CO2(X,v=00051) + N2(X,v=44) ↔ CO2(X,v=00041) + N2(X,v=45) | KustovaScaling_CO2v3_N2 | 225 |

CO2(X,v=00011) + N2(X,v=45) ↔ CO2(X,v=00001) + N2(X,v=46) | KustovaScaling_CO2v3_N2 | 46 |

CO2(X,v=00021) + N2(X,v=45) ↔ CO2(X,v=00011) + N2(X,v=46) | KustovaScaling_CO2v3_N2 | 92 |

CO2(X,v=00031) + N2(X,v=45) ↔ CO2(X,v=00021) + N2(X,v=46) | KustovaScaling_CO2v3_N2 | 138 |

CO2(X,v=00041) + N2(X,v=45) ↔ CO2(X,v=00031) + N2(X,v=46) | KustovaScaling_CO2v3_N2 | 184 |

CO2(X,v=00051) + N2(X,v=45) ↔ CO2(X,v=00041) + N2(X,v=46) | KustovaScaling_CO2v3_N2 | 230 |

CO2(X,v=00011) + N2(X,v=46) ↔ CO2(X,v=00001) + N2(X,v=47) | KustovaScaling_CO2v3_N2 | 47 |

CO2(X,v=00021) + N2(X,v=46) ↔ CO2(X,v=00011) + N2(X,v=47) | KustovaScaling_CO2v3_N2 | 94 |

CO2(X,v=00031) + N2(X,v=46) ↔ CO2(X,v=00021) + N2(X,v=47) | KustovaScaling_CO2v3_N2 | 141 |

CO2(X,v=00041) + N2(X,v=46) ↔ CO2(X,v=00031) + N2(X,v=47) | KustovaScaling_CO2v3_N2 | 188 |

CO2(X,v=00051) + N2(X,v=46) ↔ CO2(X,v=00041) + N2(X,v=47) | KustovaScaling_CO2v3_N2 | 235 |

CO2(X,v=00011) + N2(X,v=47) ↔ CO2(X,v=00001) + N2(X,v=48) | KustovaScaling_CO2v3_N2 | 48 |

CO2(X,v=00021) + N2(X,v=47) ↔ CO2(X,v=00011) + N2(X,v=48) | KustovaScaling_CO2v3_N2 | 96 |

CO2(X,v=00031) + N2(X,v=47) ↔ CO2(X,v=00021) + N2(X,v=48) | KustovaScaling_CO2v3_N2 | 144 |

CO2(X,v=00041) + N2(X,v=47) ↔ CO2(X,v=00031) + N2(X,v=48) | KustovaScaling_CO2v3_N2 | 192 |

CO2(X,v=00051) + N2(X,v=47) ↔ CO2(X,v=00041) + N2(X,v=48) | KustovaScaling_CO2v3_N2 | 240 |

CO2(X,v=00011) + N2(X,v=48) ↔ CO2(X,v=00001) + N2(X,v=49) | KustovaScaling_CO2v3_N2 | 49 |

CO2(X,v=00021) + N2(X,v=48) ↔ CO2(X,v=00011) + N2(X,v=49) | KustovaScaling_CO2v3_N2 | 98 |

CO2(X,v=00031) + N2(X,v=48) ↔ CO2(X,v=00021) + N2(X,v=49) | KustovaScaling_CO2v3_N2 | 147 |

CO2(X,v=00041) + N2(X,v=48) ↔ CO2(X,v=00031) + N2(X,v=49) | KustovaScaling_CO2v3_N2 | 196 |

CO2(X,v=00051) + N2(X,v=48) ↔ CO2(X,v=00041) + N2(X,v=49) | KustovaScaling_CO2v3_N2 | 245 |

CO2(X,v=00011) + N2(X,v=49) ↔ CO2(X,v=00001) + N2(X,v=50) | KustovaScaling_CO2v3_N2 | 50 |

CO2(X,v=00021) + N2(X,v=49) ↔ CO2(X,v=00011) + N2(X,v=50) | KustovaScaling_CO2v3_N2 | 100 |

CO2(X,v=00031) + N2(X,v=49) ↔ CO2(X,v=00021) + N2(X,v=50) | KustovaScaling_CO2v3_N2 | 150 |

CO2(X,v=00041) + N2(X,v=49) ↔ CO2(X,v=00031) + N2(X,v=50) | KustovaScaling_CO2v3_N2 | 200 |

CO2(X,v=00051) + N2(X,v=49) ↔ CO2(X,v=00041) + N2(X,v=50) | KustovaScaling_CO2v3_N2 | 250 |

CO2(X,v=00011) + N2(X,v=50) ↔ CO2(X,v=00001) + N2(X,v=51) | KustovaScaling_CO2v3_N2 | 51 |

CO2(X,v=00021) + N2(X,v=50) ↔ CO2(X,v=00011) + N2(X,v=51) | KustovaScaling_CO2v3_N2 | 102 |

CO2(X,v=00031) + N2(X,v=50) ↔ CO2(X,v=00021) + N2(X,v=51) | KustovaScaling_CO2v3_N2 | 153 |

CO2(X,v=00041) + N2(X,v=50) ↔ CO2(X,v=00031) + N2(X,v=51) | KustovaScaling_CO2v3_N2 | 204 |

CO2(X,v=00051) + N2(X,v=50) ↔ CO2(X,v=00041) + N2(X,v=51) | KustovaScaling_CO2v3_N2 | 255 |

CO2(X,v=00011) + N2(X,v=51) ↔ CO2(X,v=00001) + N2(X,v=52) | KustovaScaling_CO2v3_N2 | 52 |

CO2(X,v=00021) + N2(X,v=51) ↔ CO2(X,v=00011) + N2(X,v=52) | KustovaScaling_CO2v3_N2 | 104 |

CO2(X,v=00031) + N2(X,v=51) ↔ CO2(X,v=00021) + N2(X,v=52) | KustovaScaling_CO2v3_N2 | 156 |

CO2(X,v=00041) + N2(X,v=51) ↔ CO2(X,v=00031) + N2(X,v=52) | KustovaScaling_CO2v3_N2 | 208 |

CO2(X,v=00051) + N2(X,v=51) ↔ CO2(X,v=00041) + N2(X,v=52) | KustovaScaling_CO2v3_N2 | 260 |

CO2(X,v=00011) + N2(X,v=52) ↔ CO2(X,v=00001) + N2(X,v=53) | KustovaScaling_CO2v3_N2 | 53 |

CO2(X,v=00021) + N2(X,v=52) ↔ CO2(X,v=00011) + N2(X,v=53) | KustovaScaling_CO2v3_N2 | 106 |

CO2(X,v=00031) + N2(X,v=52) ↔ CO2(X,v=00021) + N2(X,v=53) | KustovaScaling_CO2v3_N2 | 159 |

CO2(X,v=00041) + N2(X,v=52) ↔ CO2(X,v=00031) + N2(X,v=53) | KustovaScaling_CO2v3_N2 | 212 |

CO2(X,v=00051) + N2(X,v=52) ↔ CO2(X,v=00041) + N2(X,v=53) | KustovaScaling_CO2v3_N2 | 265 |

CO2(X,v=00011) + N2(X,v=53) ↔ CO2(X,v=00001) + N2(X,v=54) | KustovaScaling_CO2v3_N2 | 54 |

CO2(X,v=00021) + N2(X,v=53) ↔ CO2(X,v=00011) + N2(X,v=54) | KustovaScaling_CO2v3_N2 | 108 |

CO2(X,v=00031) + N2(X,v=53) ↔ CO2(X,v=00021) + N2(X,v=54) | KustovaScaling_CO2v3_N2 | 162 |

CO2(X,v=00041) + N2(X,v=53) ↔ CO2(X,v=00031) + N2(X,v=54) | KustovaScaling_CO2v3_N2 | 216 |

CO2(X,v=00051) + N2(X,v=53) ↔ CO2(X,v=00041) + N2(X,v=54) | KustovaScaling_CO2v3_N2 | 270 |

CO2(X,v=00011) + N2(X,v=54) ↔ CO2(X,v=00001) + N2(X,v=55) | KustovaScaling_CO2v3_N2 | 55 |

CO2(X,v=00021) + N2(X,v=54) ↔ CO2(X,v=00011) + N2(X,v=55) | KustovaScaling_CO2v3_N2 | 110 |

CO2(X,v=00031) + N2(X,v=54) ↔ CO2(X,v=00021) + N2(X,v=55) | KustovaScaling_CO2v3_N2 | 165 |

CO2(X,v=00041) + N2(X,v=54) ↔ CO2(X,v=00031) + N2(X,v=55) | KustovaScaling_CO2v3_N2 | 220 |

CO2(X,v=00051) + N2(X,v=54) ↔ CO2(X,v=00041) + N2(X,v=55) | KustovaScaling_CO2v3_N2 | 275 |

CO2(X,v=00011) + N2(X,v=55) ↔ CO2(X,v=00001) + N2(X,v=56) | KustovaScaling_CO2v3_N2 | 56 |

CO2(X,v=00021) + N2(X,v=55) ↔ CO2(X,v=00011) + N2(X,v=56) | KustovaScaling_CO2v3_N2 | 112 |

CO2(X,v=00031) + N2(X,v=55) ↔ CO2(X,v=00021) + N2(X,v=56) | KustovaScaling_CO2v3_N2 | 168 |

CO2(X,v=00041) + N2(X,v=55) ↔ CO2(X,v=00031) + N2(X,v=56) | KustovaScaling_CO2v3_N2 | 224 |

CO2(X,v=00051) + N2(X,v=55) ↔ CO2(X,v=00041) + N2(X,v=56) | KustovaScaling_CO2v3_N2 | 280 |

CO2(X,v=00011) + N2(X,v=56) ↔ CO2(X,v=00001) + N2(X,v=57) | KustovaScaling_CO2v3_N2 | 57 |

CO2(X,v=00021) + N2(X,v=56) ↔ CO2(X,v=00011) + N2(X,v=57) | KustovaScaling_CO2v3_N2 | 114 |

CO2(X,v=00031) + N2(X,v=56) ↔ CO2(X,v=00021) + N2(X,v=57) | KustovaScaling_CO2v3_N2 | 171 |

CO2(X,v=00041) + N2(X,v=56) ↔ CO2(X,v=00031) + N2(X,v=57) | KustovaScaling_CO2v3_N2 | 228 |

CO2(X,v=00051) + N2(X,v=56) ↔ CO2(X,v=00041) + N2(X,v=57) | KustovaScaling_CO2v3_N2 | 285 |

CO2(X,v=00011) + N2(X,v=57) ↔ CO2(X,v=00001) + N2(X,v=58) | KustovaScaling_CO2v3_N2 | 58 |

CO2(X,v=00021) + N2(X,v=57) ↔ CO2(X,v=00011) + N2(X,v=58) | KustovaScaling_CO2v3_N2 | 116 |

CO2(X,v=00031) + N2(X,v=57) ↔ CO2(X,v=00021) + N2(X,v=58) | KustovaScaling_CO2v3_N2 | 174 |

CO2(X,v=00041) + N2(X,v=57) ↔ CO2(X,v=00031) + N2(X,v=58) | KustovaScaling_CO2v3_N2 | 232 |

CO2(X,v=00051) + N2(X,v=57) ↔ CO2(X,v=00041) + N2(X,v=58) | KustovaScaling_CO2v3_N2 | 290 |

CO2(X,v=00011) + N2(X,v=58) ↔ CO2(X,v=00001) + N2(X,v=59) | KustovaScaling_CO2v3_N2 | 59 |

CO2(X,v=00021) + N2(X,v=58) ↔ CO2(X,v=00011) + N2(X,v=59) | KustovaScaling_CO2v3_N2 | 118 |

CO2(X,v=00031) + N2(X,v=58) ↔ CO2(X,v=00021) + N2(X,v=59) | KustovaScaling_CO2v3_N2 | 177 |

CO2(X,v=00041) + N2(X,v=58) ↔ CO2(X,v=00031) + N2(X,v=59) | KustovaScaling_CO2v3_N2 | 236 |

CO2(X,v=00051) + N2(X,v=58) ↔ CO2(X,v=00041) + N2(X,v=59) | KustovaScaling_CO2v3_N2 | 295 |

B. Calculated concentrations of all the species considered in the model

Table 4: Densities in m^{-3} of all the species included in the model, at 2 Torr and 50 mA, for different CO_2-N_2 mixtures for the short tube (length 0.23 cm) where the CO_2 dissociation fraction and NO densities are measured.

	2 Torr					
	short tube 0.23 cm					
CO_2 fraction	0.1	0.25	0.5	0.75	0.9	1
species density (m^{-3})						
$O_2(X^3\Sigma_g^-)$	1.59E+20	5.81E+20	1.37E+21	2.14E+21	2.59E+21	2.95E+21
$O_2(a^1\Delta_g)$	1.98E+19	5.22E+19	1.05E+20	1.67E+20	2.10E+20	2.46E+20
$O_2(b^1\Sigma_g^+)$	5.12E+17	6.52E+17	7.00E+17	8.11E+17	9.15E+17	1.04E+18
$O_2(A'^3\Delta_u, A^3\Sigma_u^+, c^1\Sigma_u^-)$	2.32E+16	4.29E+16	8.00E+16	1.22E+17	1.49E+17	1.66E+17
O_2^+	2.45E+15	2.17E+15	1.54E+15	1.56E+15	2.23E+15	9.23E+15
$O(^3P)$	1.34E+21	2.00E+21	2.24E+21	2.44E+21	2.61E+21	2.85E+21
$O(^1D)$	1.65E+17	7.42E+16	4.17E+16	3.55E+16	3.56E+16	3.80E+16
O^+	6.16E+13	1.74E+13	6.47E+12	3.89E+12	3.31E+12	3.40E+12
O^-	3.87E+13	5.39E+13	8.22E+13	1.13E+14	1.34E+14	1.47E+14
O_3	9.12E+14	3.25E+15	6.29E+15	8.80E+15	1.01E+16	1.18E+16
O_3*	6.58E+11	8.55E+12	4.15E+13	9.22E+13	1.28E+14	1.64E+14
$CO_2(X^1\Sigma^+_g)$	1.20E+21	3.77E+21	8.31E+21	1.26E+22	1.49E+22	1.63E+22
CO_2^+	2.86E+14	2.11E+14	1.81E+14	1.61E+14	1.54E+14	1.56E+14
$C(^3P)$	4.25E+16	1.73E+16	9.45E+15	7.56E+15	7.22E+15	7.38E+15
$CO(a^3\Pi_r)$	4.07E+16	3.63E+16	3.54E+16	3.74E+16	3.95E+16	4.18E+16
$CO(X^1\Sigma^+)$	1.78E+21	3.39E+21	5.37E+21	7.24E+21	8.35E+21	9.24E+21
CO^+	3.21E+13	9.01E+12	3.43E+12	2.12E+12	1.83E+12	1.91E+12
$N_2(X\ ^1\Sigma_g^+)$	2.68E+22	2.14E+22	1.36E+22	6.53E+21	2.53E+21	
$N_2(A\ ^3\Sigma_u^+)$	1.59E+18	5.62E+17	1.62E+17	4.68E+16	1.45E+16	
$N_2(B^3\Pi_g)$	6.89E+16	2.08E+16	9.23E+15	4.00E+15	1.55E+15	
$N_2(C\ ^3\Pi_u)$	2.17E+14	1.16E+14	5.32E+13	2.10E+13	7.63E+12	
$N_2(w\ ^1\Delta_u)$	1.15E+16	7.55E+15	4.01E+15	1.73E+15	6.47E+14	
$N_2(a\ ^1\Pi_g)$	1.37E+16	7.25E+15	2.70E+15	8.63E+14	2.76E+14	
$N_2(a'\ ^1\Sigma_u^-)$	2.49E+17	7.33E+16	1.46E+16	3.81E+15	1.35E+15	
N_2^+	4.01E+14	1.23E+14	3.63E+13	1.08E+13	3.59E+12	
$N_2^+(B\ ^2\Sigma_u^+)$	8.11E+10	2.17E+10	6.37E+09	1.80E+09	5.77E+08	
$N(^4S)$	6.21E+18	1.26E+18	2.66E+17	7.85E+16	3.11E+16	
$N(^2D)$	1.38E+18	4.57E+17	9.19E+16	2.37E+16	7.89E+15	
$N(^2P)$	5.14E+16	5.30E+15	4.44E+14	9.03E+13	3.49E+13	
N^+	1.64E+12	1.26E+11	7.22E+09	9.67E+08	2.61E+08	
N_4^+	1.53E+13	1.56E+12	1.27E+11	7.61E+09	4.10E+08	
N_3^+	1.06E+13	6.19E+11	2.98E+10	1.95E+09	1.87E+08	
$NO(X\ ^2\Pi_r)$	7.91E+19	1.18E+20	1.87E+20	1.88E+20	1.25E+20	
$NO(A\ ^2\Sigma^+)$	1.83E+15	9.45E+14	4.22E+14	1.20E+14	2.43E+13	
$NO(B^2\Pi_r)$	7.56E+10	1.81E+10	2.73E+09	5.01E+08	1.28E+08	
NO^+	7.14E+15	7.71E+15	8.09E+15	7.84E+15	7.08E+15	

$NO_2(X^2A_1)$	8.92E+15	1.10E+16	1.28E+16	8.55E+15	4.09E+15	
$NO_2(a^4A_2)$	6.44E+13	1.42E+14	2.52E+14	2.71E+14	1.87E+14	
$CN(X^2\Sigma^+)$	1.61E+11	5.15E+10	1.66E+10	5.25E+09	1.39E+09	
$CN(B^2\Sigma^+)$	6.98E+08	2.51E+07	2.65E+06	5.49E+05	1.63E+05	
n_e	1.04E+16	1.02E+16	9.78E+15	9.46E+15	9.34E+15	9.24E+15

Table 5: Densities in m^{-3} of all the species included in the model, at 2 Torr and 50 mA, for different CO_2-N_2 mixtures for the long tube (length 0.67 cm) where the O density is measured.

	2 Torr					
	long tube 0.67 cm					
CO_2 fraction	0.1	0.25	0.5	0.75	0.9	1
species density (m^{-3})						
$O_2(X^3\Sigma_g^-)$	2.38E+20	9.65E+20	2.18E+21	3.26E+21	3.83E+21	4.25E+21
$O_2(a^1\Delta_g)$	3.10E+19	8.72E+19	1.69E+20	2.53E+20	3.06E+20	3.47E+20
$O_2(b^1\Sigma_g^+)$	1.29E+18	1.70E+18	1.68E+18	1.77E+18	1.88E+18	2.05E+18
$O_2(A'^3\Delta_u, A^3\Sigma_u^+, c^1\Sigma_u^-)$	2.79E+16	5.79E+16	1.03E+17	1.44E+17	1.67E+17	1.80E+17
O_2^+	2.20E+15	1.69E+15	1.21E+15	1.22E+15	1.67E+15	9.44E+15
$O(^3P)$	1.70E+21	2.46E+21	2.71E+21	2.95E+21	3.15E+21	3.43E+21
$O(^1D)$	3.19E+17	1.25E+17	6.38E+16	5.08E+16	4.95E+16	5.18E+16
O^+	1.27E+14	2.93E+13	9.59E+12	5.43E+12	4.49E+12	4.54E+12
O^-	3.23E+13	5.01E+13	7.41E+13	9.57E+13	1.09E+14	1.19E+14
O_3	1.31E+15	5.38E+15	1.00E+16	1.34E+16	1.49E+16	1.73E+16
O_3*	1.49E+12	2.26E+13	9.83E+13	1.98E+14	2.60E+14	3.21E+14
$CO_2(X^1\Sigma^+_g)$	5.95E+20	2.20E+21	5.30E+21	8.35E+21	9.98E+21	1.09E+22
CO_2^+	1.96E+14	1.43E+14	1.24E+14	1.09E+14	1.03E+14	1.04E+14
$C(^3P)$	3.89E+16	1.48E+16	8.44E+15	6.86E+15	6.54E+15	6.62E+15
$CO(a^3\Pi_r)$	4.34E+16	3.96E+16	3.83E+16	3.90E+16	4.03E+16	4.17E+16
$CO(X^1\Sigma^+)$	2.34E+21	4.74E+21	7.68E+21	1.02E+22	1.16E+22	1.26E+22
CO^+	7.94E+13	2.05E+13	7.57E+12	4.50E+12	3.76E+12	3.79E+12
$N_2(X\ ^1\Sigma_g^+)$	2.64E+22	2.07E+22	1.29E+22	6.06E+21	2.31E+21	
$N_2(A\ ^3\Sigma_u^+)$	1.19E+18	3.37E+17	8.76E+16	2.46E+16	7.58E+15	
$N_2(B^3\Pi_g)$	5.51E+16	1.59E+16	6.42E+15	2.54E+15	9.32E+14	
$N_2(C\ ^3\Pi_u)$	2.01E+14	1.02E+14	4.54E+13	1.74E+13	6.15E+12	
$N_2(w\ ^1\Delta_u)$	1.09E+16	6.09E+15	2.70E+15	1.03E+15	3.65E+14	
$N_2(a\ ^1\Pi_g)$	1.25E+16	5.14E+15	1.58E+15	4.77E+14	1.51E+14	
$N_2(a'\ ^1\Sigma_u^-)$	1.88E+17	3.85E+16	7.27E+15	2.03E+15	7.28E+14	
N_2^+	3.14E+14	9.22E+13	2.81E+13	8.51E+12	2.78E+12	
$N_2^+(B\ ^2\Sigma_u^+)$	7.17E+10	2.24E+10	7.44E+09	2.27E+09	7.25E+08	
$N(^4S)$	5.23E+18	7.42E+17	1.48E+17	4.57E+16	1.82E+16	
$N(^2D)$	1.11E+18	2.44E+17	4.29E+16	1.09E+16	3.58E+15	
$N(^2P)$	3.27E+16	1.79E+15	1.40E+14	3.02E+13	1.16E+13	
N^+	1.07E+12	4.25E+10	2.15E+09	2.93E+08	7.94E+07	
N_4^+	7.87E+12	6.74E+11	5.88E+10	3.50E+09	1.68E+08	
N_3^+	5.28E+12	1.93E+11	8.81E+09	5.80E+08	5.45E+07	
$NO(X\ ^2\Pi_r)$	9.61E+19	1.68E+20	2.58E+20	2.55E+20	1.80E+20	
$NO(A\ ^2\Sigma^+)$	1.66E+15	7.99E+14	3.05E+14	8.22E+13	1.76E+13	

$NO(B^2\Pi_r)$	7.88E+10	1.24E+10	1.72E+09	3.51E+08	1.00E+08	
NO^+	7.47E+15	8.36E+15	8.68E+15	8.47E+15	7.90E+15	
$NO_2(X^2A_1)$	6.90E+15	1.14E+16	1.39E+16	8.94E+15	4.23E+15	
$NO_2(a^4A_2)$	1.89E+14	3.73E+14	5.14E+14	4.92E+14	3.43E+14	
$CN(X^2\Sigma^+)$	1.45E+11	4.29E+10	1.45E+10	4.87E+09	1.39E+09	
$CN(B^2\Sigma^+)$	5.14E+08	1.46E+07	1.43E+06	3.07E+05	9.25E+04	
n_e	1.04E+16	1.03E+16	9.99E+15	9.73E+15	9.58E+15	9.44E+15

Table 6: Densities in m^{-3} of all the species included in the model, at 2 Torr and 50mA, for different CO_2-N_2 mixtures and including the reactions with N_2(A,B) from section III.1.1. for the short tube (length 0.23 cm) where the CO_2 dissociation fraction and NO densities are measured.

	2 Torr				
	short tube 0.23 cm				
CO_2 fraction	0.1	0.25	0.5	0.75	0.9
species density (m^{-3})					
$O_2(X^3\Sigma_g^-)$	2.49E+20	8.16E+20	1.65E+21	2.31E+21	2.66E+21
$O_2(a^1\Delta_g)$	3.01E+19	7.03E+19	1.25E+20	1.80E+20	2.16E+20
$O_2(b^1\Sigma_g^+)$	1.15E+18	1.07E+18	9.23E+17	9.01E+17	9.48E+17
$O_2(A'^3\Delta_u, A^3\Sigma_u^+, c^1\Sigma_u^-)$	3.17E+16	5.69E+16	9.51E+16	1.31E+17	1.52E+17
O_2^+	2.33E+15	2.12E+15	1.62E+15	1.61E+15	2.17E+15
$O(^3P)$	1.56E+21	2.11E+21	2.26E+21	2.42E+21	2.60E+21
$O(^1D)$	2.63E+17	8.93E+16	4.54E+16	3.61E+16	3.58E+16
O^+	1.01E+14	2.06E+13	6.87E+12	3.91E+12	3.31E+12
O^-	3.71E+13	5.61E+13	8.43E+13	1.14E+14	1.33E+14
O_3	1.39E+15	4.53E+15	7.59E+15	9.50E+15	1.04E+16
O_3*	1.61E+12	1.62E+13	5.78E+13	1.05E+14	1.34E+14
$CO_2(X^1\Sigma^+_g)$	7.33E+20	3.06E+21	7.53E+21	1.22E+22	1.47E+22
CO_2^+	2.21E+14	1.83E+14	1.69E+14	1.57E+14	1.52E+14
$C(^3P)$	3.49E+16	1.47E+16	8.79E+15	7.32E+15	7.15E+15
$CO(a^3\Pi_r)$	4.38E+16	3.88E+16	3.72E+16	3.80E+16	3.97E+16
$CO(X^1\Sigma^+)$	2.21E+21	4.00E+21	5.99E+21	7.59E+21	8.49E+21
CO^+	6.27E+13	1.28E+13	4.21E+12	2.29E+12	1.88E+12
$N_2(X\ ^1\Sigma_g^+)$	2.65E+22	2.11E+22	1.34E+22	6.50E+21	2.52E+21
$N_2(A\ ^3\Sigma_u^+)$	1.10E+18	3.78E+17	1.23E+17	4.20E+16	1.48E+16
$N_2(B^3\Pi_g)$	3.69E+16	9.00E+15	3.04E+15	1.06E+15	3.71E+14
$N_2(C\ ^3\Pi_u)$	2.01E+14	1.08E+14	5.10E+13	2.05E+13	7.54E+12
$N_2(w\ ^1\Delta_u)$	1.09E+16	6.68E+15	3.52E+15	1.59E+15	6.25E+14
$N_2(a\ ^1\Pi_g)$	1.25E+16	5.91E+15	2.24E+15	7.83E+14	2.66E+14
$N_2(a'\ ^1\Sigma_u^-)$	1.99E+17	5.52E+16	1.25E+16	3.60E+15	1.30E+15
N_2^+	3.39E+14	1.11E+14	3.52E+13	1.07E+13	3.56E+12
$N_2^+(B\ ^2\Sigma_u^+)$	7.54E+10	2.20E+10	6.65E+09	1.84E+09	5.81E+08
$N(^4S)$	5.41E+18	9.63E+17	2.32E+17	7.47E+16	3.01E+16
$N(^2D)$	9.82E+17	2.87E+17	6.64E+16	2.06E+16	7.86E+15
$N(^2P)$	3.14E+16	2.82E+15	3.15E+14	7.89E+13	3.34E+13
N^+	9.71E+11	6.14E+10	4.56E+09	7.87E+08	2.51E+08
N_4^+	8.94E+12	1.07E+12	1.08E+11	7.12E+09	3.96E+08

N_3^+	5.33E+12	3.12E+11	1.98E+10	1.66E+09	1.85E+08
$NO(X\ ^2\Pi_r)$	8.89E+19	1.24E+20	1.79E+20	1.81E+20	1.30E+20
$NO(A\ ^2\Sigma^+)$	1.42E+15	6.64E+14	3.03E+14	1.03E+14	2.58E+13
$NO(B^2\Pi_r)$	7.55E+10	1.44E+10	2.40E+09	4.80E+08	1.25E+08
NO^+	7.33E+15	7.80E+15	8.10E+15	7.79E+15	7.14E+15
$NO_2(X^2A_1)$	9.88E+15	1.13E+16	1.13E+16	6.59E+15	2.75E+15
$NO_2(a^4A_2)$	8.43E+13	1.58E+14	2.43E+14	2.59E+14	1.92E+14
$CN(X^2\Sigma^+)$	1.30E+11	4.28E+10	1.51E+10	4.98E+09	1.35E+09
$CN(B^2\Sigma^+)$	5.01E+08	1.69E+07	2.05E+06	4.92E+05	1.58E+05
n_e	1.04E+16	1.02E+16	9.86E+15	9.46E+15	9.34E+15

Table 7: Densities in m^{-3} of all the species included in the model, for a 50 % CO_2 50 % N_2 initial gas mixture, for different pressures, at 50mA and including the reactions with N_2(A,B) from section III.1.1. for the short tube (length 0.23 cm) where the CO_2 dissociation fraction and NO densities are measured.

	50 % CO2 50 % N2			
	short tube 0.23 cm			
Pressure (Torr)	0.6	1	2	4
species density (m^{-3})				
$O_2(X^3\Sigma_g^-)$	4.98E+20	6.34E+20	1.36E+21	3.11E+21
$O_2(a^1\Delta_g)$	4.37E+19	5.42E+19	1.05E+20	2.03E+20
$O_2(b^1\Sigma_g^+)$	6.30E+17	6.20E+17	6.97E+17	6.50E+17
$O_2(A'^3\Delta_u, A^3\Sigma_u^+, c^1\Sigma_u^-)$	8.50E+16	6.63E+16	7.93E+16	1.26E+17
O_2^+	3.74E+15	2.97E+15	1.54E+15	7.86E+14
$O(^3P)$	1.04E+21	1.60E+21	2.25E+21	2.29E+21
$O(^1D)$	6.21E+16	5.90E+16	4.18E+16	2.35E+16
O^+	3.59E+13	2.09E+13	6.49E+12	1.62E+12
O^-	1.14E+14	8.73E+13	8.17E+13	9.04E+13
O_3	9.48E+15	5.48E+15	6.27E+15	7.67E+15
O_3*	1.21E+13	1.35E+13	4.13E+13	1.19E+14
$CO_2(X^1\Sigma^+_g)$	3.77E+21	5.03E+21	8.31E+21	1.41E+22
CO_2^+	9.17E+14	4.60E+14	1.81E+14	8.53E+13
$C(^3P)$	2.49E+16	2.03E+16	9.48E+15	4.25E+15
$CO(a^3\Pi_r)$	5.69E+16	4.65E+16	3.54E+16	2.76E+16
$CO(X^1\Sigma^+)$	2.22E+21	3.10E+21	5.37E+21	9.16E+21
CO^+	2.01E+13	1.05E+13	3.43E+12	1.05E+12
$N_2(X\ ^1\Sigma_g^+)$	5.95E+21	8.07E+21	1.36E+22	2.31E+22
$N_2(A\ ^3\Sigma_u^+)$	3.60E+17	2.80E+17	1.62E+17	8.71E+16
$N_2(B^3\Pi_g)$	1.86E+16	1.49E+16	9.25E+15	5.24E+15
$N_2(C\ ^3\Pi_u)$	7.46E+13	6.66E+13	5.32E+13	4.06E+13
$N_2(w\ ^1\Delta_u)$	9.32E+15	7.34E+15	4.02E+15	1.99E+15
$N_2(a\ ^1\Pi_g)$	6.59E+15	5.28E+15	2.71E+15	1.25E+15
$N_2(a'\ ^1\Sigma_u^-)$	3.15E+16	2.60E+16	1.46E+16	8.05E+15
N_2^+	1.78E+14	9.74E+13	3.62E+13	1.48E+13
$N_2^+(B\ ^2\Sigma_u^+)$	3.78E+10	1.95E+10	6.37E+09	2.04E+09
$N(^4S)$	5.58E+17	4.52E+17	2.67E+17	1.37E+17
$N(^2D)$	1.99E+17	1.85E+17	9.25E+16	2.94E+16

$N(^2P)$	2.20E+15	1.47E+15	4.46E+14	9.14E+13
N^+	1.59E+11	7.00E+10	7.29E+09	4.45E+08
N_4^+	5.09E+11	2.79E+11	1.27E+11	7.56E+10
N_3^+	2.92E+11	1.53E+11	2.98E+10	4.06E+09
$NO(X\ ^2\Pi_r)$	9.12E+19	1.20E+20	1.87E+20	2.40E+20
$NO(A\ ^2\Sigma^+)$	4.71E+14	4.82E+14	4.23E+14	2.75E+14
$NO(B^2\Pi_r)$	2.16E+09	2.67E+09	2.75E+09	1.75E+09
NO^+	3.51E+15	5.38E+15	8.09E+15	9.79E+15
$NO_2(X^2A_1)$	9.96E+14	2.67E+15	1.01E+16	3.11E+16
$NO_2(a^4A_2)$	7.55E+13	1.49E+14	3.09E+14	3.80E+14
$CN(X^2\Sigma^+)$	1.90E+10	2.12E+10	1.67E+10	1.26E+10
$CN(B^2\Sigma^+)$	2.49E+07	1.11E+07	2.67E+06	5.87E+05
n_e	8.29E+15	8.86E+15	9.78E+15	1.06E+16

Table 8: Densities in m^{-3} of all the species included in the model, for a 50 % CO_2 50 % N_2 initial gas mixture, for different pressures, at 50mA and including the reactions with N_2(A,B) from section III.1.1. for the long tube (length 0.67 cm) where the O density is measured.

	50 % CO2 50 % N2			
	long tube 0.67 cm			
Pressure (Torr)	0.6	1	2	4
species density (m^{-3})				
$O_2(X^3\Sigma_g^-)$	8.46E+20	1.08E+21	2.18E+21	4.63E+21
$O_2(a^1\Delta_g)$	7.70E+19	9.45E+19	1.69E+20	2.97E+20
$O_2(b^1\Sigma_g^+)$	1.65E+18	1.64E+18	1.68E+18	1.35E+18
$O_2(A'^3\Delta_u, A^3\Sigma_u^+, c^1\Sigma_u^-)$	1.16E+17	8.89E+16	1.03E+17	1.57E+17
O_2^+	3.26E+15	2.41E+15	1.21E+15	6.56E+14
$O(^3P)$	1.34E+21	2.03E+21	2.71E+21	2.63E+21
$O(^1D)$	1.02E+17	9.67E+16	6.38E+16	3.31E+16
O^+	5.78E+13	3.35E+13	9.59E+12	2.14E+12
O^-	1.01E+14	7.66E+13	7.41E+13	8.26E+13
O_3	1.46E+16	8.89E+15	1.00E+16	1.13E+16
O_3*	3.51E+13	3.77E+13	9.83E+13	2.34E+14
$CO_2(X^1\Sigma^+_g)$	2.33E+21	3.10E+21	5.30E+21	9.45E+21
CO_2^+	6.14E+14	3.07E+14	1.24E+14	5.95E+13
$C(^3P)$	2.17E+16	1.75E+16	8.44E+15	3.98E+15
$CO(a^3\Pi_r)$	6.28E+16	5.09E+16	3.83E+16	2.94E+16
$CO(X^1\Sigma^+)$	3.32E+21	4.55E+21	7.68E+21	1.28E+22
CO^+	4.80E+13	2.47E+13	7.57E+12	2.16E+12
$N_2(X\ ^1\Sigma_g^+)$	5.58E+21	7.57E+21	1.29E+22	2.21E+22
$N_2(A\ ^3\Sigma_u^+)$	1.91E+17	1.48E+17	8.76E+16	4.91E+16
$N_2(B^3\Pi_g)$	1.24E+16	1.02E+16	6.42E+15	3.71E+15
$N_2(C\ ^3\Pi_u)$	6.20E+13	5.60E+13	4.54E+13	3.50E+13
$N_2(w\ ^1\Delta_u)$	6.13E+15	4.89E+15	2.70E+15	1.37E+15
$N_2(a\ ^1\Pi_g)$	3.71E+15	3.00E+15	1.58E+15	7.66E+14
$N_2(a'\ ^1\Sigma_u^-)$	1.46E+16	1.20E+16	7.27E+15	4.49E+15
N_2^+	1.31E+14	7.23E+13	2.81E+13	1.20E+13

$N_2^+(B\ ^2\Sigma_u^+)$	4.02E+10	2.16E+10	7.44E+09	2.47E+09
$N(^4S)$	3.50E+17	2.56E+17	1.48E+17	8.21E+16
$N(^2D)$	1.00E+17	8.90E+16	4.29E+16	1.41E+16
$N(^2P)$	7.82E+14	4.74E+14	1.40E+14	3.23E+13
N^+	5.29E+10	2.12E+10	2.15E+09	1.45E+08
N_4^+	1.83E+11	1.04E+11	5.88E+10	4.01E+10
N_3^+	9.66E+10	4.68E+10	8.81E+09	1.31E+09
$NO(X\ ^2\Pi_r)$	1.32E+20	1.75E+20	2.58E+20	3.02E+20
$NO(A\ ^2\Sigma^+)$	3.59E+14	3.64E+14	3.05E+14	1.86E+14
$NO(B^2\Pi_r)$	1.67E+09	1.81E+09	1.72E+09	1.13E+09
NO^+	4.29E+15	6.19E+15	8.68E+15	1.03E+16
$NO_2(X^2A_1)$	1.38E+15	3.76E+15	1.39E+16	3.94E+16
$NO_2(a^4A_2)$	1.43E+14	2.78E+14	5.14E+14	5.49E+14
$CN(X^2\Sigma^+)$	1.62E+10	1.77E+10	1.45E+10	1.17E+10
$CN(B^2\Sigma^+)$	1.61E+07	6.22E+06	1.43E+06	3.42E+05
n_e	8.30E+15	8.95E+15	9.99E+15	1.09E+16